

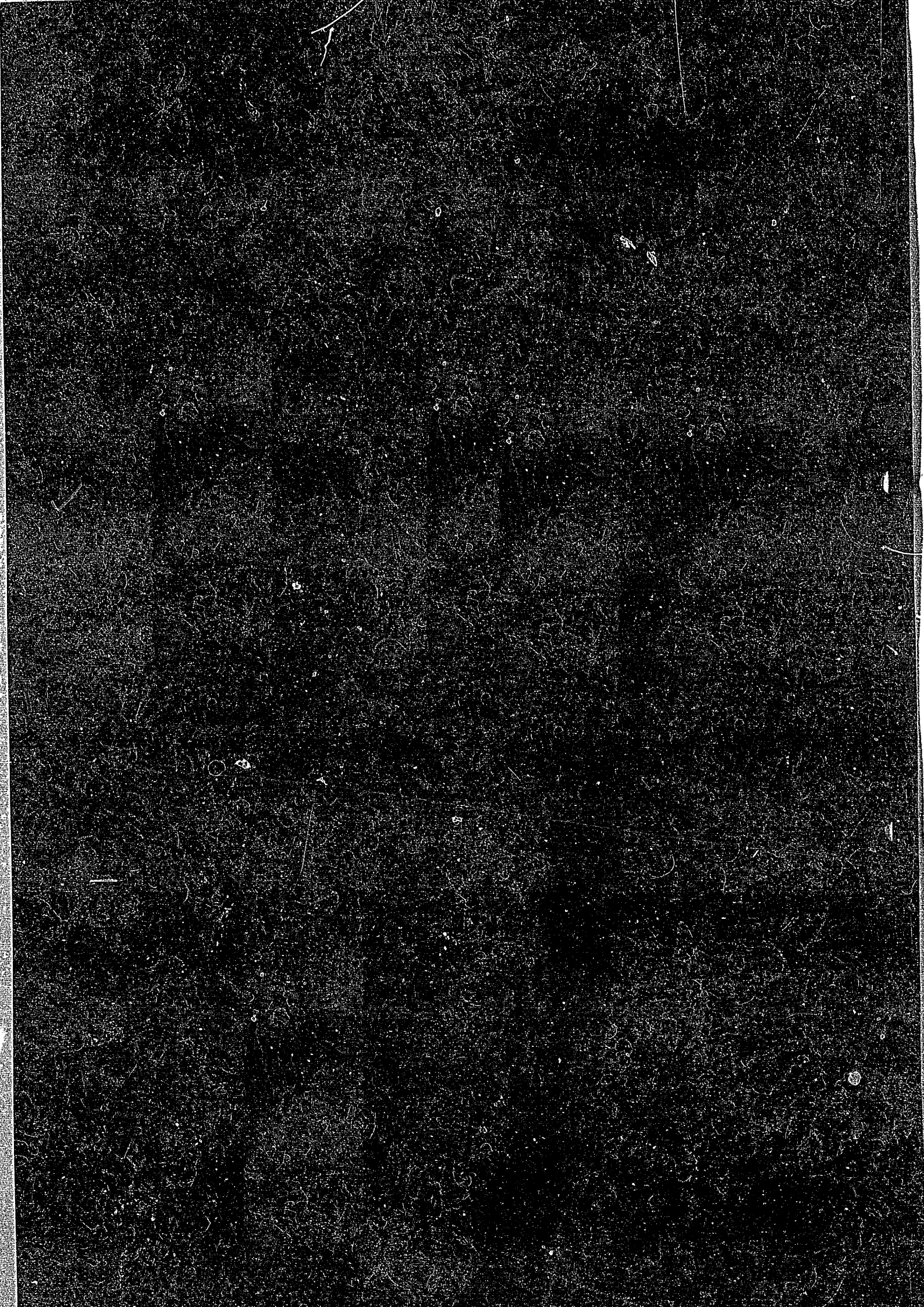
IPPJ-AM-48

**DYNAMIC PROCESSES
OF
HIGHLY CHARGED IONS**

EDITED BY Y. KANAI AND S. OHTANI

**INSTITUTE OF PLASMA PHYSICS
NAGOYA UNIVERSITY**

NAGOYA, JAPAN



IPPJ-AM-48

DYNAMIC PROCESSES OF HIGHLY CHARGED IONS

Proceedings of International Seminar
on
Dynamic Processes of Highly Charged Ions

Edited by
Yasuyuki Kanai and Shunsuke Ohtani

Institute of Plasma Physics, Nagoya University
Chikusa-ku, Nagoya 464, Japan

October 1986

This document is prepared as a preprint of compilation of atomic data for fusion research sponsored fully or partly by the IPP/Nagoya University. This is intended for future publication in a journal or will be included in a data book after some evaluations or rearrangements of its contents. This document should not be referred without the agreement of the authors. Enquiries about copyright and reproduction should be addressed to Research Information Center, IPP/Nagoya University, Nagoya, Japan.

PRÉFACE

International Seminar on Dynamic Processes of Highly Charged Ions was held as a satellite meeting of the Tenth International Conference on Atomic Physics (10th ICAP, Tokyo), on 21 - 23 August, 1986, at Fuji Institute of Education and Training, near Mt. Fuji, Japan.

The Host Institutes of this Seminar are Institute of Physical and Chemical Research (RIKEN) and Institute of Plasma Physics, Nagoya University. There were 58 participants from 6 countries, among whom were from abroad. In addition 6 family members visited. The Seminar was opened by the Guidance of the meeting by Dr. Y. Awaya, and the opening address by Dr. T. Watanabe, RIKEN, and closed by the concluding remarks by Professor Y. Kaneko, Tokyo Metropolitan University. On the 24th of August, the most participants visited the fifth uphill station of Mt. Fuji and could luckily see the top of the Mt. Fuji, on the way from the Fuji Institute to Tokyo.

The Proceedings include 18 review papers and progress reports and 10 contributed papers. The contributed papers were mainly presented in the Poster Session on 22 August. In addition, the list of participants is also attached at the end of the Proceedings.

On behalf of the organizing committee, we would like to express our sincerest thanks to all participants who gave active contribution not only by the formal presentation of papers but also through the informal, hot discussions in all possible occasions during the Seminar. We would mention the achievement of devoted secretariat Drs. Y. Awaya, T. Kambara, Y. Kanai, and I. Shimamura, and Ms. M. Nishida. We would also like to thank Meses. M. Awaya and Y. Watanabe for their friendly contribution to the family program.

S. Ohtani

T. Watanabe

Organizing Committee

Y. Awaya	(RIKEN)
T. Kambara	(RIKEN)
Y. Kanai	(RIKEN)
N. Kobayashi	(Tokyo Metropolitan Univ.)
S. Ohtani	(Inst. Plasma Phys.)
K. Shima	(Univ. of Tsukuba)
I. Shimamura	(RIKEN)
T. Watanabe	(RIKEN)

This Seminar is indebted to the following sponsors:

Nishina Memorial Foundation

Shimadzu Science Foundation

INVITED PAPERS

Thursday, August 21

19:30-20:30

Guidance

Watanabe, T.

Specificity of highly charged ions 1

Friday, August 22

9:00-10:30

Lin, C.D., Fritsch, W., and Kimura, M.

An Overview of Low-Energy Ion-Atom Collisions 3

Eichler, J.

Current Topics in High-Energy Ion-Atom Collisions 14

11:00-11:45

Dunn, G.

Overview of Electron-Ion Collisions 20

13:00-15:00

Poster Session

15:30-17:30

Matsumoto, A.

Excitation and Ionization of Ions by Electron Impact: Recent
Activities at IPP and Sophia University 24

Henry, R.J.W.

Electron-Impact Excitation and Indirect Ionization of Ions 29

Hahn, Y.

Recombination Processes in Electron-Ion Collisions 35

Younger, S.M.

Electron Impact Ionization of Heavy Ions - Some Surprises 40

Saturday, August 23

9:00-10:10

Manson, S.T., Inokuti, M., and Theodosiou, C.E.

Systematics of Energy Levels and Other Properties of Highly
Charged Ions 45

Beyer, H.F.

Atomic Physics at the ESR Storage Ring 52

10:40-12:00

Egan, P.O., Chandler, G.A., Dietrich, D.D., Ziock, K.P., Mokler,
P.H., Reusch, S., and Hoffmann, D.H.H.

X-Ray Spectroscopy of Highly Stripped Very Heavy Ions 61

Mizogawa, T., Awaya, Y., Kambara, T., Kanai, Y., Kase, M., Kumagai,
H., Mokler, P.H., and Shima, K.

Target Thickness Dependence of $K\alpha$ Satellite Intensities of Argon
Ions Colliding with Thin Carbon Foils 71

<u>Katayama, I., Fujiwara, M., Noro, T., Ikegami, H., Fukuzawa, F., Yoshida, K., Haruyama, Y., Aoki, A., Ogawa, H., and Sugai, K.</u> K-Electron Capture from Target Atoms by ^3He Ions	75
---	----

13:30-14:30

Sellin, I.A. What is New in Conroy Electron Physics?	80
<u>Yamazaki, Y., Miller, P.D., Krause, H.F., Pepmiller, P.L., Datz, S., Sellin, I.A., and Stolterfoht, N.</u> Strong Forward-Backward Asymmetries in Electron Emission from Overlapping Resonance States in Fast C^{3+} on He Collisions	88

15:00-17:00

Huber, B.A. State-Selective Measurements in Low-Energy Ion-Atom and Electron-Atom Collisions	91
Kimura, M. State Selective Electron Capture by Highly Stripped Ions from Atoms	96
<u>Okasaka, R. and Sakakibara, H.</u> Polarization Properties of Total Emission Cross Section in He^+ -He Collisions	102
<u>Koike, F., Sakaue, H., Ikezaki, Y., Wakiya, K., Takayanagi, T., Suzuki, H., and Yagishita, A.</u> Anisotropy of Electron Emission from Aligned States of Neon (Contributed Paper)	
Kaneko, Y. Concluding Remark	

CONTRIBUTED PAPERS

<u>Koike, F., Sakaue, H., Ikezaki, Y., Wakiya, K., Takayanagi, T., Suzuki, H., and Yagishita, A.</u> Anisotropy of Electron Emission from Aligned States of Neon	107
Ohyama-Yamaguchi, T. Double- and Single-Charge Transfer in Collisions of C^{6+} Ion with He Atom at Low Impact Energies	108
Shimakura, N., Sato, H., Kimura, M., and Watanabe, T. Low Velocity Collision of O^{6+} with He by MO Base Treatment	109
Phaneuf, R.A., Meyer, F.W., Havener, C.C., Stolterfoht, N., Swenson, J.K., and Shafroth, S.M. Evidence for Correlated Double-Electron Capture in Slow $\text{O}^{6+}+\text{He}$ Collisions	110
Shima, K., Umetani, K., Fujioka, S., Yamanouchi, M., Awaya, Y., Kambara, T., Mizogawa, T., and Kanai, Y. Evolution of Fast Heavy Ion Excitation in Solid Target — 0.83-2.4 MeV/u Br^{q+} , $\text{Cu}^{q+}+\text{C}$	111

Nishimura, F. and Oda, N. Angular Dependence of Loss Electrons in 0.5 MeV/amu H_2^+ , H_3^+ , and He^+ -Ar Collisions	112
Kawatsura, K., Ootuka, A., Sataka, M., Komaki, K.-I., Naramoto, H., Sugizaki, Y., Ozawa, K., Nakai, Y., and Fujimoto, F. Continuum X Rays During Ion-Atom Collisions	113
Hino, K. and Watanabe, T. Photon Angular Distribution of Radiative Electron Capture by Relativistic Strong Potential Born Calculation	114
Iwai, M., Shimamura, I., and Watanabe, T. Manifestation of Minima in the Generalized Oscillator Strengths as Minima in the Integrated Cross Sections for Ion-Atom Colli- sions	115
Msezane, A.Z., Lee, J., Reed, K.J., and Henry, R.J.W. Electron Impact Excitation of Oxygen-Like Krypton	116
List of Participants	117

SPECIFICITY OF HIGHLY CHARGED IONS

Tsutomu Watanabe

Atomic Processes Laboratory, The Institute of Physical and
Chemical Research (RIKEN), Wako-shi, Saitama 351-01, JAPAN

Highly charged ions (HCI's) have been obscure for long time and have not cut a complete figure yet even nowadays. It is quite recent that a highly charged ion has been obtained with sufficient intensity to measure in the form of ion projectile or ion target in scattering experiments. This difficulty comes from the unstable property of highly charged ions. They can easily capture an electron from the surrounding atom, molecules or free electron cloud. It is difficult to confine highly charged ions within a certain small volume as the target in scattering processes. It is also difficult to obtain an HCI with the velocity of particularly low or high compared with the charge balancing velocity. Nowadays the research activity for the dynamic processes of such highly charged ions are being developed. This is due to the improvement of production method for HCI (ion sources and recoil-ion chamber) and also due to that of the measurement techniques. Theoretically, it can be more easily being extended with aid of large scale computers. Some of them will be presented and reported in this seminar and stimulated and hot discussions on those research works will be desired.

From my opinion, one of specificity of HCI lies the existence of huge attraction potential which causes to find an electron within a wide domain. For example, the orbiting cross section in ion-atom collision with charge q and polarizability α can be written by

$$\sigma = \frac{4\pi qe}{v} \left(\frac{\alpha}{m} \right)^{1/2} \quad (1)$$

where v is the relative velocity and m is the reduced mass of the colliding system. This cross section is proportional to the charge q of the ion and the critical energy to the orbiting collision can be proportional to q^2 . The magnitude of cross section for orbiting process exceeds sometimes of the order $10^4(q/v)\pi a_0^2$.

The second specificity is the contribution of excited state of ions. This feature is closely related to the first specificity i.e. the side range of attractive potentials. If we see the oscillator strength dis-

tribution (OSD) of hydrogen like ions, the relation between the oscillator strength and energy scaled by Z^2 (Z being the atomic number of ion) is universal and doesn't depend on Z . This feature can be extended another iso-electronic sequence when we want to make qualitative discussion on the OSD. Details will be reported and discussed by Manson. Speaking of generalized oscillator strength distribution (GOSD) basically situation can be discussed similarly, the result becomes somewhat different from GOSD in the case of heavy ion collisions. According to the difference of the momentum transfer region, each GOSD is quite different from the case of electron as well as proton impact. This feature may influence on the Z -dependence of GOSD.

In the inner-shell excitation and ionization of proton absorption, so-called shape resonance spectrum or a giant band observed in the case of neutral species. However in the case of charged ion or multiply charged ion, this shape resonance spectrum is disappeared and the Rydberg spectrum appeared again. This is due to the wideness and strongness of the multi-charged Coulomb potentials. The ionization cross section of ion by electron impact is sometimes quite different from that of neutral one. The contributions of singly excited states and doubly excited states (auto-ionizing states) are sometimes relatively large. This is due to the difference of the outer-shell structure between a neutral atom and an ion.

The third specificity is the interaction of photons with HCI's. In HCI, the difference between electronic energy levels is proportional to q^2 , and the spontaneous radiative decay rate of electronic transition is proportional to the square of the energy difference (transition energy). Then decay rate is proportional to q^4 (or if we consider that transition dipole moment is the same order of magnitude rather than dipole oscillator strength, the decay rate is proportional to q^6). The role of radiative decay rate becomes important among the process which competes. The importance of dielectronic recombination and resonant-charge-transfer-and-excitation (RTE) process are often emphasized and they have been investigated extensively in recent years. The dielectronic recombination is the inverse process of double photo-excitation. The RTE is the relevant process where the part of an initial free electron in dielectronic recombination is taken by a bound electron in a target atom. Some of the phenomena, which will be reported and discussed in this seminar, can be interpreted along this concept and others might deviate from this simple speculation and these can be expected to lead to a new discovery.

An Overview of Low-Energy Ion-Atom Collisions*

C. D. Lin, W. Fritsch** and M. Kimura#

Department of Physics, Kansas State University
Manhattan, Kansas 66506 USA

**Hahn-Meitner Institute, Berlin, W. Germany

#Argonne National Laboratory, Argonne, Illinois 60439 USA

I. INTRODUCTION

Current interest in collisions between multiply charged ions (MCI) with atoms and molecules leading to electron capture into excited states of the projectile ions stems originally from applications in fusion research and in astrophysics.¹ In the last few years, many distinctive ion sources have been developed at different laboratories. Multiply charged ions produced in ECR, EBIS ion sources, as well as recoil ions produced from bombardment by fast heavy ions and by intense lasers are used routinely in collisions with neutral atoms and molecules. Early measurements by charge-state analysis of the projectiles provided many sets of total charge transfer cross sections. Stimulated by these measurements, many theoretical models have been proposed. For a recent review, the reader is referred to the article by Janev and Winter.²

Advances in recent experiments in the collision between MCI and atoms have provided cross sections to specific final excited states for a number of collision systems. These states are identified either directly by the energy-gain spectroscopy³ or indirectly by the photon-emission spectroscopy.⁴ Within the last year, there were reports of the polarization measurements of the photons emitted from de-excitation as well as differential cross section measurements.⁵ These data give information about the distribution of magnetic substates and the impact parameter dependence of the capture mechanism, respectively. These detailed measurements undoubtedly provide a greater challenge for a more accurate theoretical description of the collision dynamics between MCI and atoms. In this overview, we will give examples of the more recent measurements of collisions between MCI and simple atoms where a detailed comparison between experimental results and theoretical calculations is possible. Through such comparisons, it is hoped that we can identify the salient theoretical and experimental problems in this area for the next few years. We will also

address briefly the problems in multiple electron capture and in MCI-molecule collisions.

II. THEORETICAL MODELS

For collisions between MCI and atoms where the energy of the MCI is in the range of 0.1-30 keV/amu, it is adequate to treat the motion of the heavy particles classically. Because of the large positive charge of the MCI, it is clear that the problem has to be treated by nonperturbative methods. Two general approaches explored by various groups are: (1) direct numerical solution of the time dependent Schroedinger equation; (2) close-coupling expansion in terms of atomic or/and molecular orbitals.

In this overview, we will not address the first method⁶ or its generalization (to the time-dependent Hartree-Fock method⁷ in the case of two-electron collision systems) since these methods have not been extensively explored for collisions between MCI and atoms. Instead, we will focus on the development in the more traditional close-coupling expansion methods.

In the close-coupling method, one expands the time evolution of the electronic wave function as

$$\psi(\vec{r}, t) = \sum_j c_j(t) \phi_j(\vec{r}; t) \quad (1)$$

where ϕ_j is the eigenfunction of some operator, \vec{r} denotes the coordinates of the electrons. An important step in (1) is the determination of suitable basis functions. It would be desirable to use as few basis functions in the expansion as possible for a given collision condition. At $t \rightarrow \pm\infty$, it is clear that the suitable basis functions are the atomic orbitals (AO) of the target and of the projectiles travelling with their respective centers. Thus a convenient basis set for (1) is the travelling atomic orbitals of the two collision centers. This AO expansion method was proposed by Bates⁸ in 1958. Another familiar method is to expand (1) using the adiabatic molecular orbitals (MO) of the collision system. This model, generally known as the Perturbed Stationary State (PSS) approximation,⁹ has long been served as the basis for the qualitative as well as semi-quantitative description of slow ion-atom collisions.

The PSS model, although conceptually quite appealing, is known to have some mathematical defects. The adiabatic MO's correlate to static atomic orbitals in the asymptotic region, and not to the travelling atomic orbitals. Thus each MO basis function does not satisfy the asymptotic

boundary condition. To remedy this situation, electron translational factors (ETF) are incorporated into the MO's. Since there is no well-defined physical principles for the determination of ETF's except in the asymptotic region, various forms of ETF's have been proposed.¹⁰

One special feature in the collision of MCI with neutral atoms is that transitions occur mostly at large internuclear separations. For this reason, the AO expansion is quite adequate in giving reasonable accurate total cross sections to each subshell. In the static limit, the MO's at large internuclear separations can be accurately represented as linear combination-of-atomic-orbitals (LCAO) and thus the AO and MO expansions are equivalent. By adopting an AO expansion, however, there is no ambiguity in the choice of ETF's.

The AO expansion is not expected to be valid for collisions occurring at small internuclear separations. Thus the AO results become less reliable at lower collision energies. For one-electron collision systems, it is possible to include united-atom's orbitals in the two-center AO expansion (the AO+ model)¹¹ to span the same Hilbert space as represented by the molecular orbitals. The AO+ model (or its equivalent 3-center expansion model¹²), however, requires a larger basis set in practical applications.

An alternative unified AO-MO matching method has been proposed recently.^{13,14} This method is somewhat equivalent to the R-matrix method¹⁵ for time-independent problems. In this method, one expands the time-dependent wave functions at large internuclear separations using travelling AO's and in the inner region using static MO's. The wave functions are matched at two internuclear separations, one in the incoming part and the other in the outgoing part. In this method, the inner region is identical to the PSS model. Since the MO expansion is limited to the inner region only, problems associated with the ETF's in the PSS model are avoided.

III. SELECTIVE EXAMPLES

In this section, we compare selective experimental results with calculations based on different models to assess our understanding of the dynamics of the collision between MCI and atoms. We will first address single-electron capture only where detailed studies are available. To simplify notations, we use σ_t , σ_n , σ_{n1} , and σ_{n1m} to denote total capture, capture to n-shell, to nl-subshell and to nlm-state, respectively.

A. σ_n : Capture Cross Section for n Shell

In the low-energy region, the electron is captured predominantly to a specific n, although capture to other n-shells is also possible. The

dominant n -shell can be easily estimated by the classical barrier model¹⁶ (CBM) or from simple molecular potential curves. In Fig. 1 we show the experimental results¹⁷ for electron capture in C^{4+} -H collisions. Capture to the $n=3$ states of C^{3+} is dominant, and thus σ_3 is

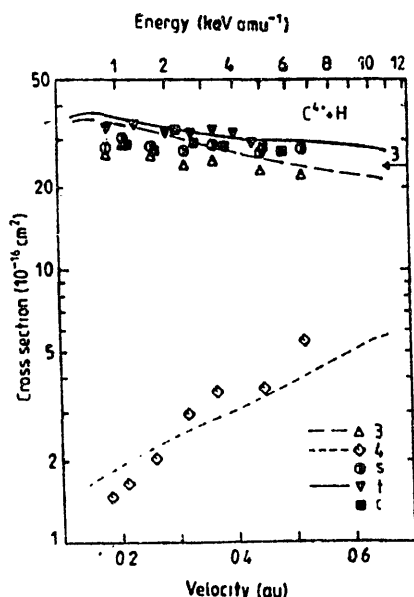


Fig. 1. Electron capture cross sections for C^{4+} -H. In the velocity range shown, σ_3 is nearly equal to σ_t . The calculations of Ref. 18 are in good agreement with the measured σ_t and σ_3 . The agreement with the small σ_4 is also quite good (from Dijkamp et al., Ref. 17).

nearly identical to σ_t obtained from charge-state analysis measurements. The experiment of Dijkamp et al. also gives cross sections for capture to $n=4$ shell. These data are compared with the AO calculations of Fritsch and Lin.¹⁸ Note that the agreement between theory and experiment is quite good even for the small σ_4 . In Fig. 2 we show the results for the C^{6+} -H system. There are no experimental measurements but there are a few calculations for this case where capture is also mostly to the $n=4$ shell. Most of the theoretical calculations agree with each other for σ_4 and with total capture cross section measurements. However, the predictions for the small σ_5 are quite different. The 33-state MO expansion calculation of Shipsey et al.¹⁹ predicts large σ_5 at low energies.

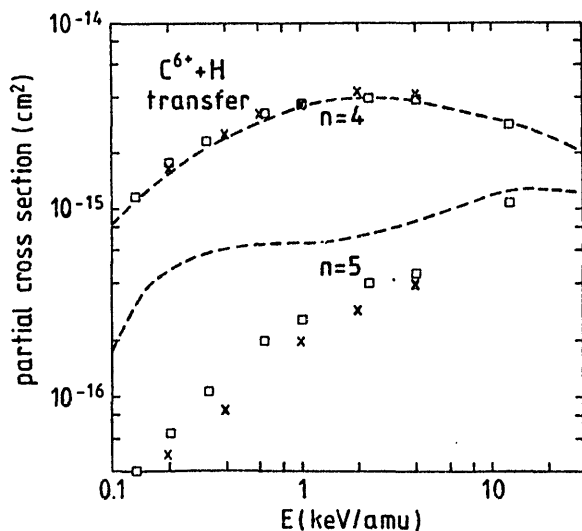


Fig. 2. Partial cross sections for transfer into C^{5+} $n=4$ and $n=5$ states in C^{6+} +H collisions. Dashed lines are from the MO calculations of Ref. 19. The AO results of Ref. 20 and the AO-MO results of Ref. 13b are shown in squares and in crosses, respectively.

The AO calculations of Fritsch and Lin²⁰ and the AO-MO matching results of Kimura and Lin^{13b} both predicted much smaller σ_5 and are in good agreement with each other. From these results it is difficult to jump into the conclusion that the MO expansion method is not valid since in the calculation of Shipsey et al. there are several approximations made in the matrix elements involving n=5 channels. Whether the discrepancy is the result of the numerical approximation or of the MO expansion remains to be resolved.

B. σ_{n1} : Subshell Cross Sections

For highly charged ions or bare projectiles, the energy separations between final nl-subshells in a given n is usually too small to be resolved using the energy gain spectroscopy. Although there are a number of theoretical calculations predicting the σ -distribution for collisions between bare projectiles and atoms, there are only indirect information about the σ -distribution from the observed Lyman radiation emitted.²¹ These measurements indicated that there is no serious discrepancy with MO-based models which include ETF's, nor with AO-based results. For lower charged heavy ions, the energy separations between nl-subshell are often large enough to be observed using the translational energy spectroscopy. An example of this is shown in Fig. 3 where cross sections for one-electron capture in C³⁺-H collisions leading to C²⁺ in specific nl-subshell is displayed. In this system, the data from the translational energy spectroscopy²² are in good agreement with those obtained from the photon-emission spectroscopy.²³ These results, surprisingly, are well predicted by calculations based on the MO expansions without including ETF's.²⁴

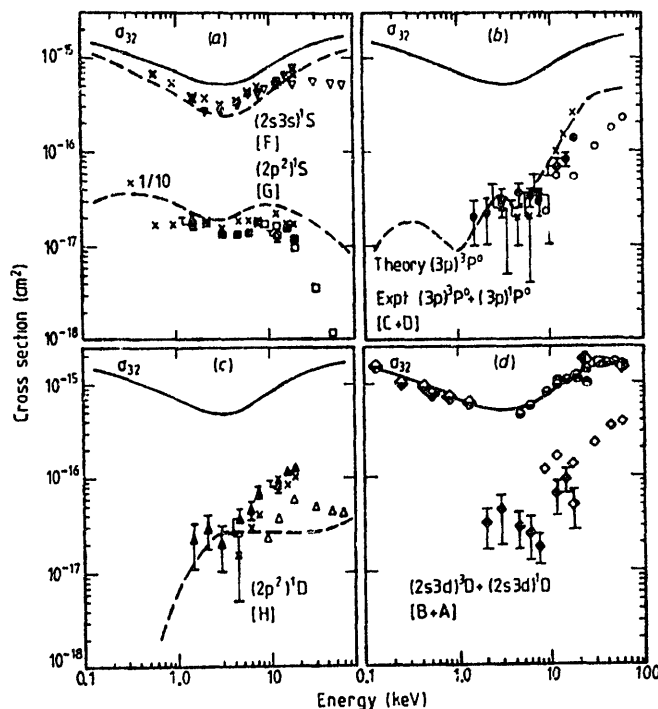


Fig. 3. Cross sections for one-electron capture in C³⁺-H collisions leading to specific C²⁺ states as indicated in the figure. For the partial nl cross sections, the experiments from Ref. 22 and from Ref. 23 are in good agreement (figures adopted from Ref. 22).

Another example where σ_{n1} 's are available for comparison is O^{6+} -He. Comparison of the experimental results of Dijkamp et al. with the results of AO expansion can be found in Fritsch and Lin.²⁵

Although σ_t and σ_n for a given target depend mostly only on the charge state of the projectiles, the ℓ -distribution depends more sensitively on the core structure of the projectiles. For example, the σ_{n1} distribution for $n=3$ in O^{6+} -He and C^{6+} -He are somewhat different. At a given collision speed, capture to the 3s tends to be smaller for the C^{6+} .

C. σ_{n1m} -Distribution

Partial information about σ_{n1m} has been obtained by observing the polarization of the photons emitted^{26,27} from the de-excitation of the electron after capture. Comparison of theoretical calculations with measurements are complicated by the need of considering the depolarization due to the spin-orbit interaction and for the effects due to cascades. There is very little theoretical analysis in this area, but work is in progress.²⁸

D. Differential Cross Sections

Measurements of angular distributions for electron capture to a specific state give information about the collision dynamics at different impact parameters. While the total cross sections σ_{n1} are often dominated by contributions from large impact parameters, angular distribution measurements can test whether the theoretical models are valid over the whole range of impact parameters. An example of angular distribution is shown in Fig. 4 for the double capture in $C^{4+}(1s^2)+He \rightarrow C^{2+}(1s^2 2s^2)+He^{++}$ collisions at 1520 keV. This is an ideal system since double capture is the dominant process in this energy region and thus the collision is well approximated by a two-channel model. The relevant molecular potential curves have also been calculated.²⁹ Using the MO expansion with the ETF's of Kimura and Thorson,³⁰ the angular distribution for this system has been calculated using both a full quantal formulation and a semi-classical method.³¹ The theoretical result is also shown in Fig. 4 where it has been folded with experimental angular resolutions.⁵ It is noted that the agreement between theory and experiment is excellent. Experiments are being carried out for other collision systems. It would be desirable to compare theoretical calculations for multi-channel systems with new measurements to check the validity of the theory.

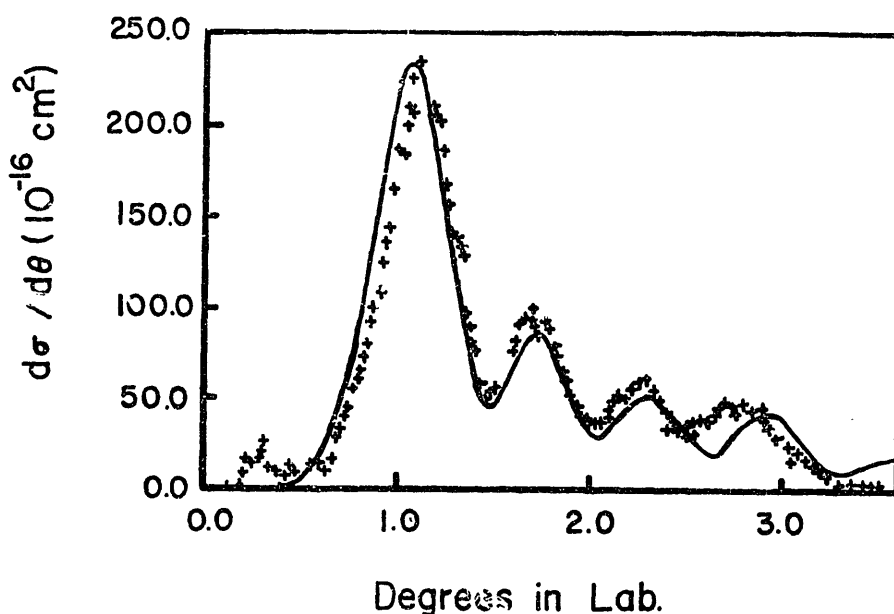


Fig. 4. Differential double electron capture cross sections for C^{4+} on He collisions. The experimental data were from Tunnell and Cocke (Ref. 5). Theoretical results shown in solid lines were the results of two-channel fully quantum-mechanical calculations by Tan et al. (Ref. 31).

IV. MULTI-ELECTRON TRANSITIONS AND MOLECULAR TARGETS

Multiple electron capture processes occur frequently in collisions between MCI and multi-electron targets, producing multiply excited states which stabilize usually by autoionization with the emission of secondary electrons. Double electron capture has been identified in energy-gain spectroscopy, and is the main contribution to transfer ionization (TI) processes in charge-state analysis measurements. Unfortunately the resolution in current energy-gain spectroscopy can identify the principal quantum numbers n and n' of the two excited electrons only. The new development in zero-degree spectroscopy³² has improved the resolution by looking at electrons emitted in the forward direction, but the method is limited to projectiles with higher velocity.

Multiple electron capture is the most efficient method of producing multiply excited states of atoms and ions. Unlike excitations by electron or by photon impacts where multiply excited states are produced only by the weak electron-electron correlation, in ion-atom collisions these states can be produced by 'multi-step' mechanism, i.e., through successive single electron capture processes during the collision. In this latter process, electron correlation plays an important role only after the collision is

over. It has been established that the cross sections for the production of doubly excited states by photon impact³³ and by electron impact follows some quasi-selection rules.³⁴ These quasi-selection rules can be understood in terms of the new classification scheme of doubly excited states.³⁵ It would be desirable to explore experimental evidence for selection rules, if any, in the production of multiply excited states in ion-atom collisions.

There are many charge-state analysis measurements for electron capture cross sections in MCI-molecule collisions. Since the dominant contribution to the total capture cross sections derives from large impact parameters, the process can be approximated by using a model potential for the molecule or by neglecting the strong coupling region of the ion-molecule complex. Calculations based on these models by Kimura^{36,37} have produced good total capture cross sections. Exciting experiments in ion-molecule collisions in the future, however, probably will study the fragmentation of the resulting molecular ions. For diatomic molecules, coincidence measurements tell how the capture process depends on the orientation of the molecule. Production of different polyatomic molecular ions has been observed³⁸ in abundance; many of these ions have not been isolated by chemists. This area of 'hot chemistry' would allow the study of complex molecular ions. These ions are believed to play an important role in the formation of complex molecules in interstellar space through chains of ion-molecule reactions.

IV. SUMMARY AND DISCUSSION

The progress in the study of collisions of MCI with atoms in the last few years clearly indicates that both theory and experiment have passed their infancy. Improved data on subshell cross sections, polarizations, and differential cross sections will provide more stringent tests of the different sophisticated theoretical models in use. Currently, multi-variable coincidence measurements are being carried out by the group from Orsay.³⁹ In their study, the charge state of the target and of the projectile, the energy gain and the angular distribution were measured in coincidence. These data allow a clear identification of specific final state. In particular, this group has been able to identify triple and quadruple electron capture events in a single collision, although the resolution is not good enough to isolate specific states.

From the theoretical viewpoint, it is fair to say that model calculations for one- and quasi-one-electron systems are in good shape in the

energy region where the number of states populated are small. For multi-electron target atoms, ab initio calculations are much more difficult. A detailed study would require proper consideration of collision dynamics as well as electron correlations. For two-electron collision systems, calculations based on AO expansions have shown that the results are in good agreement with measured σ_{n1} . However, the computational effort is not trivial for each system. Neither the MO with ETF's nor the AO-MO matching methods have yet been applied extensively to obtain partial cross sections in MCI-atom collisions, although there is no reason to expect that these calculations would give erroneous results since these models have been successfully applied to other ion-atom collisions.

In this overview, we have not considered the role of ionization. For MCI-atom collisions at low energies, it is adequate to neglect ionizations. At increasing collision energies, many $n1$ subshells are populated. Detailed full close-coupling calculations become nearly impossible because of the large number of channels. A reasonable approximation is then to treat each n -manifold separately⁴⁰ or to include the coupling between the dominant n -manifold with each weaker n -manifold separately in each calculation. Although the capture probability to each n -manifold is small, the sum of the capture probabilities to many n -manifolds is large. So far, it has not been possible to include ionization channels in the MCI-atom collisions in the intermediate energy region despite that the effect of ionization can be included in the close-coupling formulation using pseudostates.⁴¹ Recent calculations⁴² indicated that the neglect of ionization channels can give errors up to a factor of two in total capture cross sections at high energies.

Finally it is important to mention that the basic collision dynamics in MCI-atom collision is not very different from the conventional ion-atom collisions studied using small accelerators. Theoretical methods developed for MCI-atom collisions are applicable to other ion-atom collisions. It is fitting to say that many experimental data in proton-helium collisions performed almost two decades ago have now been explained⁴³ using the AO-MO matching method. The same calculation can also explain the recent measurements of alignment⁴⁴ and of orientation parameters⁴⁵ of H(2p) produced in p-He collisions.

*The research work reported here was supported in part by the US Department of Energy, Office of Energy Research, Division of Chemical Sciences.

REFERENCES

1. R.J. Fonck, D.S. Darrow and K.P. Jaehnig, Phys. Rev. A29, 3039 (1984).
2. R.K. Janev and H. Winter, Phys. Rep. 117, 265 (1985).
3. C. Schmeissner, C.L. Cocke, R. Mann and W. Meyerhof, Phys. Rev. A30, 1661 (1984); K. Okuno et al., Phys. Rev. A28, 127 (1983).
4. D. Dijkkamp et al., J. Phys. B18, 737 (1985).
5. L.N. Tunnell, Ph.D. thesis, Kansas State University (1986).
6. H.J. Ludde and R.M. Dreizler, J. Phys. B15, 2713 (1982).
7. A. Henne, A. Toepfer, H.J. Ludde and R.M. Dreizler, J. Phys. B19, L361 (1986).
8. D.R. Bates, Proc. Phys. Soc. A247, 294 (1958).
9. H.S.W. Massey and R.A. Smith, Proc. Roy. Soc. London A142, 142 (1933).
10. See C.D. Lin, Comm. At. Mol. Phys. 11, 261 (1982).
11. W. Fritsch and C.D. Lin, J. Phys. B15, 1255 (1982).
12. T.G. Winter and C.D. Lin, Phys. Rev. A29, 567 (1984).
13. a) M. Kimura and C.D. Lin, Phys. Rev. A31, 590 (1985); b) *ibid.*, A32, 1357 (1985).
14. T.G. Winter and N.F. Lane, Phys. Rev. A31, 2698 (1985).
15. E.P. Wigner and L. Eisenbud, Phys. Rev. 72, 29 (1947).
16. H. Ryufuku, K. Sasaki and T. Watanabe, Phys. Rev. A21, 745 (1980).
17. D. Dijkkamp, D. Ciric, E. Vlieg, A. de Boer and F.J. de Heer, J. Phys. B18, 4763 (1985).
18. W. Fritsch and C.D. Lin, J. Phys. B17, 3271 (1984).
19. T.A. Green, E.J. Shipsey and Browne, Phys. Rev. A25, 1364 (1982).
20. W. Fritsch and C.D. Lin, Phys. Rev. A29, 3039 (1984).
21. A. Chetioui, J.P. Rozet, D. Vernhet, K. Wohrer, P. Bcuisset, A. Tourti and C. Stephan, Nuc. Instr. Meth
22. F.G. Wilkie, R.W. McCullough and H.B. Gilbody, J. Phys. B19, 239 (1986).

23. D. Ciric et al., J. Phys. B18, 3639 (1985).
24. S. Bienstock, T.G. Heil, C. Bottcher and A. Dalgarno, Phys. Rev. A25, 2850 (1982).
25. W. Fritsch and C.D. Lin, J. Phys. B (1986) to be published.
26. D. Vernhet, A. Chetioui, K. Wohrer, J.P. Rozet, P. Piquemal, D. Hitz, S. Dousson, A. Salin and C. Stephan, Phys. Rev. A32, 1256 (1985).
27. L.J. Lembo, K. Danzmann, Ch. Satoller, W.E. Meyerhof and T. W. Hansch, Phys. Rev. Lett. 55, 1874 (1985).
28. A. Jain and C.D. Lin, (in progress).
29. M. Kimura and R.E. Olson, J. Phys. B17, L713 (1984).
30. M. Kimura and W.R. Thorson, Phys. Rev. A24, 1780 (1981).
31. J. Tan, C.D. Lin and M. Kimura (to be published).
32. N. Stolterfoht, C.C. Havener, R.A. Phaneuf, J.K. Swanson, S.M. Shafroth and F.W. Meyer, Phys. Rev. Lett. 57, 74 (1986).
33. P.R. Woodruff and J.A. Samson, Phys. Rev. A25, 848 (1982).
34. P.J.M. Van dear Burgt and H.G.M. Heideman, J. Phys. B18, L755 (1986).
35. C.D. Lin, Phys. Rev. Lett. 51, 1348 (1983); Phys. Rev. A29, 1019 (1984).
36. M. Kimura, Phys. Rev. A32, 802 (1985).
37. M. Kimura, Phys. Rev. A33, 4440 (1986).
38. T.J. Gray and J. Legg (private communication, 1986).
39. P. Roncin and M. Barat, Europhys. Lett. (to be published, 1986).
40. H. Ryufuku and T. Watanabe, Phys. Rev. A20, 1828 (1979).
41. W. Fritsch and C.D. Lin, Phys. Rev. A27, 3361 (1983).
42. A. Jain, C.D. Lin and W. Fritsch, Phys. Rev. A (to be published, 1986).
43. M. Kimura and C.D. Lin, Phys. Rev. A34, 176 (1986).
44. R. Hippler, W. Harbich, M. Faust, H.O. Lutz and L.J. Dube, J. Phys. B19, 1507 (1986).
45. H.O. Lutz (private communication, 1986).

CURRENT TOPICS IN HIGH-ENERGY ION-ATOM COLLISIONS

J. Eichler

Hahn-Meitner-Institut für Kernforschung Berlin, Germany F.R.

In a large number of laboratories, ion-atom collisions can now be investigated experimentally at high collision energies. By high energy it is usually understood that the projectile velocity considerably exceeds all electronic orbital velocities occurring in either projectile or target. In a few cases experimental investigations have even been carried into the relativistic velocity regime. From the theoretical point of view, high-energy collisions are simpler to describe in some respects, because many of the finer details of atomic structure do not contribute or are currently not measurable. In the following, I shall summarize some of the results that have recently been obtained. Since the selection is necessarily limited, it is far from complete and hence involves personal preferences.

1. Nonrelativistic High-Energy Collisions

1.1 Excitation and Ionization

At high projectile velocities, the process of target excitation or ionization is generally well understood. First-order theories, as for example the plane-wave Born approximation (PWBA) or the semiclassical approximation (SCA) give reasonably good agreement with experiment. These theories predict a projectile charge dependence of the cross section as Z_p^2 . For high charges Z_p , however, the first-order cross section exceeds the unitarity limit, so that non-perturbative methods have to be applied. Recently Brendlé and Gayet¹ have developed a method based on Schwinger's variational principle to calculate excitation cross sections. If $|i\rangle, |f\rangle$ are initial and final unperturbed states, G_T^\pm is the unperturbed target Green function, and V the perturbing potential, the scattering wave functions are

$$|\psi_i^\pm\rangle = |i\rangle + G_T^\pm V |\psi_i^\pm\rangle$$

$$|\psi_f^-\rangle = |f\rangle + G_T^- V |\psi_f^-\rangle.$$

The Schwinger amplitude then is given¹ by

$$T_{fi} = \frac{\langle f|V|\psi_i^+\rangle \langle \psi_f^-|V|i\rangle}{\langle \psi_f^-|V - VG_T^+V|\psi_i^+\rangle}$$

and is known to be stationary with respect to small errors in $\psi_{f,i}^\pm$. The evaluation is performed¹ by an expansion on a truncated basis set. Without going into details, one can immediately see that since

$$\langle V \rangle \propto Z_p$$

$$\langle VG_T^+V \rangle \propto Z_p^2$$

the Schwinger amplitude tends to a finite limit as $Z_p \rightarrow \infty$. This leads to the so-called saturation effect. Recently, Wohrer et al.² have experimentally investigated the nuclear charge dependence of $1s^2 \rightarrow 1s2p$ and $1s^2 \rightarrow 1s3p$ excitation cross sections of Fe^{24+} projectiles at 400 MeV. They clearly find the saturation effect in agreement with the predicted behavior.

1.2 Electron Capture

Being a rearrangement collision electron capture is by far more difficult to treat theoretically than is excitation or ionization. The development in the last years has been guided to a large extent by the attempt to reproduce the asymptotic high-energy behavior and the so-called "Thomas peak" in the differential cross section. While this is a second-order effect, the first-order theory, since more than thirty years, has been identified with the Oppenheimer-Brinkman-Kramers approximation (OBK), irrespective of the fact that the OBK cross sections are off by a factor 3 or 4. Only recently the reason for this defect and other problems has been pointed out by Dewangan and Eichler³: The long-range nature of the Coulomb potential renders conventional scattering theory inapplicable and requires a special treatment. (In collisions without rearrangement this does not lead to serious difficulties) By rewriting the first-order (and similarly higher-order) transition amplitude into a first-order B1B ("boundary corrected 1st-Born") amplitude for a

short-range potential one obtains³

$$A_{B1B} = i \int_{-\infty}^{\infty} \langle \Phi_f e^{i v_T \ln(R+vt)} \left| \frac{Z_T}{r_T} - \frac{Z_T}{R} \right| \Phi_i e^{i v_p \ln(R-vt)} \rangle dt$$

where $\Phi_{i,f}$ involve translational factors and $v_T = Z_T(Z_p - 1)/v$, $v_p = Z_p(Z_T - 1)/v$. It turns out that this first-order amplitude which is consistent with the long range nature of the Coulomb interaction yields encouraging agreement with experimental data even without any further corrections. This shows the need to reformulate more sophisticated theories in such a way that Coulomb boundary conditions are satisfied from the outset.

1.3 Resonant Transfer and Excitation (RTE)

For the processes discussed so far, electron-electron correlations do not play an important role at high collision energies. If several electrons are involved one usually gets satisfactory estimates by assuming independent electrons and applying appropriate statistical factors. In contrast to this, RTE comes about just by electron-electron correlations. In RTE, which is closely related to dielectronic recombination, a quasi-free electron (bound e.g. in an H₂ gas target) is captured into a multicharged ion while at the same time the energy gain is used to simultaneously excite an electron, say from the K- to the L-shell. The process occurs in resonance, with a width that is determined by the Compton profile of the target electrons. Subsequently, the decay of the excited electronic states is detected by the emission of x-rays or Auger electrons. Reusch et al.⁴ have performed experiments with a Ti¹⁹⁺ ion beam of 260-420 MeV and a H₂ target. By measuring the K x-rays, they clearly identify two peaks arising from KLL and KLn(n>2) capture. The data are in agreement with theoretical predictions⁵.

In another measurement by Swenson et al.⁶ RTE has been detected by the measurement of Auger electrons in collisions of Li-like O⁵⁺ ions with He. A resonance in the cross section for production of Be-like (1s2s2p²)³D and (1s2s2p²)¹D states as a function of ion energy has been observed at ~13 MeV with a width of 7 MeV, in excellent agreement with the impulse approximation model⁷ for the RTE.

1.4 High-Resolution Projectile Spectroscopy

The experiment just mentioned has been performed using techniques

of zero degree Auger electron spectroscopy. This powerful technique first used by Itoh et al.⁸ takes advantage of the fact that at forward angles the Doppler broadening vanishes in first order so that after a deceleration of the electrons an energy resolution of 0.1% can be achieved. It is then possible to obtain very detailed spectra of highly charged projectile ions.

2. Relativistic Collisions

In very recent times it has become possible to accelerate heavy ions to relativistic velocities⁹. The coupling of accelerators known as the Berkeley BEVALAC has opened up new frontiers in physics by producing ions up to uranium with maximum energies up to 1 GeV/amu. Under these conditions, even high-Z ions can be stripped to one- or two-electron systems, their atomic structure and QED corrections for high Z can be investigated. Theoretically, aside from relativistic effects, atomic collisions become basically simple since $v \gg v_e$ in all cases.

2.1 Ionization

Since a long time the theory of target ionization has been the basis of estimates for electronic stopping powers. Ionization is well treated by the PWBA or SCA which leads to the transition amplitude

$$A_{fi} = \int dt \int d\vec{r} \Phi_f^+(\vec{r}, t) [-V_{\text{ret}} + \vec{\alpha} \cdot \vec{A}_{\text{ret}}] \Phi_i(\vec{r}, t)$$

where the first term describes the retarded longitudinal and the second term ($\vec{\alpha}$ being the Dirac matrix) the retarded transverse contribution. Adopting the dipole approximation, it can be shown that the asymptotic cross section behaves as $\sigma \propto \ln \gamma^2$ where $\gamma = (1 - v^2/c^2)^{-1/2}$. Detailed calculations by Anholt⁹ yield excellent agreement with experimental data for 4.88 GeV protons on various targets. Recent more rigorous calculations by Becker et al.¹⁰ give results that are generally 10% lower than the values of Ref. 9.

2.2 Electron Capture

If one considers that the nonrelativistic capture cross section decreases with energy as $1/E^6$ or $1/E^{5.5}$ one may ask whether at relativis-

tic velocities there is still a measurable cross section left. Yet there are two reasons why the relativistic cross section decreases less rapidly: (i) There is a finite maximum velocity c . (ii) Because of the Lorentz contraction of the space wave functions, the momentum wave function have extended tails in the direction of the relative velocity thus leading to a less rapidly decreasing momentum overlap between target and projectile. Relativistic OBK calculations by Moiseiwitsch and Stockman¹¹ indeed give an $1/E$ behavior but cross section values that are much too high compared to experimental data¹². The required reduction of the cross section has been achieved by Eichler in his relativistic eikonal theory of electron capture¹³. In this theory, the capture amplitude is derived in the form

$$A_{fi} = i \int dt \int d\vec{r} \psi_f^{i+}(\vec{r}_p, t') S \frac{Z_p}{r_{p'}} \psi_i(\vec{r}_T, t)$$

where the primed coordinates refer to the moving projectile system and S is a transformation matrix transforming a spinor from the target to the projectile system. For ψ_f the eikonal approximation is used. Calculations have been performed for transitions from initial K,L,M shells into final states up to $n=10$ giving good agreement with measured total cross sections¹⁴ for a large variety of projectile-target combinations and collision energies.

2.3 Electron-Positron Pair Creation

A process that is specific to relativistic collisions occurs when virtual photons from the moving Coulomb field of the projectile scatter from the static Coulomb field of the target and decay into electron-positron pairs. This process has already been studied theoretically by von Weizsäcker 1934 and Williams 1935. Recent accurate calculations by Becker et al.¹⁵ start from the amplitude

$$A_{fi} = i\gamma Z_p \int dt e^{i(E_p + E_e)t} \langle \psi_e | \frac{1}{r'} (1 - \frac{v}{c} \alpha_z) | \psi_p \rangle$$

and lead to an asymptotic cross section

$$\sigma \propto Z_p^2 Z_T^2 (\ln \gamma)^3$$

Since this cross section keeps increasing with energy it is of great practical importance for the design of relativistic ion accelerators and colliders for projected energies up to 100 GeV/amu.

1. B. Brendlé, R. Gayet, J.P. Rozet, and K. Wohrer, Phys. Rev. Lett. 54 (1985) 2007
2. K. Wohrer, A. Chetoui, J.P. Rozet, A. Jolly, F. Fernandez, C. Stephan, B. Brendlé, and R. Gayet, J. Phys. B 19 (1986) in press
3. D.P. Dewangan and J. Eichler, J. Phys. B 18 (1985) L65; *ibid.* (1986) in press.
4. S. Reusch, P.H. Mokler, R. Schuch, E. Justiano, J. Konrad, A. Müller, and Z. Stachura, Report EAS-7 (1986) 68
5. D.J. McLaughlin and Y. Hahn, Phys. Lett. A 88 (1982) 394
6. J.K. Swenson, Y. Yamazaki, P.D. Miller, H. Krause, P.F. Dittner, P. Pepmiller, S. Datz, and N. Stolterfoht, submitted for publication.
7. D. Brandt, Phys. Rev. A 27 (1983) 1314
8. A. Itoh, D. Schneider, T. Schneider, T.J.M. Zouros, G. Nolte, G. Schiwietz, W. Zeitz and N. Stolterfoht, Phys. Rev. A 31 (1985) 684
9. R. Anholt and H. Gould, LBL-20661 Report and private communication R. Anholt Phys. Rev. A 19 (1979) 1009
10. U. Becker, N. Grün, and W. Scheid, J. Phys. B 18 (1985) 4589
11. B.L. Moiseiwitsch and S.G. Stockman, J. Phys. B 13 (1980) 2975
12. R. Anholt and J. Eichler, Phys. Rev. A 31 (1985) 3505
13. J. Eichler, Phys. Rev. A 32 (1985) 112
14. W.E. Meyerhof, R. Anholt, J. Eichler, H. Gould, Ch. Munger, J. Alonso, P. Thieberger, and H.E. Wegner, Phys. Rev. A 32 (1985) 3291
15. U. Becker, N. Grün, and W. Scheid, J. Phys. B 19 (1986) 1347

OVERVIEW OF ELECTRON-ION COLLISIONS

Gordon H. Dunn

Joint Institute for Laboratory Astrophysics of the National
Bureau of Standards and the University of Colorado,
Boulder, CO 80309, USA

The consequential roles of electron-ion collisions in a variety of plasmas - astrophysical, fusion, laser, etc. - have been responsible in substantial measure for a keen interest in these kinds of collisions in the past two decades. Elastic scattering, excitation, ionization, and recombination are all conceptually simple processes that have been studied and considered in electron-atom collisions for more than 70 years. Yet, these same processes, when pertaining to electron-ion collisions, continue to challenge the creative efforts of many to gain a detailed understanding.

Technological breakthroughs leading to crossed beams experimental measurements on the various processes have led to impressive progress, and continued advances in technology have led to continued progress in electron-ion collision studies. For example, the introduction of ECR and EBIS ion sources have made it feasible to study a far broader range and variety of target ions, and only now is it possible to make colliding beams measurements with ions having $Q > 5$. Similarly, it is only in the past three years that the important process of dielectronic recombination has lent itself to cross section measurements.

For each of the collision processes there remain different needs and exist different problems. However, some common issues emerge from the work that has been done, pointing the way to some general features of what should be done in the next few years. Indirect ionization mechanisms like excitation-autoionization, resonant-capture-double-autoionization, and resonant-capture-auto-double-ionization have been shown to become very important for highly charge ions - especially for moderate and high Z ions. In some cases, these processes dominate over the direct ionization mechanism by an order of magnitude or more. Similarly, dielectronic resonances may enhance excitation cross sections by large factors. Dielectronic recombination itself has been shown to be a "tuneable" process which is changed and controlled by angular momentum mixing parameters in the environment.

Thus, there should be a systematic study of these processes - all of which involve autoionization phenomena - as a function of atomic number Z and ion charge Q . Since radiative lifetimes become comparable to autoionization lifetimes for $Q \approx 20$, the range $15 < Q < 25$ would seem to be a particularly attractive and important range to study. The lower limit of this range has just become technologically feasible, and the remainder of the range will require some continued creative effort. Perhaps the use of ion-storage rings coming on line in the future will provide the technological answer to this need.

technological answer to this need.

Another important challenge lies in the study of the basic electron-ion collision processes for heavy ions, where electron correlations and relativistic effects may be amplified.

For excitation one finds that theory has been tested by experiment for only a very narrow range of transitions and ionization stages. Most measurements have been made using crossed beams of electrons and ions and observing fluorescence in the third orthogonal direction with a detection efficiency $<10^{-4}$. The energy-loss/angular distribution measurements which have been made are not absolute (strictly relative), are over a narrow range of angle, and have suffered a similarly low detection efficiency. This low detectability coupled with low target densities characteristic of colliding beams put severe limitations on what systems can be studied. A new technique is being developed which will also lead to energy loss measurements, but will enjoy a detection efficiency near 1.0. This will allow measurements on a variety of transitions and for the more highly charged ions now obtainable with modern ion sources. There is an important need - as already pointed out - to get experimental tests of the effects on excitation of dielectronic resonances, since theoretically these resonances can influence the average cross sections by substantial factors, and local cross sections are affected even more.

The three body nature of ionization continues to leave "simple" knock-on ionization as a challenge to theorists. However, by introducing an arbitrary (maximum) phase, quantum calculations (notably Coulomb Distorted Wave) now usually give results that compare well with experiment. A variety of semi-empirical formulae (notably the Lotz formula) have met with some success in predicting direct knock-on ionization. Further progress on the understanding of this process probably awaits a fundamental breakthrough in the description of many-body interactions, and not on more experimental results. However, it has been demonstrated in the last few years that direct ionization is very often not the dominant ionization mechanism. Rather, indirect mechanisms such as excitation-autoionization (EA), resonant-capture double autoionization (REDA), and resonant-capture auto-double ionization (READI) often dominate (sometimes by more than an order of magnitude) the ionization of ions. Similar statements apply to both single and multiple ionization. Thus, as with excitation, autoionizing resonances play a major role in the ionization process. It is essential to more clearly document and identify that role and, again, to do it through the range of ion charge where autoionization and radiative rates are competitive. In comparisons of experimental and theoretical data on work to date, there is little difficulty in identifying a very strong role of EA, but the roles of REDA and READI are much more hypothetical - these processes need clear identification and measurement.

The status of work on recombination is somewhat similar to that on excitation - the theoretical situation is highly developed, whereas the experimental data are sparse and limited. Apparently, there have been no

published direct measurements of radiative recombination cross sections, though progress in that direction may be imminent with the implementation of ion storage rings for atomic physics studies. Cross section measurements for dielectronic recombination (DR) have just been made over the past three years. Though much of the disparity between experimental and theoretical data has now been rationalized by recognizing the "tuneable" nature of DR, there remain discrepancies which need to be resolved. It is now totally obvious that all future experiments on DR must recognize its "tuneable" nature and make provision for careful control and measurements of those variables that lead to tuning, or comparisons with theory will always be tentative and conjectural. As with excitation and ionization, the measurements on DR should be made through the charge state range where autoionization and radiative rates are comparable. This is a goal that will rely upon future technology - probably for all three processes.

Bibliographies¹ published by the Institute for Plasma Physics serve as a guide to both the experimental and theoretical literature. Reviews of the theoretical methods and data for excitation have been done by Seaton² and by Henry³. A relatively recent review of the experimental excitation work has been written by Crandall⁴. An evaluated compilation of theoretical data for electron-impact excitation of atomic ions has recently been published by Gallagher and Pradhan⁵, and this work also contains discussions of the approximation methods for obtaining the data. As with excitation, electron impact ionization of ions has been reviewed a number of times, with more recent reviews being those of Dunn⁶ and of Younger⁷. The compilation of Tawara et. al.⁸ is a complete and useful collection of the data (both experimental and theoretical) for electron impact ionization. Experimental data and methods for dielectronic recombination have recently been reviewed by Dunn⁹. Reviews by Seaton and Storey¹⁰ and by Hahn¹¹ treat the theory, though recent advances in the effects of fields are not covered in these reviews, and the original literature should be consulted¹².

Great progress has been made in the study and understanding of electron-ion collisions, and much of that progress has occurred during the past 5 years since modern ion sources and other technological advances have become available. The near term should bring continued advance, and as one looks to the long term when ion storage rings become available for use in these studies, many of the outstanding issues in this field should be fully addressable.

REFERENCES

1. K. Takayanagi and T. Iwai, "Bibliography on Electron Collisions with Atomic Positive Ions: 1940 through 1977", Institute of Plasma Physics, Nagoya University, Report IPPJ-AM-7, June 1978. Also, Y. Itikawa, "Bibliography on Electron Collisions with Atomic Positive Ions: 1978 Through 1982", Report IPPJ-AM-24, Sept. 1982.
2. M. J. Seaton, Adv. At. Mol. Phys. 11, 83 (1975).

3. R. J. W. Henry, Phys. Rep. 68, 1 (1981).
4. D. H. Crandall, in "Physics of Ion-ion and Electron-ion Collisions", ed. by F. Brouillard and J. W. McGowan (Plenum, New York, 1983), p. 201.
5. J. W. Gallagher and A. K. Pradhan, "An Evaluated Compilation of Data for Electron-Impact Excitation of Atomic Ions", JILA Information Center Report No. 30, Oct. 1, 1985.
6. G. H. Dunn, in "Electron Impact Ionization", ed. by T. D. Mark and G. H. Dunn (Springer-Verlag, New York, 1985), p. 277.
7. S. M. Younger, in "Electron Impact Ionization", ed. by T. D. Mark and G. H. Dunn (Springer-Verlag, New York, 1985), p.1.
8. H. Tawara, T. Kato, and M. Ohnishi, "Ionization Cross Sections of Atoms and Ions by Electron Impact", Institute of Plasma Physics, Nagoya University, Report # IPPJ-AM-37, Feb. 1985.
9. G. H. Dunn, in "Physics of Electron-ion and Ion-ion Collisions", ed. by F. Brouillard and P. Defrance, (Plenum, New York, 1986).
10. M. J. Seaton and P. J. Storey, in "Atomic Processes and Applications", ed. by P. G. Burke and B. L. Moiseiwitsch, (North Holland, Amsterdam, 1977), p. 134.
11. Y. Hahn, in "Advances in Atomic and Molecular Physics Vol. 21", ed. by D. R. Bates and B. Bederson, (Academic Press, New York, 1986).
12. For example, see: K. LaGattuta, I. Nasser, and Y. Hahn, Phys. Rev. A33, 2782 (1986); D. C. Griffin, M. S. Pindzola, and C. Bottcher, Phys. Rev. A33, 3124 (1986); C. Bottcher, D. C. Griffin, and M. S. Pindzola, Phys. Rev. A34, #2 (1986); D. Harmin, Phys. Rev. Lett. (1986); K. Sakimoto, J. Phys. B. (1986).

Excitation and Ionization of Ions by
Electron Impact: Recent Activities at
IPP and Sophia University

Atsushi Matsumoto
Hiroshima Institute of Technology
Saeki-ku, Hiroshima, 731-51, Japan

In the course of experimental investigation on atomic process at Institute of Plasma Physics (IPP), Nagoya University, a research program was started in 1981, for studies of ionization of multiply charged ions by electron impact, as a collaboration program at IPP, which was raised to a guest program in 1984, and have been continuing up to now. The purpose of the project is not only to obtain total ionization cross section data useful for the nuclear fusion research but also to deepen our understanding of the electron-ion collision process by means of electron spectroscopy technique. The group consists of 10 physicists from various institutions:

A. Danjo	(Niigata Univ.)
T. Hirayama	(Sophia Univ.)
A. Matsumoto	(Hiroshima Institute of Technology)
S. Ohtani	(IPP)
H. Suzuki	(Sophia Univ., Guest Prof. of IPP)
Y. Takayanagi	(Sophia Univ.)
H. Tawara	(IPP)
K. Wakiya	(Sophia Univ.)
I. Yamada	(IPP)
M. Yoshino	(Shibaura Institute of Technology)

The research program done by this group is called the ACE-IT project. ACE-IT means Atomic Collision Experiments-Ion Target.

In this presentation, we describe two kinds of experimental apparatus, which are in operation for measurements of ionization cross sections of ions and electron energy loss spectra using the crossed beams technique, and some examples of the results.

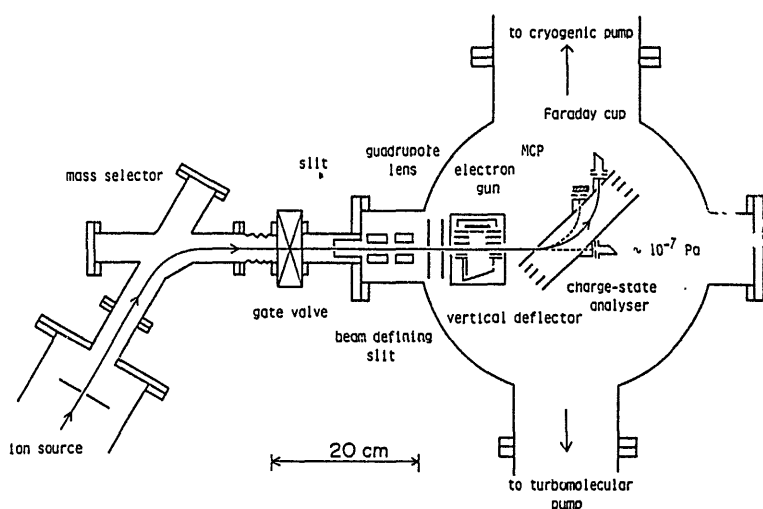


Fig. 1 Schematic of crossed beams apparatus.

Figure 1 shows a crossed beams apparatus constructed at IPP for measurements of cross sections for electron impact ionization of ions. Ions extracted from an ECR ion source are accelerated, mass analysed and transported to an interaction chamber, which is evacuated with a turbomolecular pump and a cryogenic pump providing a pressure less than 1×10^{-7} Pa. A typical ion current arriving at interaction region is 150 nA for Ar^{2+} ions. Electrons from a conventional electron gun are accelerated to the desired impact energies and cross the ion beams at right angles. The ion and electron beams are both chopped in order to separate signals from backgrounds. After crossing the electron beam, the primary ions and the ionized ions are separated spatially with an electrostatic charge state analyser. The ionized ions are detected with a microchannel plate (MCP) by single counting technique. The counting efficiencies of the MCP are experimentally determined for triply charged rare gas ions.

The measured cross sections for electron impact ionization of doubly charged rare gas ions, Ne^{2+} through $\text{Xe}^{2+,1)}$ are shown in Figs 2. Systematic trend is seen from data shown in Fig. 2; as the total number of electrons increases, the measured cross sections become larger than those of Lotz calculation²⁾ at around peak and rise more steeply than expected for direct ionization at near threshold, except for Ne^{2+} . As for Ar^{2+} ion, there is a small bump at around 160 eV. Similar bump is also observed at around 140 eV in the cross section curve of Kr^{2+} . Figure 3(a) shows the measured cross sections for electron impact ionization of S^+ ion³⁾ together with those of Lotz calculation. From threshold to 60 eV, the cross sections rise more rapidly than expected for direct ionization, and above

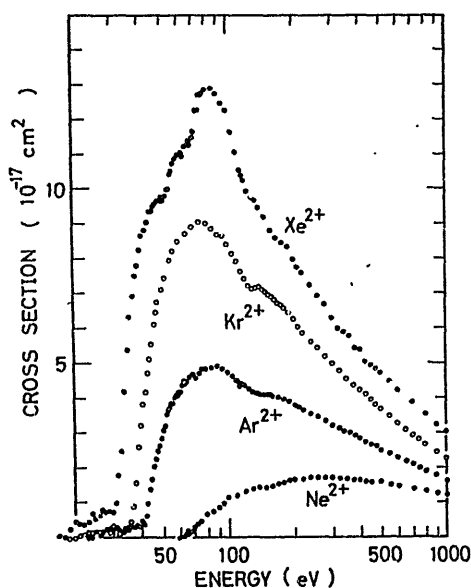


Fig. 2 Single ionization cross sections for Ne^{2+} through Xe^{2+} .

100 eV, they are in good agreement with Lotz formula. Figure 3(b) shows the measured cross sections for S^{2+} ion³⁾ together with Lotz calculation. Similarly to the case for S^+ , the measured cross sections show a rapid rise from threshold to 70 eV, and furthermore, they show a clear bump at around 100 eV. These features are very similar to those for Ar^{2+} and for Kr^{2+} .

On the other hand, measurements of cross sections for electron impact ionization of alkali ions and alkaline earth ions have been made using the other crossed beams apparatus constructed at Sophia Univ., which is similar with the preceding one except for the ion source. The measured cross sections for single and double ionization of Na^+ and K^+ ions⁴⁾ are shown in

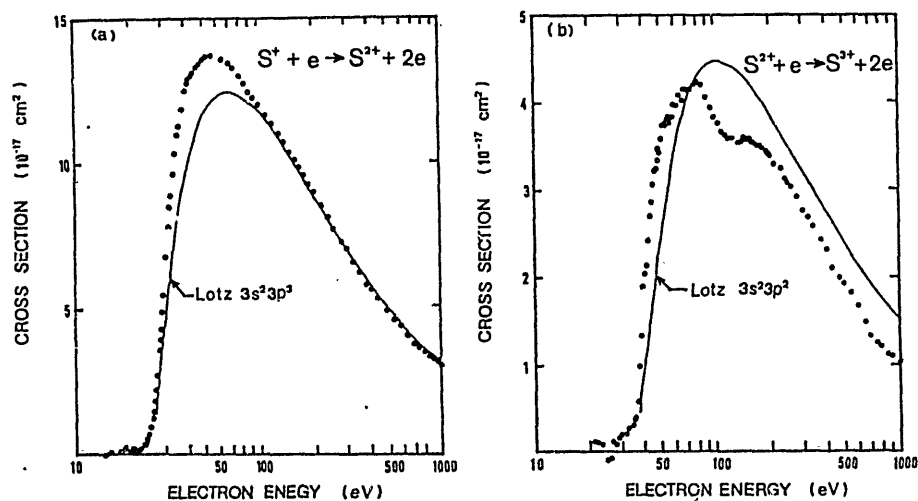


Fig. 3 Ionization cross sections for (a) $\text{S}^+ \rightarrow \text{S}^{2+}$ and (b) $\text{S}^{2+} \rightarrow \text{S}^{3+}$. The solid line is Lotz calculation for direct ionization from the outermost shell.

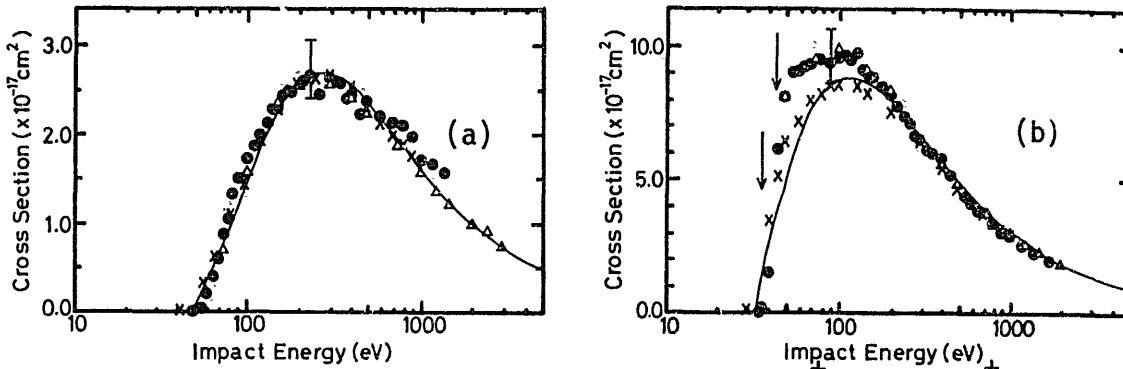


Fig. 4 Single ionization cross sections for (a) Na^+ and (b) K^+ ions. Closed circles — present results, open triangles — Peart and Dolder⁸⁾, crosses — Hooper et al.,⁹⁾ solid line — Lotz calculation.

Figs. 4 and 5, respectively. The results for single ionization of Na^+ and K^+ are in good agreement with the previous crossed-beam data within experimental uncertainties. Double ionization cross sections for Na^+ and K^+ are shown in Fig. 5 together with those for the other alkali metal ions Li^+ 5), Rb^+ 6) and Cs^+ 7). From this figure, one can find a similar trend to the rare gas ions in which the cross section increases with atomic number Z of the ion. In the results of K^+ , there is an evidence of structure at about 400 eV of impact energy. This structure is thought to be attributed to the contribution from the L-shell ionization-antioionization (Auger effect).

One of the most general and useful method for measurements of the differential cross sections for inelastic collision of electrons with atoms and molecules is the electron-impact spectroscopy, which is based on measurements of energy loss spectra of scattered electron resulting from

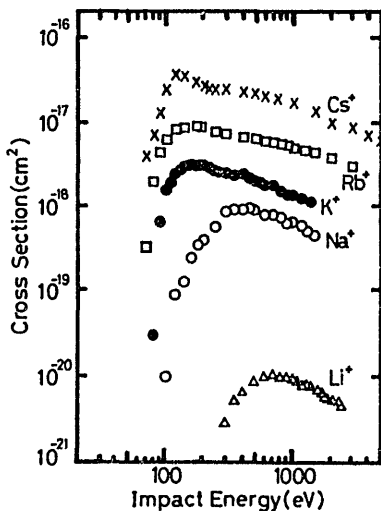


Fig. 5 Double ionization cross section for Na^+ and K^+ together with the results for Li^+ , Rb^+ and Cs^+ .

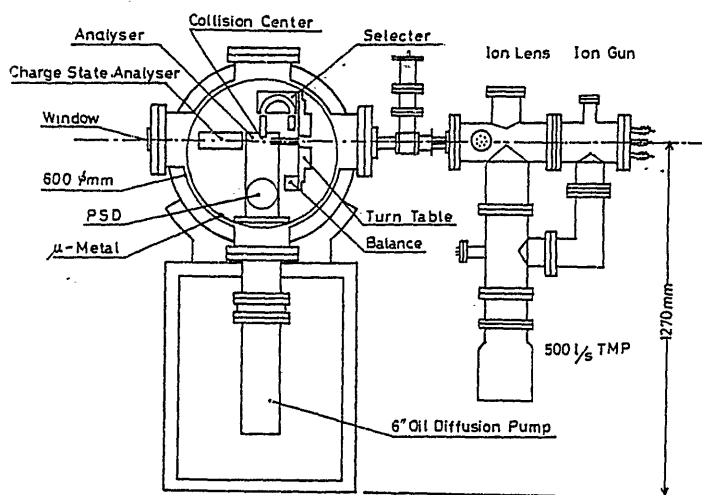


Fig. 6 Schematic drawing of ACE-IT.

the transfer of electron kinetic energies to excitation energies of target atoms and molecules. Besides this, the ejected-electron spectroscopy is also a useful method to study the autoionization or Auger effect in atoms and molecules. A somewhat ambitious experiment which attempts to apply the electron spectroscopy technique to the electron-ion experiments is in progress at IPP. Figure 6 shows a schematic diagram of the experimental apparatus, which consists of an electron energy selector and an electron energy analyser of quasi-hemispherical type, in addition to a conventional crossed beams arrangement.

References

- 1) A. Danjo, A. Matsumoto, S. Ohtani, H. Suzuki, H. Tawara, K. Wakiya and M. Yoshino: *J. Phys. Soc. Jpn.* 53 (1984) 4091.
- 2) W. Lotz: *Z. Phys.* 216 (1968) 241.
- 3) I. Yamada, A. Danjo, A. Matsumoto, S. Ohtani, H. Tawara, H. Suzuki, K. Wakiya and M. Yoshino: Abstracts of 10th ICAP (1986) Tokyo.
- 4) T. Hirayama, K. Oda, Y. Morikawa, T. Ono, Y. Ikezaki, T. Takayanagi, K. Wakiya and H. Suzuki: *J. Phys. Soc. Jpn.* 55 (1986) 1411.
- 5) B. Peart and K.T. Dolder: *J. Phys.* B2 (1969) 1169.
- 6) D.W. Hughes and R.K. Feeney: *Phys. Rev.* A23 (1981) 2241.
- 7) K.R. Heartling, R.K. Feeney, D.W. Hughes and W.E. Sayle II: *J. Appl. Phys.* 53 (1982) 5427.
- 8) B. Peart and K.T. Dolder: *J. Phys.* B1 (1968) 240
- 9) J.W. Hooper, W.C. Lineberger and F.M. Bacon: *Phys. Rev.* 141 (1966) 165.

Electron-Impact Excitation and Indirect Ionization of Ions

Ronald J. W. Henry
Department of Physics and Astronomy
Louisiana State University, Baton Rouge, LA, USA

Due to experimental difficulties encountered especially for multiply-ionized species, determination of collision strengths must rely primarily on calculations. Reviews of calculations include Seaton¹⁾, Henry²⁾ and Gallagher and Pradhan³⁾.

Figure 1 summarizes the various ions on which calculations have been made. In addition to the light ions, the impetus for the field of electron-ion scattering has come from astrophysics as evidenced by the work on cosmically-abundant ions Ne, Fe, Si, Mg, S, and Ar. Also, tokamak plasmas have introduced data needs for Ti, Fe, and Mo. Experiments which yield direct values for integral cross sections or collision strengths are given by the open squares. Open circles represent ionization experiments from which cross sections for excitation have been deduced.

How do we judge the reliability of the calculations? We will consider the effect of various physical approximations and compare results with different types of measurements.

The collision strength $\Omega(i,f)$ is related to the excitation cross section $\sigma(i \rightarrow f)$ (measured in units of πa_0^2) by:

$$\Omega(i,f) = \omega_i k_i^2 \sigma(i \rightarrow f) \quad (1)$$

where k_i^2 is the energy (in Ry.) of the incident electron relative to the lower state i , and ω_i is the statistical weight of the lower atomic state. We introduce the parameter x , the energy in threshold units defined by

$$x_i = k_i^2 / \Delta E_{if} \quad (2)$$

where ΔE_{if} is the excitation energy (in Ry.) for the transition from level with energy E_i to level with energy E_f .

The essential physics which should be considered for all calculations of electrons scattering from ions includes target state correlations, unitarization, exchange, channel coupling, resonances and relativistic mixing of target states. The best quantum mechanical description for the solutions of the collision problem is a converged close-coupling method. A discussion of the equations may be found in the review articles^{2,3)} and in Burke and Seaton⁴⁾. Other approximate methods are also discussed in the various reviews.

The main type of resonance which dominates electron-ion scattering is the Feshbach or closed-channel resonance. An infinite series of resonances converges on to each of the states of the target ion due to the attractive Coulomb potential. When the initial and final states are more strongly coupled to the closed channel than to each other, then the resonance effects are large.

For many systems, configuration mixing in the description of the target ion must be included. It follows from the variational principle used in the formulation of the scattering problem, that the error in the collision strengths is directly related to the first order error in the target wave functions. A figure of merit for collision strengths is probably provided by the accuracy of oscillator strengths obtained with the same target wave functions. This is correct at least at very high energies where the collision strength is directly proportional to the oscillator strength.

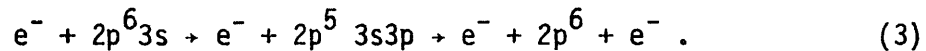
As the nuclear charge of the target ion increases, relativistic effects become important, especially for $Z > 20$. These have a striking effect on a spin-forbidden collision strength such as $\Omega(2s^2 \ ^1S_0, 2s2p \ ^3P_1^0)$ for Fe XXIII. The spin-orbit term mixes the $2s2p \ ^3P_1^0$ and $2s2p \ ^1P_1^0$ configurations and so the dipole allowed transition $2s^2 \ ^1S - 2s2p \ ^1P_1^0$, which has a collision strength ~ 0.5 , dominates.

There are four major types of experiments which involve measurement of direct integral cross sections, direct angular distributions, indirect integral cross sections from ionization, and rate coefficients deduced from plasma experiments.

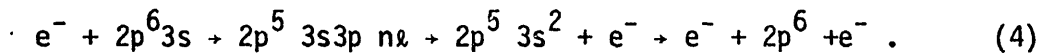
Filled circles in Figure 2 represent emission results for $^2S_{1/2} \rightarrow ^2P_{3/2}^0$ transition in Cd II by Hane et al.⁵⁾ The open triangle is deduced by Chutjian⁶⁾ from experimental differential cross sections obtained in an energy loss experiment. For comparison, a simple Gaunt approximation calculation is given by the dashed line. It gives agreement within 30% at threshold but underestimates the cross section by a factor of 2.5 at higher energies.

Figure 3 compares a calculated differential cross section for $4^2S \rightarrow 4^2P^0$ excitation in Zn II with $5^2S \rightarrow 5^2P^0$ in Cd II in same threshold units. For these homologous ions it was not anticipated that there would be a striking difference in both magnitude and shape for the two cross sections. Further, measurements of Hane et al.⁵⁾ show that the cross section for the $5s^2 \ ^2D$ state of Cd II is of the same order of magnitude as the $5p \ ^2P^0$ state, whereas for comparable transitions in Zn II, Msezane and Henry⁷⁾ found that the resonance transition was an order of magnitude larger than the inner shell $4s \ ^2S \rightarrow 4s^2 \ ^2D$.

A significant contribution to electron-impact ionization may come from excitation of an inner-shell electron, which subsequently loses its energy by ejection of a more loosely bound electron from an outer shell. An example of this excitation-auto-ionization process is



Another significant contribution to electron-impact ionization comes from the temporary capture of the incident electron with simultaneous excitation of an inner-shell electron. This resonance decays with emission of two electrons. An example of this resonance-excitation-double autoionization (REDA) process is



The ORNL group⁸⁾ has reported on electron impact ionization cross sections for 37 target ions. Other groups are involved in this active area, such as the measurements on Ne III, Ar III, Kr III, and Xe III by Danjo et al.⁹⁾

Figure 4 gives electron impact ionization cross section for the ground $3s^2 1S$ state of S^{4+} . Solid circles represent experimental data of Howald et al.¹⁰⁾ Direct ionization distorted wave cross sections obtained by using Younger's parameters¹¹⁾ are given by the dashed line. The upper and lower solid lines represent distorted wave¹²⁾ and close coupling¹³⁾ calculations, respectively, for excitation autoionization plus distorted wave cross section for direct ionization.

Research was supported in part by the U.S. Department of Energy, Division of Chemical Sciences.

REFERENCES

- 1) M. J. Seaton, *Adv. Atom. Molec. Phys.* 11, (1975) 83.
- 2) R. J. W. Henry, *Phys. Reports* 68, (1981) 1.
- 3) J. Gallagher and A. N. Pradhan, JILA Report (1985).
- 4) P. G. Burke and M. J. Seaton, *Methods in Computational Phys.* 10, (1971) 1.
- 5) K. Hane, T. Goto and S. Hattori, *Phys. Rev. A* 27, (1983) 124.
- 6) A. Chutjian, *Phys. Rev. A* 29, (1984) 64.
- 7) A. Z. Msezane and R. J. W. Henry, *Phys. Rev. A* 25, (1982) 692.
- 8) D. C. Gregory *et al.* ORNL Report TM-9501 (1985).
- 9) A. Danjo *et al.* *J. Phys. Soc. Jpn.* 53, (1984) 4091.
- 10) A. M. Howald *et al.*, *Phys. Rev. A* 33, 3780 (1986).
- 11) S. M. Younger, *Atomic Data for Fusion*, edited by D. H. Crandall, C. F. Barnett, and W. L. Wiese, vol. 7, p. 190.
- 12) M. S. Pindzola, D. C. Griffin, and C. Bottcher, *Phys. Rev. A* 33, 3788 (1986).
- 13) S. S. Tayal and R. J. W. Henry, *Phys. Rev. A* 33, 3825 (1986).

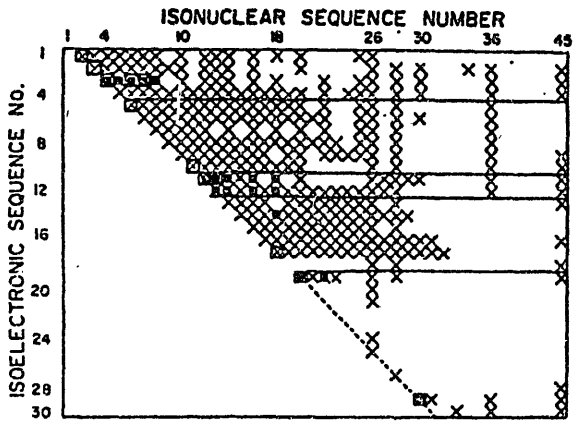


Fig. 1 Electron ion excitation calculations and measurements.

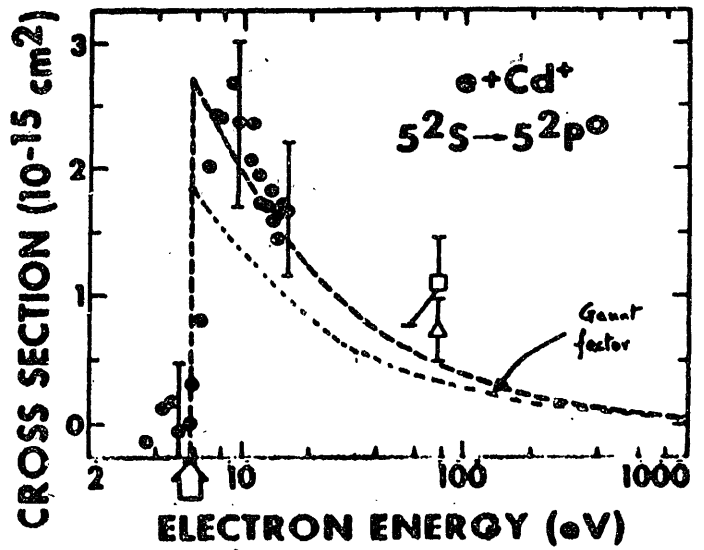


Fig. 2

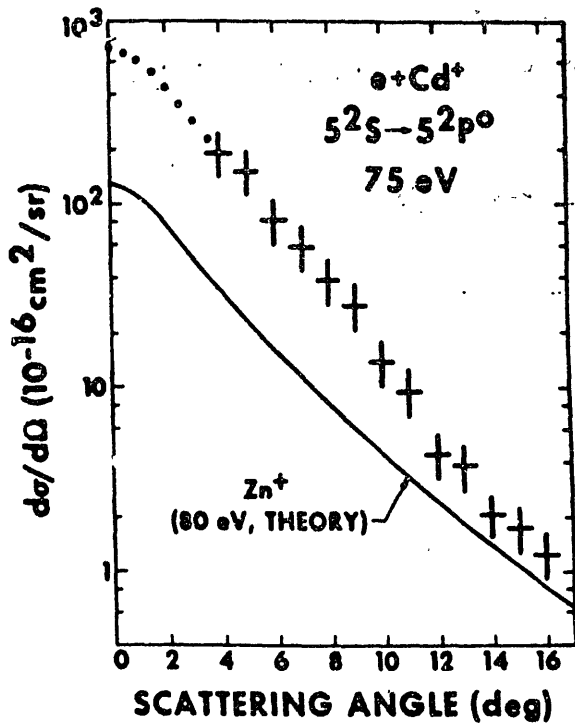


Fig. 3

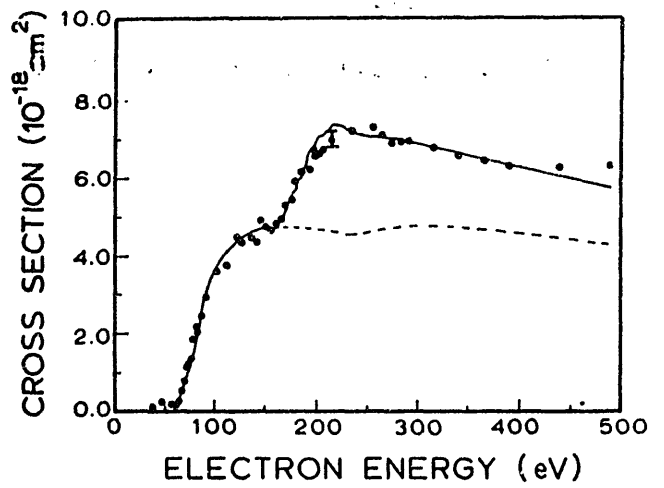


Fig. 4

RECOMBINATION PROCESSES IN ELECTRON-ION COLLISIONS

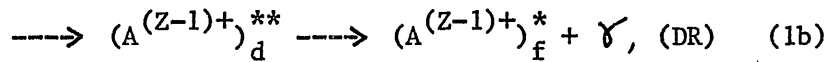
Yukap Hahn

Physics Department, University of Connecticut

Storrs, connecticut 06268 USA

Magnetically confined fusion plasmas consist mainly of electrons and protons, with the electron kinetic energies in the 1-5 keV range and density of about 10^{13} - 10^{14} cm^{-3} . Also present are many different species of impurity ions, with the nuclear core charges $Z_c=2$ -60 and typical density of 10^8 - 10^{10} cm^{-3} . At such high temperatures ($1 \text{ keV} \approx 10^7 \text{ K}$), ions with $Z_c \lesssim 30$ are nearly completely stripped of their electrons. On the other hand, the temperature near the container walls is lower and the ions there are presumably much less ionized. Therefore, to analyze the behavior of such plasmas, comprehensive and reliable atomic data on the important e-e, e-I and I-I collision processes are needed for many Z_c and Z =degree of ionization. We focus our discussion here on the e-I capture process, with emphasis on high Z region. As is well-known, the e-I capture process is, together with the collisional excitation, one of the main radiation cooling mechanisms of high temperature plasmas. Much of the background material for our discussion was covered in several recent reviews¹⁻³.

The electron-ion recombination proceeds in two distinct modes, (i) direct radiative recombination (RR) and (ii) indirect dielectronic recombination (DR), described schematically



where the singly-excited states are denoted with one (*) and doubly-excited states (d) by (**). The amplitude is given by²

$$T_{fi} = (\Psi_f | D | \Psi_i) + (\Psi_f | DG^\Gamma V | \Psi_i) = T_{fi}^{\text{RR}} + T_{fi}^{\text{DR}} \quad (2)$$

where D and V are the electron-radiation and electron-electron couplings, respectively, and G^Γ is an intermediate state propagator with the correct radiative and Auger width operators². The cross section is given by

$$|T_{fi}|^2 \approx |T_{fi}^{\text{RR}}|^2 + |T_{fi}^{\text{DR}}|^2 \propto \sigma_{fi}^{\text{RR}} + \sigma_{fi}^{\text{DR}}, \quad (3)$$

where we neglected the interference term between the RR and DR amplitudes; this is reasonable when T_{fi}^{DR} consists of a series of sharp resonances.

For the direct capture, RR, we have the simple Kramer's formula, which was found⁴ to be very effective when an effective charge⁵ $Z_{\text{eff}}=(Z+Z_c)/2$ was used. For high Z ions where the electronic orbitals are nearly Coulombic, the cross section scales in $n'=Z/p_c$, where $p_c = 2me_c$ for the continuum electron energy e_c . Therefore, with the above Z_{eff} , σ^{RR} may be⁵ conveniently tabulated for all ions in terms of n' .

The DR cross section is given in the isolated resonance approximation (IRA)² by

$$\sigma_i^{DR} = \sum_f \sigma_{fi}^{DR} \approx \sum_d \frac{4\pi}{p_c^2} \frac{g_d}{2g_i} A_a(d \rightarrow i) \omega(d) \tilde{\delta}(E_d - E_i) (\pi a_0^2), \quad (4)$$

where the g 's are the statistical factors and $\tilde{\delta}$ is a Lorentzian line shape given by $\tilde{\delta} = (\Gamma/2) [(E_d - E_i)^2 + \Gamma^2/4]^{-1}$. The fluorescence yield ω is defined in terms of the radiative and Auger transition probabilities A_r and A_a , respectively, as

$$\omega(d) = \Gamma_r(d) / [\Gamma_r(d) + \Gamma_a(d)] \approx \Gamma_r / \Gamma \quad (5)$$

with

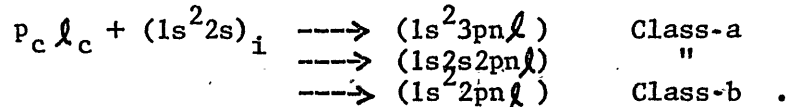
$$\Gamma_r(d) = \sum_f A_r(d \rightarrow f) \quad \text{and} \quad \Gamma_a(d) = \sum_j A_a(d \rightarrow j).$$

The DR rate coefficient α^{DR} is defined as a velocity-weighted Maxwellian average of σ^{DR} and is given by

$$\alpha_i^{DR} = \sum_d \left(\frac{4\pi Ry}{k_B T} \right)^{3/2} \frac{g_d}{2g_i} A_a(d \rightarrow i) \omega(d) \exp(-e_c/k_B T) \quad (6)$$

In (5) and (6), the cross terms between different resonance states d were neglected, in accordance with our IRA. Evidently, the general structure of σ^{DR} and α^{DR} is the same, and A_a and A_r are the basic building blocks for these quantities, as it is also the case with other resonant processes in e-I collisions¹.

The DR process may be conveniently divided into two excitation classes, (a) $\Delta n_t \neq 0$ and (b) $\Delta n_t = 0$, each with distinctive behavior in Z, n and other parameters. For example, in the $e + \text{Fe}^{23+}$ system,

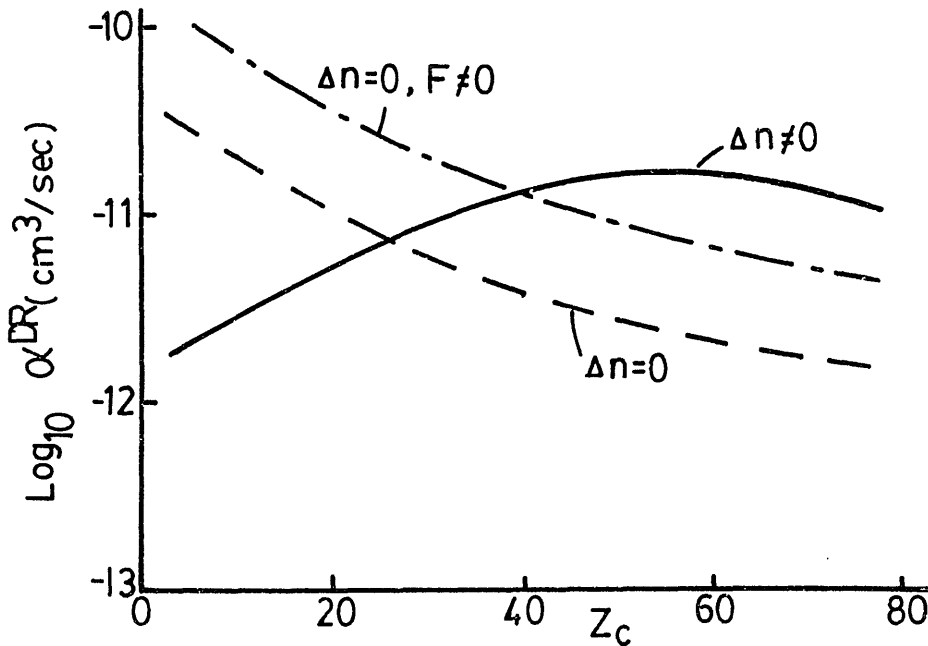


In the class-a excitation, the excitation energies for $2s \rightarrow 3p$ and $1s \rightarrow 2p$ are large and approximately scale as Z^2 , while a Z^1 behavior is expected for class-b mainly due to spin-orbit interaction. In Table I, we summarize the Z-scaling properties for high Z ions. The Z dependence of α^{DR} and σ^{DR} is inferred from that of A_a and A_r using the relations (4) and (6).

Table I. The Z-scaling of A_a , A_r and the related quantities is summarized in terms of the exponent S of an assumed behavior Z^S .

	Class-a; $\Delta n_t \neq 0$		Class-b; $\Delta n_t = 0$		
	$\omega \ll 1$	$\omega \approx 1$	$\omega \ll 1$	$\omega \approx 1$	
Energy	2	2	1	1	
A_a	0	0	1/2	1/2	
A_r	4	4	1	1	
ω	4	0	1/2	0	
$\xi \equiv 1 - \omega$	0	-4	0	-1/2	
α	1	-3	-1/2	-1	*
σ	0	-4	-1	-3/2	

Figure 1 illustrates the behavior of α^{DR} as a function of Z_c for a typical isoelectronic sequence (i.e. same $N = Z_c - Z =$ number of electrons).



Detailed theoretical data on the both class-a and b processes and comparison with the latest available data will be presented.¹⁷ Some of the outstanding theoretical problems of current interest in connection with the DR process will be summarized.

The work reported here was supported in part by a DOE grant.

References

1. Y. Hahn, Comments on Atom. & Molec. Phys. 13, 103 (1983) and (1986)
2. Y. Hahn, Advances in Atom. & Molec. Phys. 21, 123 (1985)
3. Y. Hahn, NATO Workshop, Belgium Oct. 1985, F. Brouillard, ed.
4. C. M. Lee and R. H. Pratt, Phys. Rev. A12, 1825 (1975) and A14, 990 (1976); Y. S. Kim and R. H. Pratt, *ibid* A27, 2913 (1983)
5. Y. Hahn and D. W. Rule, J. Phys. B10, 2689 (1977)
6. D. S. Belic et al, Phys. Rev. Lett. 50, 339 (1983); A. Muller et al, *ibid* 56, 127 (1986)
7. P. F. Dittner et al, Phys. Rev. Lett. 51, 31 (1983)
8. K. LaGattuta and Y. Hahn, Phys. Rev. Lett. 51, 558 (1983); K. LaGattuta, I. Nasser, and Y. Hahn, Phys. Rev. A33, 2782 (1986)
9. D. G. Griffin, M. S. Pindzola and C. Bottcher, Phys. Rev. A33, 3124 (1986) and ORNL preprint, 1986
10. B. A. Mitchell et al, Phys. Rev. Lett. 50, 335 (1983)
11. J. F. Williams, Phys. Rev. A29, 2936 (1984)
12. J. Kohl, unpublished
13. J. A. Tanis et al, Phys. Rev. Lett. 49, 1325 (1982) and 53, 2551 (1984)
14. J. A. Tanis et al, to be published, (Phys. Rev. A (RC))
15. M. Clark et al, Phys. Rev. Lett. 54, 544 (1985) and Phys. Rev. A33, 17 (1986)
16. D. Brandt, Phys. Rev. A27, 1314 (1984)
17. D. J. McLaughlin, I. Nasser and Y. Hahn, Phys. Rev. A31, 1926 (1985); G. Omar and Y. Hahn, Phys. Rev. A, to be published.

ELECTRON IMPACT IONIZATION OF HEAVY IONS - SOME SURPRISES

Stephen M. Younger
A-Division
Lawrence Livermore National Laboratory
Livermore, Ca. 94550 USA

The scattering dynamics of heavy atoms and ions can be strongly influenced by the highly localized charge density associated with many electron subshells. This localization can lead to the formation of potential barriers and multi-well scattering potentials which can, in turn, lead to shape resonances in the cross sections. Also, term-dependence in the continuum channels can cause very large perturbations in cross sections for non-resonant systems. These effects are in addition to the compound-resonance (excitation-autoionization) processes which also occur in lighter systems.

This paper reports the results of calculations of electron impact ionization cross sections for a variety of heavy ions using a distorted wave Born-exchange approximation.¹ The target is described by a Hartree-Fock wavefunction. The scattering matrix element is represented by a triple partial wave expansion over incident, scattered, and ejected (originally bound) continuum states. These partial waves are computed in the potentials associated with the initial target (incident and scattered waves) and the residual ion (ejected waves). A Gauss integration was performed over the distribution of energy between the two final state continuum electrons. For ionization of closed d- and f-subshells, the ejected f-waves were computed in frozen-core term-dependent Hartree-Fock potentials, which include the strong repulsive contribution in singlet terms which arises from the interaction of an excited orbital with an almost closed shell.² Ground state correlation was included in some calculations of ionization of d^{10} subshells.³

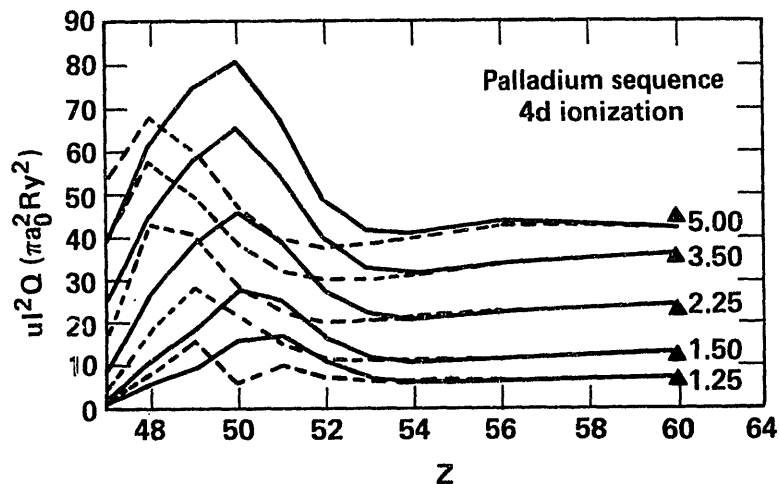


Fig. 1: Scaled distorted wave Born-exchange cross sections, uI^2Q , for electron impact ionization of the 4d subshell in the palladium isoelectronic sequence plotted as a function of Z . Solid line: Term-dependent partial waves. Dotted line: term independent partial waves. Triangles: Predictions of the simple Lotz formula:⁵

As an example of the non-classical behavior of electron impact ionization for heavy ions, we show in Figure 1 the cross section for ionization of the 4d subshell in the palladium isoelectronic sequence ($4d^{10} \ ^1S$ ground state).⁴ This is an important isoelectronic sequence in that it is the prototype for 4d excitations in all heavier atoms and ions and is itself free of the complications introduced by additional valence subshells.

As the nuclear charge increases along the isoelectronic sequence, the ejected orbitals are pulled in toward the core, experiencing a more complex continuum-core interaction than occurs in silver. The scaled cross section first increases, reaches a peak at Sn^{4+} , and then begins to decrease. As the nuclear charge approaches 54, the complex exchange interaction between the d^9 core and the ejected f-wave decreases in importance compared to the nuclear charge + direct electrostatic interaction, resulting in a gradual return of the cross section to classical scaling. Classical scaling is not recovered until approximately the tenth ionization state. This is very different from low-Z isoelectronic sequences where classical scaling is obtained either from the neutral atom itself or at worst from the first or second ionization stage.

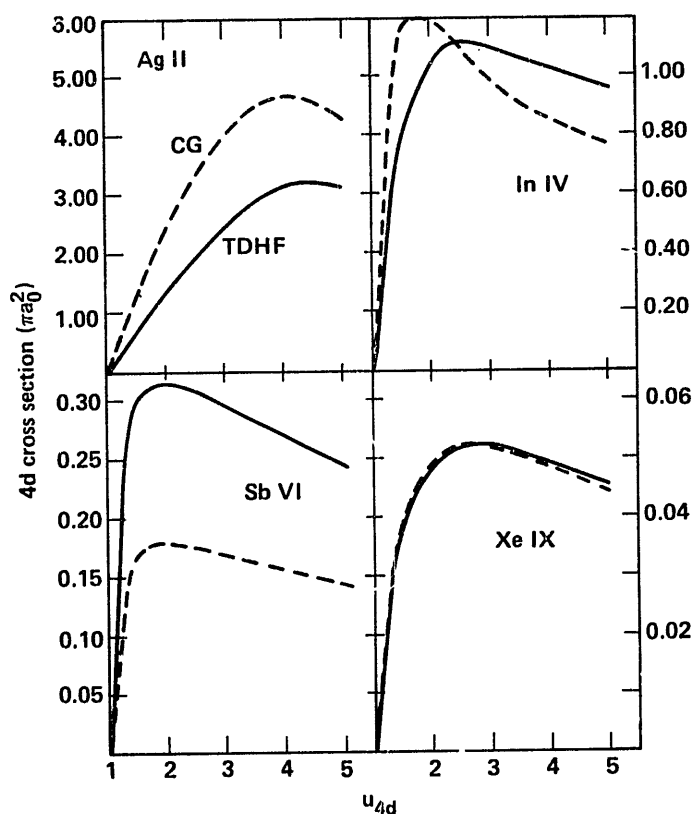


Fig. 2: Electron impact ionization cross sections for several palladium-like ions illustrating the variation in the shape the cross section with increasing nuclear charge.

In addition to non-classical scaling of the cross section along an isoelectronic sequence, the shape of the cross section can change significantly between nearby ions. Figure 2 compares scaled cross sections for ionization of several Pd-like ions. For the intermediate Z ions, the scattering potential has a double well character, with an inner well corresponding roughly to the tightly bound core and a very shallow well at large radii corresponding to the asymptotic Coulomb potential of the ion. The two wells are separated by a potential barrier which in some cases projects above zero energy. Under the right conditions of potential structure and continuum energy, the partial waves can "resonate" in the inner well, i.e., there will be a rapid buildup of continuum orbital density near the bound orbitals. Such a transition of orbital density can be accompanied by a rapid increase in the scattering cross section. Even if a true resonance does not occur (indicated by a partial wave phase shift increment of π), there can still be significant modifications of scattering orbital density which can affect the cross section.

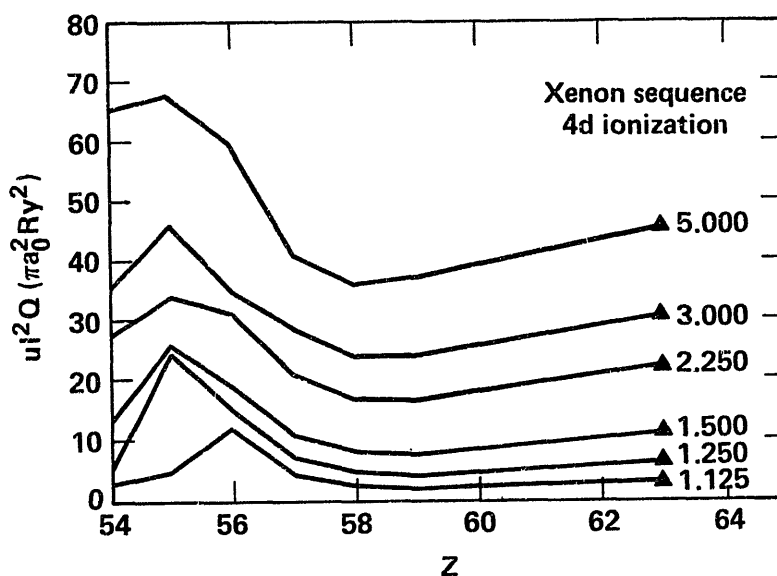


Fig. 3. Scaled distorted wave Born-exchange cross sections, uI^2Q , for electron impact ionization of the 4d subshell in the xenon isoelectronic sequence plotted as a function of Z . Results of the simple Lotz approximation⁵ are given as solid triangles.

An illustration of both resonant and non-resonant modifications of the electron ionization cross section can be seen in ionization of the 4d subshell in xenon-like ions. This process leaves the residual ion in a singly autoionizing configuration resulting in effective double ionization of the initial target by a single electron impact. The breakdown of classical scaling is shown in Figure 3. The presence of a shape resonance in the Cs^+ cross section is illustrated in Figure 4.⁶ The large structure at $u=1.35$ is due to a shape resonance in the potential for the scattered electron. The normal maximum in the cross section occurs at 3.5 threshold units. The theoretical calculations, which include the effects of ejected wave term dependence and ground state correlation, are in good agreement with the measurements of Hertling et. al.⁷

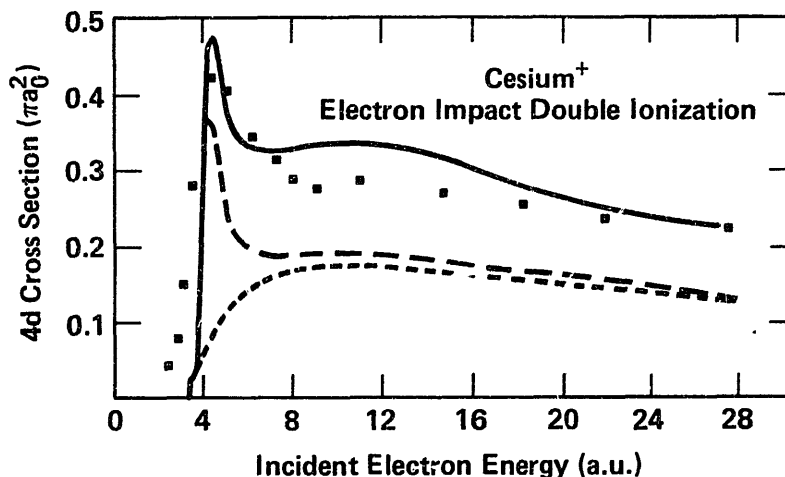


Fig. 4: Electron impact double ionization cross section of Cs^+ illustrating the giant resonance at low scattering energies. Theoretical curves correspond to 4d ionization followed by single autoionization. Solid curve: distorted wave Born-exchange calculation including effects of ejected wave term dependence and ground state correlation. Dashed curve: distorted wave Born calculation neglecting term dependence and correlation. Dotted curve: Coulomb-Born calculation. Points: Crossed-beam measurements of Hertling et. al.⁶

Survey calculations have been performed to determine whether such giant resonances occur in other heavy ions. A resonance similar to the one in Cs^+ was found for neutral xenon. For Ba^{++} resonance behavior occurs in the exchange matrix elements only, implying that a measurement of the cross section for Ba^{++} will provide a sensitive test of partial wave scattering theories for electron exchange in scattering processes. Strong resonances were also found for 4d ionization of Xe^+ and I^+ . The existence of resonances in both of these ions is confirmed by experimental data.⁸

Figure 5 presents calculated cross sections for ionization of the 4f electron of the $4f^{14} 1S$ (metastable) configuration of Tm^+ . Cross sections computed with simple scattering potentials show a very large resonant enhancement at low energies, followed by an even larger principle maximum at $u=3.25$. Although the magnitude of the second maximum is reduced when term-dependent ejected f-waves are employed, the resonance at low energy remains strong. Although the resonance in $4f^{14} \rightarrow 4f^{13}$ ionization is quite strong, it disappears in the next ion in the isoelectronic sequence, Yb^{++} . An investigation of several heavier ions (W^+ and Hg^+) was made to determine if the presence of additional large-radii screening electrons would cause the structure to reappear. It did not, however, indicating that the increased nuclear charge is strong enough to prevent the formation of a potential barrier compatible with shape resonances. Strong shape resonances were found, however, for other singly ionized rare earth ions such as Eu^+ where the $4f^7 6s$ configuration does not possess the very strong term-dependent excited spectrum found for closed-subshells.

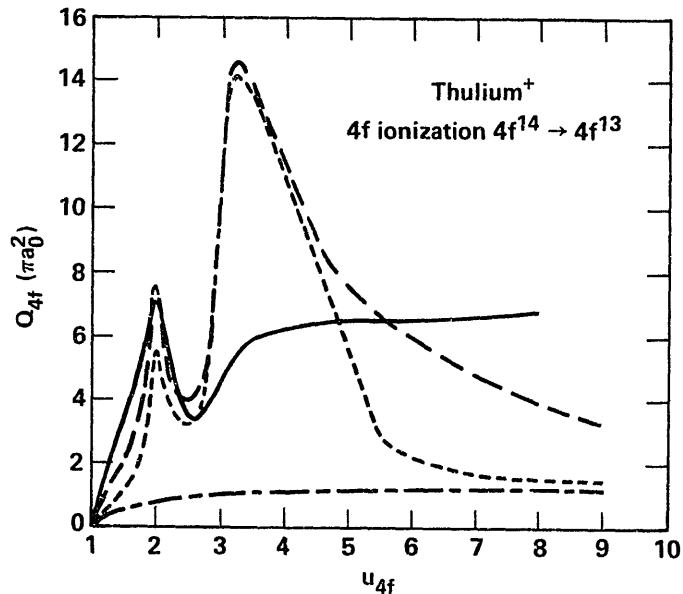


Fig. 5: Distorted wave calculations of the cross section for electron impact ionization of the $4f^{14} 1S$ subshell of Tm^+ . Solid curve: Born-exchange calculation including term-dependent ejected f -waves. Dashed curve: Born-exchange without term-dependent potentials. Dotted curve: Same as dashed curve, but without exchange. Chain curve: Coulomb-Born calculation without exchange or term-dependence.

In conclusion, we have shown that the electron impact ionization of heavy atoms and ions is considerably more complex than is the case for light ions. Non-classical scaling of the cross section can persist to ionization stages as high as ten, and giant resonance structures can significantly perturb the cross sections of few times ionized atoms at low scattering energies.

This work was performed under the auspices of the U.S. Department of Energy by Lawrence Livermore National Laboratory under contract #W-7405-Eng-48.

REFERENCES

1. S.M. Younger, Phys. Rev. A22, 2682 (1980), Phys. Rev. A23, 1981 (1981).
2. M.S. Pindzola, D.C. Griffin, C. Bottcher, D.H. Crandall, R.A. Phaneuf, and D.C. Gregory, Phys. Rev. A29, 1749 (1984).
3. M.S. Pindzola, D.C. Griffin, and C. Bottcher, J. Phys. B16, L355 (1983).
4. S.M. Younger, Phys. Rev. A (In press).
5. W. Lotz, Z. Phys. 216, 241 (1968).
6. S.M. Younger, Phys. Rev. Lett. 56, 2618 (1986).
7. D.R. Hertling, R.K. Feeney, D.W. Hughes, and W.E. Sayle, J. Appl. Phys. 53, 5427 (1982).
8. Ch. Achenbach, A. Müller, and E. Salzborn, Phys. Rev. Lett. 50, 2070 (1983).

SYSTEMATICS OF ENERGY LEVELS AND OTHER PROPERTIES
OF HIGHLY CHARGED IONS*

S.T. Manson, M. Inokuti,[†] and C.E. Theodosiou[§]

Department of Physics and Astronomy

Georgia State University, Atlanta, GA 30303, USA

[†]Argonne National Laboratory, Argonne, IL 60439, USA

[§]Department of Physics and Astronomy

The University of Toledo, Toledo, OH 43606, USA

Our knowledge of energy levels and other properties of highly charged ions is rather meager compared to our knowledge of the neutrals. Nevertheless, such knowledge is often required to interpret the complex phenomena which occurs in collisions of these highly charged ions. In this paper we report on our initial efforts to understand the systematics of the properties of highly charged ions. This effort is based on the use of (relatively) simple central-field calculations, which, as shall be shown, are surprisingly accurate for highly charged ions.

We stress the point of view, based on extensive experience with neutrals, particularly in the context of quantum-defect theory,¹⁻³ that diverse observable data can be represented in terms of a small set of key numerical parameters (e.g., phase shifts, oscillator strength densities, and amplitudes at the nucleus). The variation of such parameters from one ion species to another lends itself to easy and instructive mapping using realistic atomic models. By mapping these parameters throughout the periodic system and for all ionic charges, one can establish trends that will form a reliable basis for predicting unmeasured properties of ions. In addition, this survey is useful for establishing to what extent such well-known spectral features as Cooper zeros and shape resonances,⁴ so important in neutral atoms, control the spectral behavior of ions.

Any property of ions can be considered as a function of two variables, the nuclear-charge number (or atomic number) Z and the number of electrons N . Data can then be analyzed in terms of at least three alternative pictures: isoelectronic (N kept constant), isonuclear (Z kept constant), and isoionic ($z = Z - N + 1$ kept constant). Note that the spectroscopist calls z the order of the spectrum and that an electron at large distances sees a Coulomb potential due to the net charge ze . Each of these pictures

brings out different aspects of the variation of a given quantity over Z and N .

The isoelectronic picture is the most straightforward from a computational view point. Further, it is closely related to the $1/Z$ expansions.⁵ Each of the properties approaches the known hydrogenic values asymptotically⁶ when plotted against $1/Z$ ($1/Z \rightarrow 0$). The isonuclear picture simplifies the variation of ionic properties from one order of the spectrum to the next. In addition, the isonuclear picture is the most suitable for certain applications. For example, if we consider a given impurity in a fusion plasma, the many ions of that impurity nuclide which are relevant constitute an isonuclear sequence. This is also true for astrophysical applications.⁷ The isoionic picture maintains a constant asymptotic potential $-ze^2/r$ seen by an electron, and focuses on the interplay between increasing Z and increasing N . This provides a framework for the transfer of the extensive experience with neutral atoms, $z = 1$, gained by traditional spectroscopy and collision physics.

At an ionization threshold there is a union between discrete states, usually characterized by their quantum defects and treated by spectroscopic methods, and continuum states, usually characterized by their scattering phase shifts and treated by collision theory. Quantum-defect theory¹⁻³ shows, among other things, that these two manifolds of states are smoothly connected when the data are suitably renormalized. This reveals the Rydberg series to be an appendage to the continuum so that the most basic wave-function parameters, viz., phase and amplitude, vary smoothly through threshold. In particular, the quantum defect μ_ℓ at the limit of the Rydberg series and the zero-energy scattering phase shift δ_ℓ (with respect to the Coulomb phase) are related simply by

$$\pi\mu_\ell(n \rightarrow \infty) = \delta_\ell(E = 0), \quad (1)$$

where ℓ is the orbital angular-momentum quantum number, and n is the principal quantum number. In approaching the problem of mapping out the behavior of phase shifts as a function of both atomic number and ionic charge, we decided to begin by limiting the scope of the study to a single standard energy. We have chosen as our standard energy the ionization limit where the asymptotic kinetic energy E of the one-electron states equals zero. Consequently, our discussion pertains directly to properties of nearby states both below and above the threshold for ionization.

In addition to threshold phase shifts, we shall discuss systematics of inner shell properties of atomic ions. In particular, results shall be presented for x-ray transition energies, dipole matrix elements, and photoionization cross sections showing the systematics of these properties.

Before presenting any of the results, it is of interest to point out that these calculations were performed using simple Hartree-Slater (or Dirac-Slater in the relativistic case) wave functions⁸ which are quite amenable to large-scale calculation. In addition the use of these wave functions has been shown to be reasonably accurate for the neutrals;^{9,10} this accuracy is expected to be even better for positive ions. This can be seen by consideration of the potential of electrons in an ion of atomic number Z with N electrons,

$$V = - \sum_{i=1}^N \frac{Ze^2}{r_i} + \sum_{i<j} \frac{e^2}{r_{ij}} = -Ze^2 \left[\sum_{i=1}^N \frac{1}{r_i} - \frac{1}{Z} \sum_{i<j} \frac{1}{r_{ij}} \right] \quad (2)$$

For a fixed N , the $1/Z$ coefficient causes the second term in Eq. (2) to decrease in magnitude relative to the first term with increasing Z . Since the second term, the interelectron repulsion, is just the part of the potential being approximated, it is clear that the approximation improves as Z increases and the nuclear attraction dominates.

As a first example, a selection of quantum defect results¹¹ are shown in the isoionic picture ($z = Z - N + 1 = \text{constant}$) in Fig. 1. The variation of each of the μ_ℓ 's with Z for the neutrals ($z = 1$) is seen to be rich in structure;

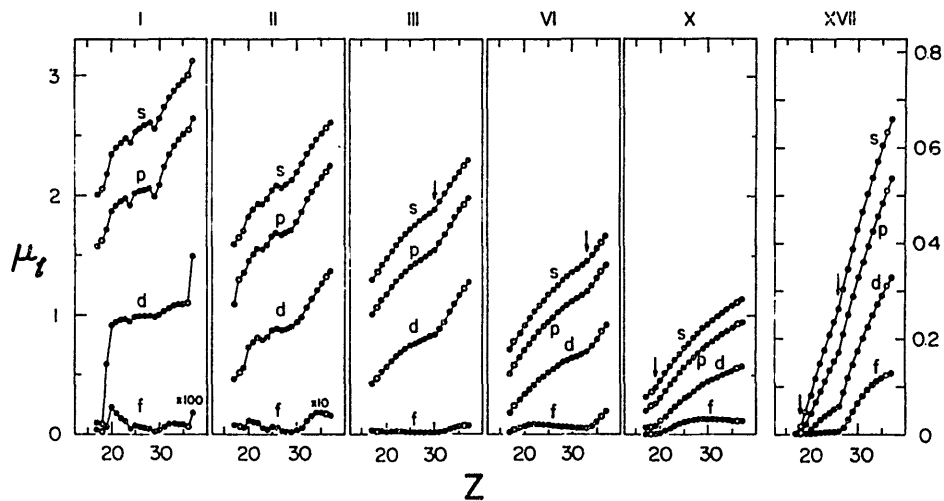


Fig 1. Isoionic pictures of the zero-energy phase shift in units of π (quantum defect μ_ℓ at the series limit). The Roman numerals indicate the order of the spectrum, or $z = Z - N + 1$. The arrows indicate the positions of the hydrogenic magic numbers, while the open circles denote noble-gas nuclides. Note the change of vertical scale on the rightmost panel.

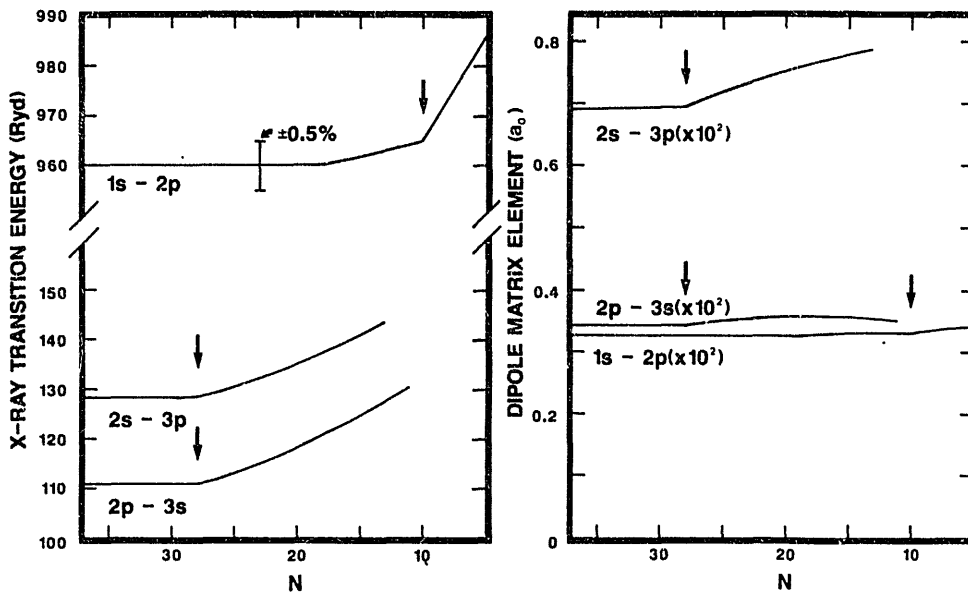
this structure is associated with the chemical properties of the elements. Note that this structure is considerably diminished for the $z = 2$ results and essentially gone for $z = 3$ and higher. The structure for the neutrals is due to the delicate balance between three forces; the nuclear attraction, the interelectron repulsion, and the centrifugal repulsion. With increasing z , the interelectron repulsion becomes proportionally weaker, thereby destroying the balance.

Note also, that for the neutrals, there are slope discontinuities in the curves for $N = 2, 10, 18,$ and 36 , the noble gas electron numbers. By the third spectrum ($z = 3$), these discontinuities occur for $N = 2, 10$ and 28 , as seen in Fig. 1. Thus the closed shell systems for the neutrals, the noble gas configurations, differ from the closed shells for multicharged atoms where the closed shells are hydrogenic represent the filling of the $n = 1, n = 2,$ and $n = 3$ subshells. This is, of course, exactly what one would expect as the deviation from hydrogen-like behavior, the interelectron repulsion, grows smaller. By these arguments, similar behavior should be found for $N = 60$ where the $n = 4$ shell is filled; such behavior has been found.¹¹

In the comparison of our results with experiment (which has generally shown excellent agreement) irregularities have been noted in the quantum defects of the higher members of certain Rydberg series. These irregularities are likely due to external perturbations, e.g., collisions or stray fields. In these cases, it is felt that the theoretical quantum defects give more reliable energy levels; a tabulation is presented elsewhere.¹²

The next example relates to x-ray transitions filling inner shell vacancies. In atomic collisions, identification of the various excitation and ionization processes is made by observing these x-rays. Nevertheless, in many of these collisions, multicharged ions result. The question, then, is to explore to what extent x-ray energies and intensities are modified by the existence of outer-shell vacancies.

To investigate this matter, we have looked at the isonuclear sequence of Rb and its ions. The results of calculations of x-ray energies and dipole matrix elements (whose squares are proportional to the transition probabilities) are shown in Figs. 2 for three different transitions. Looking first at the transition energies vs. N , we see the remarkable result that at first, removing electrons has no effect, but at some critical point the x-ray energies start changing with decreasing N . For the $2s - 3p$ and $2p - 3s$ transition this break comes at the 28 electron system, while for the $1s - 2p$ x-rays the break is at $N = 10$. Furthermore, looking at the dipole matrix elements, exactly the same effect is seen.



Figs. 2. Isonuclear pictures of the x-ray transition energies and dipole matrix elements for 1s - 2p, 2s - 3p, and 2p - 3s transitions for Rb ($Z = 37$) and its ions, plotted vs. number of electrons, N . The arrows indicate the 10- and 28-electron hydrogenic closed shell systems.

Neither the 2s - 3p nor the 2p - 3s change until we come to the 28 electron system, the hydrogenic closed shell system. The next electron removed is a 3d electron; thus when we break into the $n = 3$ shell, matrix elements and energies involving other $n = 3$ electrons change, but removing outer shell ($n = 4, 5$) electrons leaves them unchanged. The same thing happens to 1s - 2p when we break into the $n = 2$ subshell.

To understand these results, note that $\langle r \rangle$ for a given subshell is a function of principal quantum number n and very little else. Thus, as far as an inner shell is concerned, an outer shell electron is just a shell of charge at its $\langle r \rangle$. This is crucial because a shell of charge exerts no force in its interior. Thus, removal of an outer shell electron only changes the potential in the inner region by a constant, leaving energy differences and matrix elements unaffected. Clearly, then, removing outer shell electrons does not change inner shell x-ray energies or intensities. Once electrons are removed from the same shell (not necessarily the same subshell), by the above arguments, energies and matrix elements should change; this is seen in Figs. 2.

Note further that this argument is not perfect. Looking at the 1s - 2p x-ray energy, it is seen that a

change starts to occur after $N = 18$; in other words, removing 3d electrons have no effect, but 3p and 3s electrons, being more penetrating, do have some effect, but a very minor one ($< 0.5\%$). Thus we see that this constancy is good to at least 0.5%. Furthermore, we would expect the invariance to removal of outer shell electrons to be true for other inner shell properties as well, not just transition energies and dipole matrix elements.

What, however, occurs if the inner shell electron makes a transition to the continuum? How is the inner shell ionization process affected by removal of outer shell electrons? To explore this question, the next example relates to photoionization of inner shells. Fig. 3 shows the photoionization cross section of Fe 2s for the iron isonuclear sequence¹³ plotted vs. incident photon energy. Note that a separate calculation was performed for each stage of ionization. For the lower stages of ionization, the cross sections all lie on the same line (to within the thickness of the line). The cross section begins to change only for Fe⁺¹⁷ where we break into the 10 electron system and remove a 2p electron.

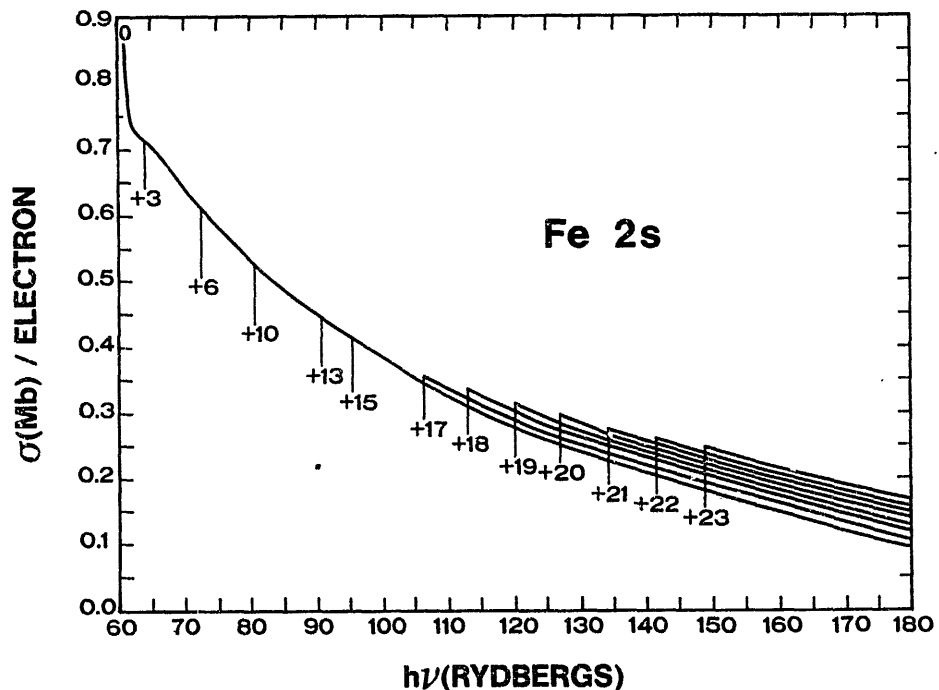


Fig. 3. Photoionization cross section (per electron) for the 2s subshell of the Fe isonuclear sequence from the neutral to Fe⁺²³. The vertical lines are the thresholds for the given stage of ionization.

The explanation for the invariance of the photoionization cross section is precisely the same as outlined above for x-ray transitions, with one added proviso. The continuum wave function is not localized within the outer shells, but the matrix element is localized due to the localization of the initial state, so the matrix element is essentially unaffected by outer shell electron removal. The transition energy is, however, affected. Thus the invariance shows up only when plotted vs. photon energy.

This result has been found in many other cases as well. Perhaps the most remarkable case studied was thorium ($Z = 90$) where the 2p photoionization cross section was found to agree to within a few percent for neutral thorium and 80-times-ionized neon-like thorium¹⁴.

REFERENCES

* This work was supported by the U.S. Army Research Office and the U.S. Department of Energy, Office of Health and Environmental Research.

1. M.J. Seaton, Mon. Not. Roy. Astron. Soc. 118, 504 (1958).
2. M.J. Seaton, Rep. Prog. Phys. 46, 167 (1983).
3. C. Greene, U. Fano, and G. Strinati, Phys. Rev. A 19, 1485 (1979).
4. U. Fano and J.W. Cooper, Rev. Mod. Phys. 41, 441 (1968).
5. D. Layzer, Ann. Phys. (N.Y.) 8, 271 (1959).
6. M.W. Smith and W. Wiese, Ap. J. Supp. 23, 103 (1973).
7. B.C. Fawcett, Adv. Atom. Mol. Phys. 10, 223 (1974).
8. F. Herman and S. Skillman, Atomic Structure Calculations (Prentice-Hall, Englewood Cliffs, N.J., 1963).
9. S.T. Manson, Phys. Rev. 182, 971 (1969).
10. U. Fano, C.E. Theodosiou, and J.L. Dehmer, Rev. Mod. Phys. 48, 49 (1976).
11. C.E. Theodosiou, S.T. Manson and M. Inokuti, Phys. Rev. A 34, (in press).
12. C.E. Theodosiou, M. Inokuti, and S.T. Manson, At. Data Nuc. Data Tables (in press).
13. R.F. Reilman and S.T. Manson, Phys. Rev. A 18, 2124 (1978).
14. W. Ong, S.T. Manson, H.K. Tseng, and R.H. Pratt, Phys. Lett. 69A, 319 (1979).

ATOMIC PHYSICS AT THE ESR STORAGE RING

◇

Heinrich F. Beyer

GSI D-6100 Darmstadt, W-Germany

Abstract

The study of the physics of few-electron very heavy ions such as U^{91+} looks very promising as an approach to interesting and fundamental points in atomic physics. The GSI Heavy-Ion-Synchrotron (SIS) and the Experimental-Storage-Ring (ESR) facilities to be built will offer unique possibilities for such an experimental program to be carried out. We give an overview of the SIS and ESR projects, a more general introduction to phase-space cooling concepts being applied at storage rings and an outline of the atomic-physics program being presently in discussion.

1 Introduction

A highly charged few-electron ion Z^{q+} , $q \approx Z \approx 92$ is in many respects a unique tool for addressing fundamental topics in atomic physics. Many familiar rules of thumb for collisional and radiative processes of one- and two-electron atoms fail when the charge of the nucleus gets as high as 92. At the same time atomic structure keeps impressively clean as opposed to the many-electron case where it is, very often, difficult to discriminate interesting physics from the morass of complicated multi-level structure.

A single free ion at rest would be the ideal spectroscopic sample and many interesting attempts [1] have been made to approach such a situation (for lower charge states). In many accelerator-based experiments one seeks for a dense sample of fast ions filling a small phase space. Therefore various techniques for increasing phase-space density (cooling) have been developed. Notably electron cooling of an ion beam by heat exchange with a cold electron beam has proven very promising. After the pioneering work at Novosibirsk [2] there is now an increasing number of storage rings employing electron cooling some of which are more or less operational others being in the status of being installed or planned [3]. In the following the new projects at GSI are sketched.

2 The New Accelerator Projects at GSI

An outline of the accelerator complex[4] to be built at GSI is given in figure 1. The existing UNILAC linear accelerator, capable of accelerating ions throughout the periodic table up to 20 MeV/u, will be used as an injector to the new Heavy-Ion Synchrotron SIS. The SIS will further accelerate ions up to uranium to the 1 GeV/u region whereas the Experimental Storage Ring ESR coupled to the SIS will be used to improve the quality of the beam and adapt it to the needs of the actual experiment.

2.1 The Heavy-Ion Synchrotron SIS

The SIS, having a circumference of 216.7 m, has a magnetic bending power of $B \cdot \rho = 18Tm$ and will be operated at a cycling rate of 1-5 Hz. Maximum achievable energies depend on the charge-to-mass ratio q/A of the injected ions and drop from 2 to 0.9 GeV/u (Ne to U) using a foil stripper at 11.4 MeV/u after the UNILAC. Corresponding particle currents are in the order of 10^{12} to 10^{10} ions/s. Injection of the UNILAC beam into the SIS will be accomplished during 10 to 30 turns and space-charge limits are reached with injected particle currents of $2 \cdot 10^{14} s^{-1} U^{78+}$ and $2 \cdot 10^{15} s^{-1} Ne^{10+}$. Such high currents will be obtained by a newly developed high-current ion source and an RFQ structure [5] replacing the first Wideröe linac.

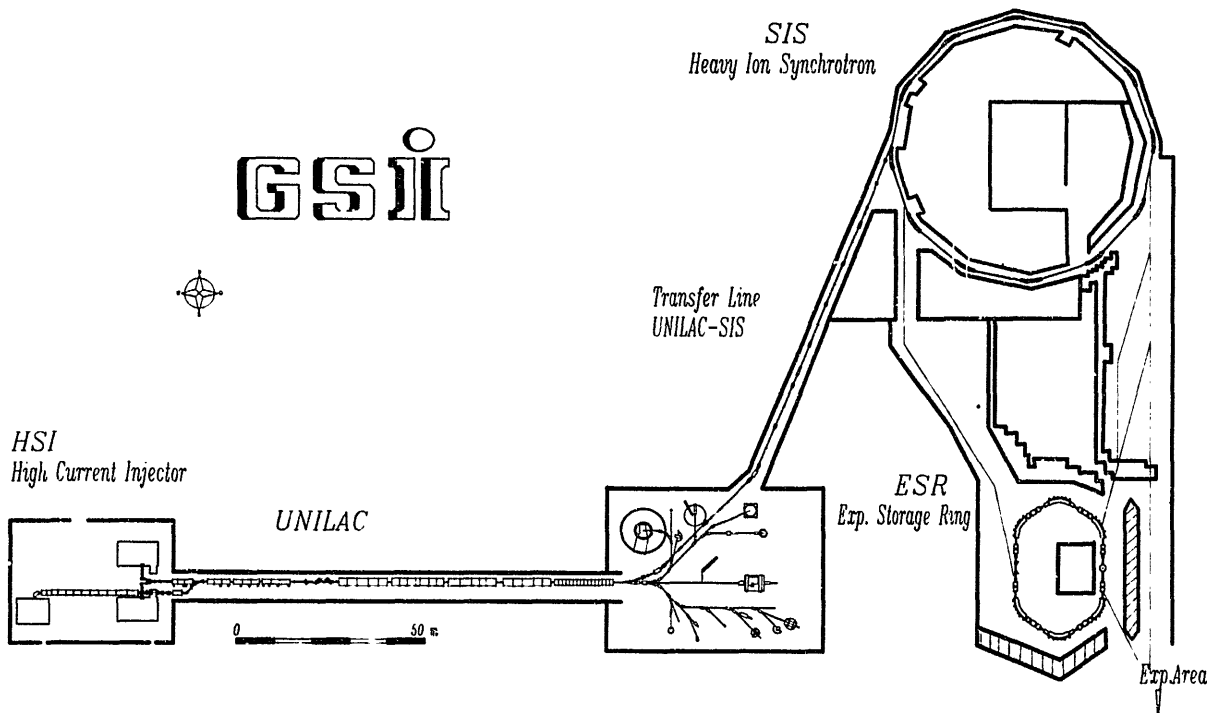


Figure 1: Schematic view of the planned accelerator facilities at GSI. The existing UNILAC linear accelerator will be used as an injector for the new Heavy-Ion Synchrotron SIS to which the Experimental Storage Ring ESR will be coupled.

2.2 The Experimental Storage Ring ESR

As indicated already by its name operation of the ESR [6] is regarded as an experiment on its own and, as we will see below, a number of atomic-physics issues are encountered. The ESR has exactly half the circumference of the SIS which enables a convenient transfer of one half of the SIS turn into one ESR turn using the rf frequency of the SIS. Figure 2 shows the layout of the small ring. The magnets have a bending power of 10 Tm . This allows storage of Ne^{10+} ions with a maximum energy of 834 MeV/u and of U^{92+} with 556 MeV/u . In connection with the SIS the ESR offers a variety of very attractive features:

As a *storage ring* it can store completely stripped heavy ions. Even for uranium the stripping yield of bare ions is high at energies above 500 MeV/u [7]. Via the fast extraction channel the fully stripped ions may be reinjected into the SIS for acceleration to maximum energy. The flexible ion optics of the ring allow various modes of operation. For accepting ion beams of large momentum spread ($\Delta p/p = 0.02$) and emittance ($140\pi 10^{-6} \text{ m}$), such as hot fission fragments, a moderate dispersion can be used. If a zero dispersion is selected in the straight section multi-charge ($\text{U}^{89+} - \text{U}^{92+}$) operation is possible. In yet another mode, with large dispersion, two beams of slightly different momenta can be stored and can be brought to intersect at a small angle of about 100 mrad [8]. The *intersecting-beam* technique can be used to study interactions of two few-electron ions at collision energies corresponding to a fixed-target equivalent energy of up to 7 MeV/u .

As a *stretcher ring* the ESR can store coasting beams with a duty factor of up to about 90%. But also focussing the beam to bunches of 1 ns duration with repetition rates of about 40 MHz should be possible using the rf cavities installed. The latter may also be used for deceleration down to UNILAC energies. Both modes of operation, however, require phase-space cooling to compensate for the emittance growth.

As a *cooler ring* it employs various cooling devices (see below) most important being the

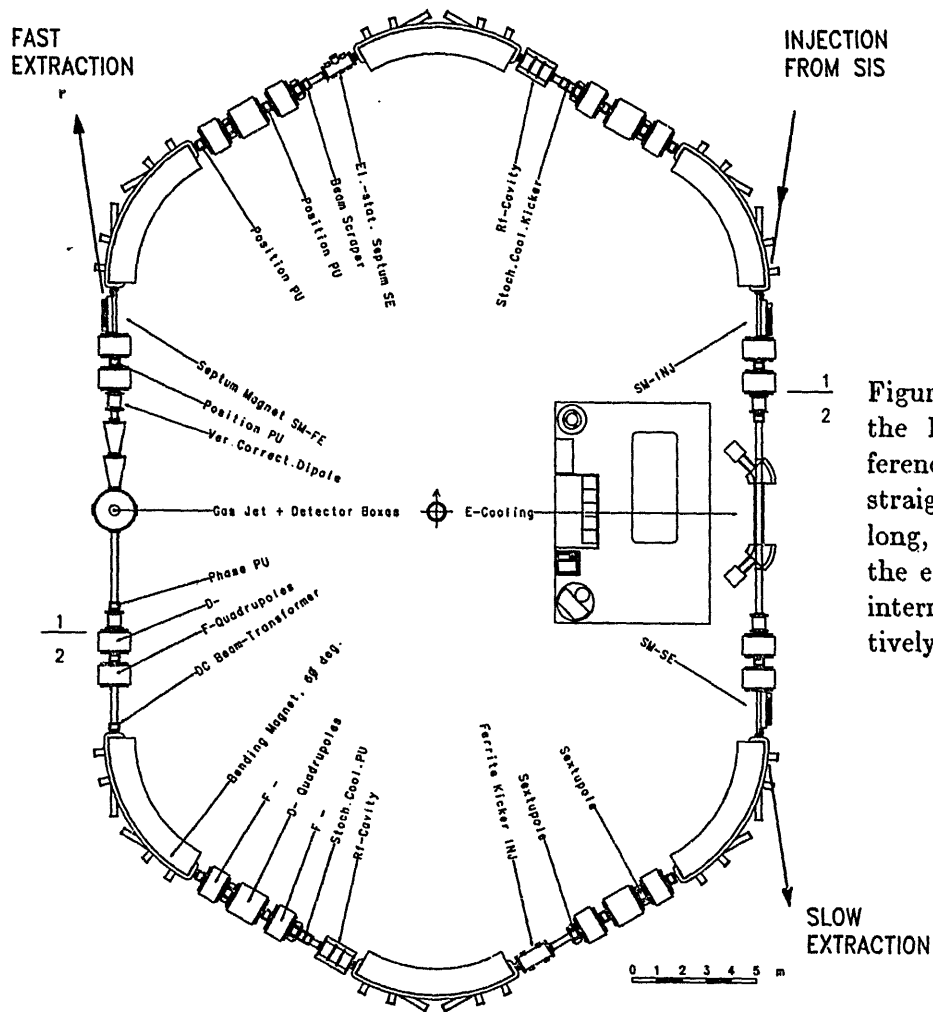


Figure 2: The structure of the ESR with a circumference of 108.4m. Two straight sections, each 9.5m long, are used for insalling the electron cooler and an internal gas target, respectively.

electron cooler which will be installed in one of the long straight sections. One anticipates cooled ion beams with a momentum spread of as low as 10^{-5} and emittances of $0.1\pi 10^{-6}m$.

Using the *internal target* (normal or polarized atomic or ionic beam) installed in the second straight section, together with the circulating cool ion beam, collision processes can be studied. All experiments which need thin targets will gain in luminosity by the circulating beam current ($\sim 2MHz$) as compared to single-pass experiments.

3 Phase-Space Cooling

There are mainly three different techniques feasible for compressing the six-dimensional phase space of an ion beam circulating in a storage ring.

Stochastic cooling [9] makes use of a feedback system. For cooling transverse betatron oscillations a pick-up electrode senses a position error of a particle on each traversal. The error signal is amplified in a broad-band amplifier and is applied to a kicker located $(2n+1)/4$ betatron wavelengths apart from the pick up. The kicker deflects the particle by an angle proportional to it's error. In reality we have a large number N of particles in the ring and the sensing and correction process will be applied to a group of particles (sample). The cooling rate is proportional to the bandwidth of the amplifier and to the inverse of the ion density. Due to the statistical nature of the process and the quite low signal-to-noise ratio stochastic cooling works best at rather hot beams.

Range of specific ion energy	4-560 MeV/u
Working range for the electron beam	2-320 keV
Electron current	1-10 A
Electron current density	0.1-1.0 A/cm ²
Electron beam diameter	35-50 mm
Cathode temperature	0.1 eV (1100 K)
Effective length of cooling section	2.50 m
Installation length	4.50 m
Aperture diameter (horiz.)	250 mm
$B_{ }$ (Solenoids, Toroids)	0.2-0.3 T

Table 1: Parameters of the ESR Electron Cooling Section.

Electron Cooling introduces a dissipative force via Coulomb interactions between the circulating particle beam and a dense co-streaming beam of cold electrons serving as a cold reservoir. In the subsequence of Budkers [10] initial proposal electron cooling was studied both experimentally [2] and theoretically [11]. The main components of an electron-cooling device are the electron gun, a straight interaction region, a collector, where most of the electron kinetic energy is recuperated, and a longitudinal magnetic field for guiding and confining the electron stream. In Table I the relevant parameters are given for the ESR cooler. If there was no heating mechanism cooling takes place until the effective temperatures of the heavy-particle and electron beam become equal, $T_i = T_e$. Neglecting the magnetic field a simple estimate of the cooling (friction) force may be obtained by considering the stopping power of an ion in an electron gas [11] (in the moving mean-electron frame of reference). For a Maxwellian velocity distribution function the corresponding cooling time is

$$\tau = \frac{m_i m_e}{q^2 e^4 n_e L_c} \begin{cases} (4\pi)^{-1} v_i^3 & v_i > v_e \\ \frac{3}{4} (2\pi)^{-1/2} \left(\frac{T_e}{m_e}\right)^{3/2} & v_i < v_e \end{cases} \quad (1)$$

Equation (1) shows the scaling of the cooling time proportional to m_i/q^2 of the ion and to the inverse of the electron density, n_e^{-1} . Figure 3 compares electron cooling with stochastic cooling as a function of ion-beam temperature. As can be seen, the two techniques are complementary: electron cooling starts to be effective at lower beam temperature where stochastic cooling gets inefficient. As the ion beams injected from the SIS will allready have a momentum spread of $\Delta p/p \approx 5 \cdot 10^{-3}$ electron cooling will be the method used throughout with the exception of hot nuclear fragments which need stochastic precooling. For the ESR typical cooling times range from 0.15 to 650 ms (30MeV/u U^{92+} to 500MeV/u Ne^{10+}).

It may be argued that the cathode temperature T_c is the minimum achievable temperature of the electron beam. However, one has to take into account two effects. *First*, after electrostatic acceleration the longitudinal temperature $T_{||}$ of the electron beam (as measured in the mean particle rest frame) is strongly reduced to

$$T_{||} = T_{\perp} \frac{T_{\perp}}{2\gamma^2 \beta^2 m_e c^2} \ll T_{\perp} = T_c \quad (2)$$

where β and γ are the usual relativistic factors. *Secondly*, the presence of the guiding magnetic field tends to freeze the transverse degrees of freedom of the electrons as the ions interact with Larmor discs slowly drifting along the magnetic-field lines rather than with rapidly travelling electrons. Consequently a very fast ‘supercooling’ down to very low temperatures can occur [12].

Laser cooling of circulating ion beams adopts the principal which was successfull in cooling

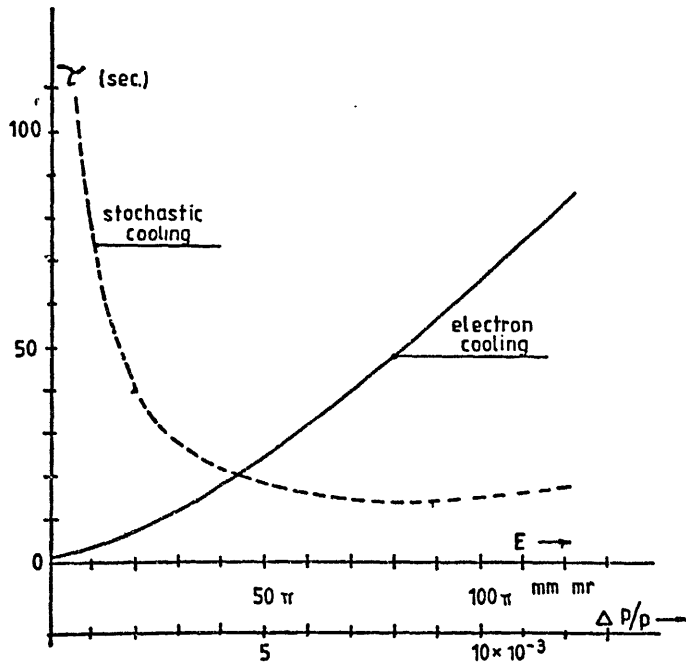


Figure 3: Cooling times for stochastic and for electron cooling as a function of beam emittance or momentum spread [9]

thermal atomic beams or ions in electromagnetic traps [1]. Absorption of highly directional photons from a laser tuned to within the absorption profile of an ionic resonance and a random reemission results in a net momentum transfer. This can lead to a velocity compression which eventually may proceed faster than electron cooling. Both transverse [13] and longitudinal schemes [14] have been proposed.

In a storage ring the cooling procedures are in competition with various heating mechanisms. Among them are scattering in the residual gas ($\sim 10^{-10}$ mbar) and in internal gas targets ($< 10^{14} \text{ cm}^{-2}$) and intra-beam scattering [15]. In electron cooling space charge in the intense electron beam and stability of the high voltage of the power supply cause a modulation of the electron velocity.

4 Experimental Programme at the ESR

As already stressed in the introduction, the domain of the ESR will be the physics of ions with both high nuclear and high ionic charge. Once the anticipated brilliant beams are available experiments under well defined and controlled conditions will become feasible with a considerable increase of measuring resolution and precision. What follows is a (necessarily incomplete) outline of experiments which become possible with the ESR [16].

4.1 Nuclear/Astro Physics

Nuclear-physics experiments, such as the study of compressed nuclear matter and its equation of state or of rare radioactive nuclei with the ESR operated as a high-quality mass spectrometer [17], are not within the scope of the present talk. However, it might be worthwhile to note some of the processes at the borderline between nuclear, astro and atomic physics.

Beta decay into unoccupied bound states of highly ionized atoms must have played a key role during nucleosynthesis and the knowledge of these processes are of great importance for establishing a cosmological clock [18]. Bound β^- decay may get energetically allowed only at high degrees of ionization as for the process ${}_{66}^{163}\text{Dy}_{5/2}^{66+} \rightarrow {}_{67}^{163}\text{Ho}_{7/2}^{66+}$. In neutral matter the reverse electron capture process takes place. In the ESR bare ions Z^{Z+} might be stored and

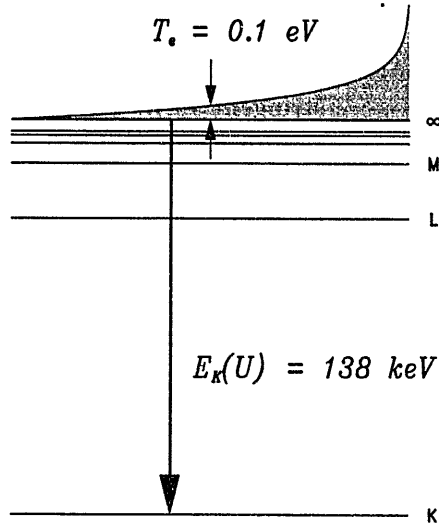


Figure 4: Radiative electron capture of cold electrons

cooled and the breeding of $(Z+1)^{Z+}$ being observed as a function of time. Thereby, for the first time, a simulation of nucleosynthesis in the laboratory will become possible in a broad range of plasma temperatures.

4.2 Atomic Physics

4.2.1 Electron - Ion Radiative Recombination

The recombination of a free electron with an ion can only proceed via the emission of a photon



and is the reverse process of photoionization. The capture can proceed directly (the only way for bare ions) to the final state $Z^{(q-1)+}$ or, in case of $q < Z$ via a doubly excited intermediate state $Z^{(q-1)+**}$. The two processes are referred to as radiative electron capture (REC) and dielectronic recombination (DR) [19], respectively and may be studied at the electron cooler. Especially REC, whose cross section diverges for small relative velocities, may as a loss process limit the efficiency of electron cooling. As the REC cross section is proportional to the final-state binding energy [20] the highest rate is expected for capture into the uranium 1s orbital. For this case a time constant of $\tau_{REC} \approx 20s$ is estimated for typical ESR parameters and is much bigger than typical cooling times.

As indicated in figure 4 the REC may serve as a diagnostic for the cooling process because the width of the spectrum profile is given by the temperature of the electron beam in case the ions are cooled down already or by a combination of ion and electron temperature when cooling starts. The spike of the REC spectrum, which is still enhanced by the flattening of the electron velocity distribution, is located at the boundary to the continuum. This allows a direct determination of inner-shell (1s) binding energies with a high precision. Similarly resonance energies can be measured in multi-electron ions making use of the dielectronic recombination. For this purpose the electron velocity must be detuned over the resonances. Evidently, the precision, which will finally be achieved, crucially depends on how well cooling works. It has also been proposed[21] to enhance the capture by laser radiation. This will be most advantageous for light ions where the spontaneous rate is low.

4.2.2 Ion - Ion Collisions

With the intersecting-beam technique, mentioned before, it becomes possible to prepare experimental conditions for collisions where only one electron is involved. Charge exchange between two heavy ions in well prepared states might be studied this way. But especially the study of

quasiatoms, where, during the collision, the binding energy of an inner electron becomes comparable to its rest mass could be studied in a more stringent way. Quasi-molecular x-ray and spontaneous positron emission, a field having already a tradition at GSI [22], would be measured and hopefully the puzzles given by present experimental findings would be disentangled.

4.2.3 Ion - Atom Collisions

Various stripping and capture processes in a wide range of ions and energy can be studied making use of the internal gas target. Let me note here only two collision regimes which are important for populating the atomic states of interest for precision spectroscopy: the dressing of a (bare) circulating ion with *one* electron out of a low- Z target gas and the production of high-charge low-velocity recoil ions. The latter process has been investigated extensively with beams from the UNILAC [23]. In the collision regimes involving very high charges low target densities are required, therefore advantage is taken of the beam recirculation [24].

4.2.4 Precision Atomic Spectroscopy

It has been speculated that the theory of quantum electrodynamics (QED) might have limitations for an electron bound in the strong field of a heavy nucleus [25]. This question is closely related to the relative importance of higher-order terms in the Lambshift which are only at the 10^{-6} level in neutral hydrogen but dominate in hydrogenlike uranium. Therefore a Lambshift measurement at very high Z would be interesting already at a modest precision. The lowest levels of intrinsic limitations, due to natural linewidths, are encountered for the $1s$ Lambshift. However, it is most demanding regarding the needed precision of x-ray spectroscopy [26]. The $1s$ Lambshift in U^{91+} for instance is $\sim 0.5keV$ out of a transition energy of $\sim 100keV$. On the other hand the $n = 2 \rightarrow 2$ transitions should be mentioned which, due to relativistic effects, gain a notable branching especially in the heliumlike system. The latter has also the advantage of a smaller linewidth as compared to the hydrogenlike $2p \rightarrow 2s$ transition. As already mentioned, the relevant states are prepared by the internal gas target either in the circulating beam or in the recoil ions.

Another kind of experiment makes use of resonant laser excitation in a collinear geometry. The $1s$ hyperfine splitting and the resulting bound-state g factor in one-electron heavy ions can be measured this way [27]. Due to the transformation of wavelength into the lab system (at angles $\alpha = 0^\circ, 180^\circ$ for collinear geometry) a wide range of ions $50 \leq Z \leq 92$ can be covered with existing laser frequencies. Also a two-photon excitation [28] can be tuned to a real intermediate level by absorbing one photon travelling parallel (red shifted) and another one antiparallel (blue shifted) to the ion beam. A wide range of relative spacings in a three-level system can be accessed depending on the size of β .

4.2.5 Fundamental Symmetries

Parity violation in atoms could be studied in a much cleaner way if an adequate few-electron scheme can be found avoiding the many-electron atomic structure uncertainty. A candidate might be the $2s \rightarrow 1s$ transition in hydrogenlike heavy ions. When the initial state is populated by electron capture from a polarized electron target the signature of parity-violating admixtures should be observable in the anisotropy of the emission.

4.2.6 Collective Phenomena in Very Cold Ion Beams

If one can sustain cooling down to very low temperatures a phase transition to an ordered 'Coulomb solid' may take place [29]. This is expected to happen when the ion temperature T_i

gets lower than about 0.6% of the internal Coulomb energy

$$T_i < 0.0058 \frac{q^2 e^2}{4\pi\epsilon_0} n_i^{1/3} \quad (4)$$

It is unclear whether such a situation will be reached in one of the cooler rings presently being built or whether a special ring structure has to be optimized for this purpose. In the Novosibirsk experiments [2] a threshold behavior around $10\mu A$ was found in the temperature of the proton beam as a function of beam current. This was attributed to an ordering effect. However, the temperature was much higher than (4) and even for a collapse into a *one*-dimensional array it was much too high. It should be pointed out that the achievement of such an ultra-cold ionic sample will have a large impact on precision atomic spectroscopy.

4.2.7 Heavy-Ion Pumped Lasers

It was demonstrated by Ulrich et al. [30] that infrared laser action can be achieved by depositing energy of about $10^{11}W/cm^2$ into a gaseous target by means of a pulsed beam from the Munich tandem or from the UNILAC. The extension towards the (soft) x-ray region is limited by the power-density (P/A) requirements, the minimum wavelength achievable scaling like $\lambda \sim (P/A)^{-1/3}$. With a bunched high-intensity beam from the new accelerator an increase in the power density up to about $10^{13}W/cm^2$ should be possible resulting in a three to four-times smaller wavelength.

5 Conclusion

The new installations at GSI will open the field of few-electron very heavy ions in a wide energy range particularly interesting for many atomic-physics experiments. The success of cooling off particle noise will crucially determine the feasibility and ultimate precision in most of the experiments identified above.

It is a pleasure to thank all my colleagues for the opportunity of working with them together on the projects presented above. I am particularly indebted to Fritz Bosch and Bernhard Franzke for valuable discussions.

References

- [1] see for instance: W.D. Phillips, J.V. Prodan and H. Metcalf in *Atomic Physics 9* (R.S. Van Dyck and E.N. Fortson eds.) p.338
- [2] G.I. Budker et al. *Particle Accelerators* **7** (1976) 197
- [3] for a survey see: B. Franzke *IEEE NS-32* No.5 (1985) 3297
- [4] Die Ausbaupläne der GSI, March 1984
P. Kienle, The SIS-ESR Project of GSI *GSI report* 85-16 (1985)
- [5] R.W. Müller et al. *GSI Scientific Report* (1985) p. 375
- [6] B. Franzke, H. Eickhoff, B. Franczak and B. Langenbeck Zwischenbericht zur Planung des Experimentier-Speicherrings (ESR) der GSI, GSI-SIS-INT/84-5 (1984)
- [7] H. Gould et al. *Phys.Rev.Lett.* **52** (1984) 180

- [8] B. Franzke and Ch. Schmelzer *IEEE NS-32* No.5 (1985) 2678
- [9] D. Möhl in *Cern Accelerator School* (P. Bryant and S. Newman eds., Geneva 1984) p.97 and references therein.
- [10] G.I. Budker *Atomic Energy* **22** (1967) 346
- [11] Ya.S. Debrennev and A.N. Skrinsky *Particle Accelerators* **8** (1977) 1
A.H. Sørensen and E. Bonderup *Nucl.Instr.Meth.* **215** (1983) 27
- [12] Ya. S. Debrennev and A. N. Skrinsky *Particle Accelerators* **8** (1978) 235
V.V. Parkhomchuk in *ECOOOL* (H. Poth ed.) (KfK Karlsruhe 1984) p.71
- [13] P.J. Channell *J.Appl.Phys* **52** (1981) 3791
- [14] J. Javanainen et al. *J.Opt.Soc.Am.* **B2** (1985) 1768
- [15] A. Piwinski in *9-th Intern. Conf. on High-Energy Accelerators* (Stanford 1974) p.405
I. Hofmann and R. Meyer-Prüßner in *GSI-Report* GSI-85-19 (1985)
- [16] *Workshop on the Physics with Heavy Ion Cooler Rings* (Heidelberg 1984)
Arbeitstreffen über Experimente am geplanten Experimentier-Speicherring der GSI
(Rauischholzhausen 1984)
- [17] H. Wollnik, T. Schwab and M. Berz *GSI Scientific Report* (1985) p.372
- [18] K. Takahashi and K. Yokoi *Nucl.Phys.* **A404** (1983) 578
F. Bosch *proceedings of the 18th EGAS Conference* (Marburg, 1986)
- [19] Y. Hahn *these Proceedings*
- [20] M. Stobbe *Ann.Phys.* **7** (1930) 661
- [21] R. Neumann, H. Poth, A. Winnacker and A. Wolf *Z.Physik* **A313** (1983) 253
- [22] see e.g.: P. Kienle *invited talk at the 10th ICAP* (Tokyo,1986)
- [23] for a review see: H.F. Beyer and R. Mann in *Progress in Atomic Spectroscopy* Part C (H. Beyer and H. Kleinpoppen, eds.) (Plenum, New York 1984) p.397
- [24] see also: H. Schmidt-Böcking in ref. [16]
S. Kelbch et al. *GSI Scientific Report* (1985) p.203
- [25] K.W. Kugel and D.E. Murnick *Rep.Prog.Phys.* **40** (1977) 297
- [26] R.D. Deslattes in ref. [16]
- [27] T. Kuehl, G. Huber in ref. [16]
- [28] O. Poulsen and N.I. Winstrup *Phys.Rev.Lett.* **47** (1981) 1522
- [29] N.S. Dikansky and D.V. Pestrikov in *ECOOOL* (H. Poth ed.) (KfK Karlsruhe 1984) p.275
J.P. Schiffer and P. Kienle *Z.Physik* **A 321** (1985) 181
J.P. Schiffer and O. Poulsen *preprint* (1985)
- [30] A. Ulrich, H. Bohn, P. Kienle and G.J. Perlow *Appl.Phys.Lett.* **42** (1983) 782 and in ref.[16]

X-RAY SPECTROSCOPY OF HIGHLY STRIPPED VERY HEAVY IONS

P. O. Egan, and G. A. Chandler, D. D. Dietrich, K. P. Ziock

Lawrence Livermore National Laboratory

Livermore, CA 94550, USA

P. H. Mokler, S. Reusch

Gesellschaft für Schwerionenforschung (GSI)

D-6100 Darmstadt, FRG

D. H. H. Hoffmann

Max Planck Institute for Quantum Optics (MPQ)

D-8046 Garching, FRG

The spectroscopy of very highly-charged ions presents a number of intriguing challenges for atomic physics from the viewpoint of both theory and experiment. In particular the precise solution of the multi-electron QED problem and the development of accurate multi-electron relativistic wave functions are two of the outstanding challenges facing atomic theory. The extension of experimental tests of QED to the regime of high Z , where one can test higher order terms and search for possible high field failures of the theory is also an exciting possibility with the development of new techniques for producing highly charged ions.

Most precision highly stripped ion spectroscopy experiments have concentrated on the case of hydrogen-like (or helium-like) systems, with a view to testing QED in a high Z system whose wavefunction is well known. A number of recent experiments using fast beams^{1,2,3,4} (beam-foil), recoil ions⁵ and plasmas⁶ have measured the Lyman- α energy ($2P - 1S$) in hydrogenic C^{+16} , Ar^{+17} , Fe^{+25} and Kr^{+35} . By subtracting off the Dirac energy in such experiments one can arrive at the Lamb shift of the $1s$ state which can then be compared with theory. Although significant progress has been made recently, all the experiments

determine the 1s Lamb shift to an accuracy of 1-15%, while theoretical estimates of higher order contributions are about two orders of magnitude lower.^{7,8} Thus the experiments serve the purpose of ruling out radical breakdown of the theory but are not as yet at the accuracy level to probe finer features of the standard theory.

An important new development has been the recent measurement by Gould and Munger⁹ of the $3p_0$ lifetime in helium-like uranium (U^{+90}) at the LBL Bevelac using a 219 MeV/amu U beam. Since the leading QED terms go as $(\alpha Z)^4$ one can put the theory to a stringent test at lower levels of experimental precision at very high Z. In addition one tests higher order terms in the theory which have much lower relative size at low Z. Future experimental facilities, in particular the SIS project at GSI described at this seminar by H. Beyer,¹⁰ should yield higher rates and more accurate values for high Z hydrogenic systems.

We have taken a slightly different approach in our experimental program by concentrating on the spectroscopy of few electron systems, in particular ions isoelectronic to Ne I (10 electrons). Neon like systems are attractive because they feature a closed L-shell and thus have $n=3 \rightarrow 2$ spectra which are relatively simple to measure and calculate. Closed shell ions are also important for plasma applications and diagnostics since they exist over a wide range of temperature and density. For example, the laser driven x-ray laser work at LLNL¹¹ observed lasing in Se^{+24} neon-like $n=3 \rightarrow 3$ transitions, and spectra of neon-like Ag^{+37} have been measured at PLT,¹² while neon-like line ratios have been used as a density diagnostic in laser produced plasmas.¹³

Our focus in neon-like spectroscopy experiments is not on a pure single electron QED test as in the H-like experiments, but rather on providing benchmark experiments in a two-fold attack of testing both the QED theory of a many electron system and the energy calculations requiring a relativistic multi-electron wavefunction. The ten electron system is simple enough that one can hope to make real progress on the theory, yet has enough electrons (and complexity) to give theory and experiment a real workout. Ultimately, one would hope that a refined

theory would be able to predict energy levels in heavy neutral atoms to the same level of precision as the currently existing x-ray spectroscopic data.¹⁴

Another attractive feature of L-shell spectroscopy is that we can examine very high Z systems (for example the region around Z=80 at GSI) at conventional heavy ion accelerators, while for K-shell systems at the same facilities we are only able to reach a Z of about 32. Thus, neon-like spectroscopy is a kind of "poor man's" Bevelac or SIS experiment.

The experimental technique we use to produce the highly charged ions is the brute force approach of stripping relativistic ions from an accelerator in a thin foil. The charge state one can achieve is then determined by the energy of the ions which can be produced, and can be predicted approximately using semi-empirical formulae. We have found that we can produce neon-like ions¹⁵ at the LBL SuperHILAC (E = 8.5 MeV/amu) for Z up to 57 (La), and by moving to the GSI UNILAC (14.9 MeV/amu) we were able to reach Ne-like Bi (Z=83).

The main problem which faces spectroscopic experiments on fast ion beams is how to deal with the large Doppler shifts associated with beam velocities, $\beta = v/c = 0.1 - 0.2$, without sacrificing experimental counting rate. At LLNL we have developed^{15,16} a new x-ray spectrometer to specifically deal with this problem. The instrument (Fig. 1) features two Johann crystal spectrometers which are set up with their Rowland circles lying in exactly the same plane. This spectrometer plane is set up approximately ± 2 m perpendicular to the incoming ion beam, with the final excitation foil positioned at its center. The angular acceptance of the crystals is quite large and unrestricted by slits in the dispersion plane, so that the full height of the crystals (~5 mm) can be used. The observed spectra are two-dimensional and to capture them with highest resolution we use x-ray film (Kodak DEF 392) as the detecting medium. Because of the Doppler shift, the x-rays emitted by

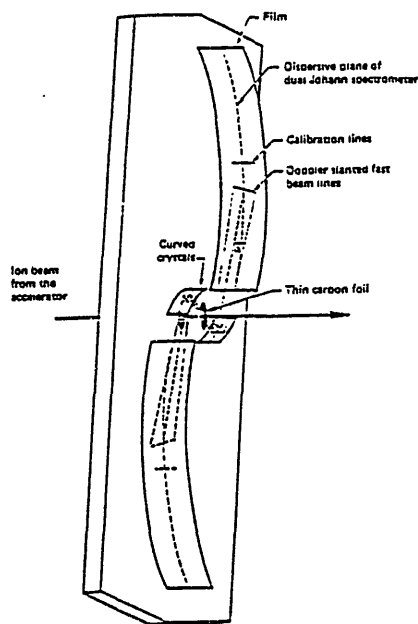


Fig. 1 Diagram of the LLNL dual Johann crystal spectrometer.

the fast ions in the lab frame do not have a unique wavelength, but rather a wavelength correlated with the emission angle α with respect to the perpendicular to the beam direction,

$$\lambda = \gamma\lambda_0 (1 - \beta\sin\alpha)$$

This means that the ion lines on the film will be slanted with respect to stationary calibration lines as shown in Fig. 1. The film position with respect to the central instrument plane can be determined by observing shadows of prepositioned wires. Any deviation of the spectrometer from perpendicularity to the beam line can be taken out by averaging the wavelengths on both sides of the instrument -- since the two Rowland circles are coplanar, a blue shifted line on one side will be cancelled by a red shifted line on the other in averaging. The average wavelength, $\lambda = \gamma\lambda_0$, can then be corrected to the true wavelength at rest by measuring the beam velocity accurately to determine γ . The instrument actually comprises two interchangeable dual spectrometers; a 30-cm Rowland circle spectrometer with Bragg angle coverage of 30°-65°, and a 1-m device with θ_B ranging from 10° to 18°.

An example of a typical fast ion spectra, showing lines from Bi⁺⁷³ as well as stationary calibration lines is shown in Fig. 2.

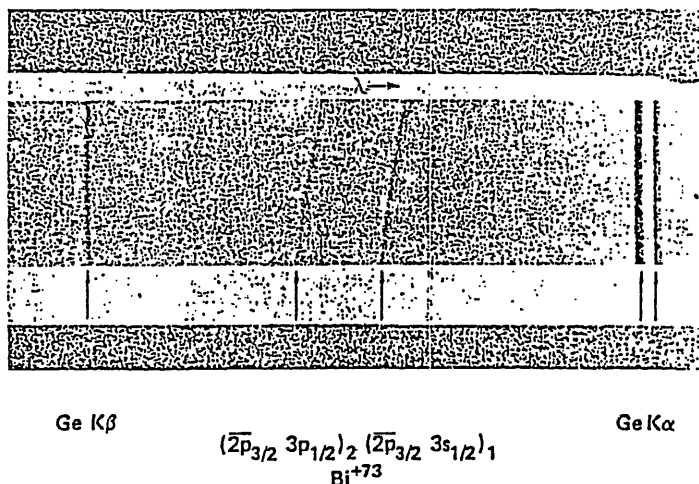


Fig. 2. Example of raw film data showing lines from neon-like Bi (slanted) together with germanium calibration lines (straight).

In our most recent experiment at GSI we have measured the $n = 3 \rightarrow 2$ spectra of Ne-like Bi and Au (Bi^{+73} and Au^{+69}). A partial level diagram of the 10 electron bismuth system, showing the transitions we expected to observe is shown in Fig. 3. Note that in addition to the "allowed" Δl transitions, the E2, $J=2-0$ p-p transitions have large enough transition rate at this high Z to be observed in the viewing region after the foil. The dispersing crystal in this experiment was Ge 220 which gave a coverage of 10-15 keV with the $1m$ ($\theta = 10^\circ - 18^\circ$) instrument, sufficient to observe all the $n=3-2$ lines.

The experiment ran with beam currents of 5-10 pA, and it took approximately five hours to get a reasonable exposure on the film. An example of a typical digitized output from the 2-d film spectrum is shown

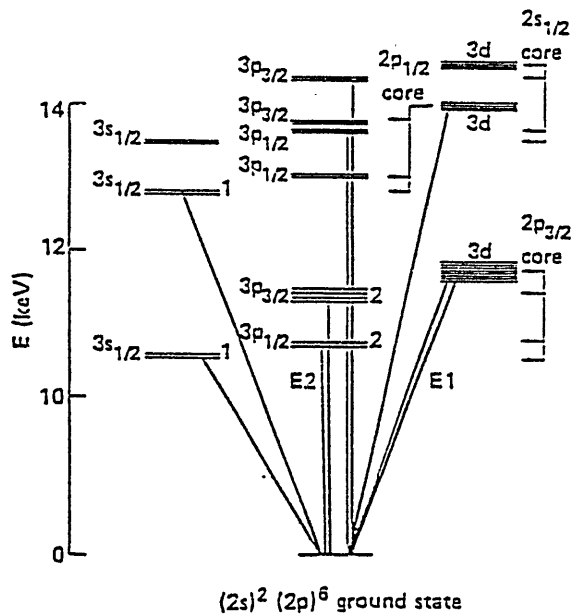


Fig. 3 Level diagram for n=3 and n=2 states of Bi⁺⁷³ showing transitions we expect to see.

in Fig. 4 with line identifications showing the Bi⁺⁷³ transitions expected in Fig. 3. The spectra are dominated by radiation from the

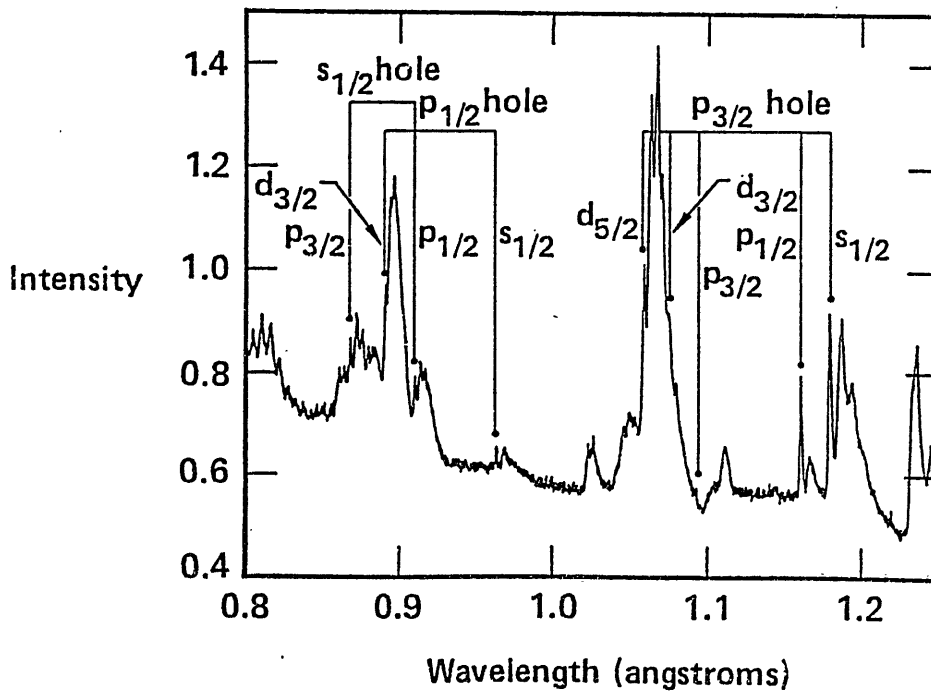


Fig. 4 Experimental spectrum with Bi⁺⁷³ lines identified.

lower (Na- and Mg-like) states in the beam, but the neon-like lines are nonetheless clearly visible.

The absolute accuracy to which the strongest lines are determined is 4 eV, or 400 ppm, limited principally by the determination of the central plane wire shadows. The relative accuracy of the positions of lines is much better, 1 eV or 100 ppm.

The energy levels in the Bi^{+73} can be calculated using one of several multi-electron codes. Chen and Scofield¹⁷ have evaluated this system using the code of I. P. Grant,¹⁸ which explicitly calculates the various QED corrections to the energy levels. This code also contains a phenomenological correction to handle the screening contributions of inner shell electrons to the QED self-energy terms. The results of running the code both with the phenomenological screening correction and without screening, using simple hydrogenic QED terms, are shown in Table I. The theoretical calculations are compared with our preliminary

Upper State (HOLE/ELEC) _J	Expt. (eV)	Theory (MCDF-S)	Theory (MCDF-H)	Expt-Theor (MCDF-S)	(MCDF-H)
(2P _{3/2} 3s _{1/2}) ₁	10508(4)	10507.4	10507.7	0.6(4.0)	0.3
(2P _{3/2} 3p _{1/2}) ₂	10679(4)	10678.9	10677.0	0.1(4.0)	2.0
(2P _{3/2} 3p _{3/2}) ₂	11344(10)	11349.2	11347.2	-5.2(10.)	-3.2
(2P _{3/2} 3d _{3/2}) ₁	11534(11)	11530.7	11528.2	3.3(11)	5.8
(2P _{3/2} 3d _{5/2}) ₁	11719(4)	11725.9	11723.5	-6.9(4.)	-4.5
(2P _{1/2} 3s _{1/2}) ₁	12872(5)	12872.1	12872.3	-0.1(5.)	-0.3
(2P _{1/2} 3d _{3/2}) ₁	13925(6)	13928.4	13926.0	-3.4(6.)	-1.0
(2s _{1/2} 3p _{1/2}) ₁	13625(6)	13633.1	13627.1	-8.1(6.)	2.1
(2s _{1/2} 3p _{3/2}) ₁	14296(7)	14300.2	14294.2	-4.2(7.)	1.8

(MCDF-S) -- THEORY USING SCREENED SELF ENERGY

(MCDF-H) -- THEORY USING HYDROGENIC SELF ENERGY

Table I. Comparison of our preliminary data on Bi^{+73} 3→2 energies with theory.

experimental results in Table I. A very interesting result can be seen immediately: the hydrogenic corrections give generally better agreement with the preliminary experimental data than the results using phenomenological screening!

The QED corrections to the experimentally observed lines in this system are largest for levels where an electron is excited out of the 2s state. For example, even with screening, the 2s3p levels have radiative corrections of about -28 eV, arising from self-energy (Lamb shift) corrections of ≈ -36 eV and vacuum polarization terms of $\approx +8$ eV. Since the experiment can determine these lines to a relative accuracy of 1 eV, we can in principle determine the Lamb shift at $Z=83$ to 3%. However, we are presently limited by theory, which can be seen from Table I to be currently able to get things to about 5 eV with some uncertainty about how the screening works. However a 5 eV Lamb shift measurement at $Z=83$ is still a fairly strong test of the QED higher order terms -- at about the same level as the U^{+90} measurement.

If there were real problems with QED we might expect to see difficulties with the neutral atom K x-ray energies. These can be measured quite precisely,¹⁴ but it's not easy to say how well the theory¹⁹ can calculate such things. Our results, and future experiments along these lines, can hopefully bridge the gap between spectroscopic measurements on hydrogen-like and neutral high Z systems.

One interesting aspect of the data is that the p-p E2 transitions allow us to imply values for n=3-3 transitions which begin or end on these states. This analysis was used in our earlier Xe experiments and also applies here, although the $\overline{2p_{3/2}3p_{3/2}}$ line observed in Bi^{+73} is anomalously weak when compared to the Xe experiment.

Data for Au^{+69} are presently being analyzed.

In conclusion, by concentrating on the spectroscopy of very highly ionized neon-like systems, we have arrived at results which pose interesting problems for the theory of few electron systems, particularly

the treatment of screening, and which provides one of the strongest tests of high field ($\alpha Z > 0.5$) QED.

Acknowledgment

Work performed in part under the auspices of Gesellschaft für Schwerionenforschung (GSI), and the U.S. Department of Energy by Lawrence Livermore National Laboratory under contract #W-7405-Eng-48. We would like to thank the staff of GSI and J. Geier, D. Leneman and R. Morales for their help in this experiment.

References

1. J. P. Briand, M. Tavernier, P. Indelicato, R. Marrus and H. Gould, Phys. Rev. Lett. 50, 832 (1983).
2. P. Richard, *et al.*, Phys. Rev. A. 29, 2939 (1984).
3. M. Taverier, J. P. Briand, P. Indelicato, D. Liesen and P. Richard, J. Phys. B. 18, L327 (1985).
4. R. D. Deslattes, R. Schuch and E. Justiniano, Phys. Rev. A. 32, 1911 (1985).
5. H. F. Beyer, R. D. Deslattes, F. Folkmann and R. E. LaVilla, J. Phys. B18, 207 (1985).
6. E. Källne, J. Källne, P. Richard and M. Stöckli, J. Phys. B17, L115 (1984).
7. P. Mohr, Atomic Data and Nucl. Data Tables 29, 453 (1983).
8. W. R. Johnson and G. Soff, Atomic Data and Nucl. Data Tables 33, 405 (1985).
9. H. Gould and C. Munger, ICAP-X Abstracts (Tokyo, 1986) p. 10.

10. H. Beyer, Proceedings of this seminar.
11. D. Matthews, et al., Phys. Rev. Lett. 54, 110 (1985).
12. P. Beiersdorfer, et al., Phys. Rev. A. 34, 1297 (1986).
13. J. Bailey, et al., submitted to J. Phys. B. (UCRL preprint 92620).
14. E. G. Kessler, Jr., et al. Phys. Rev. A. 26, 2696 (1982).
15. D. Dietrich, et al., Phys. Rev. Lett. 54, 1008 (1985).
16. C. J. Hailey, et al., J. Phys. B18, 1443 (1984).
17. M. H. Chen and J. Scofield, private communication.
18. I. Grant, Nucl. Inst. and Meth B9, 471 (1985).
19. M. H. Chen, B. Crasemann, Nils Martenson, B. Johansson, Phys. Rev. A.31, 556 (1985).

245F/jg

Target thickness dependence of $K\alpha$ satellite intensities
of Argon ions colliding with thin carbon foils

T. Mizogawa, Y. Awaya, T. Kambara, Y. Kanai, M. Kase,
H. Kumagai, P. H. Mokler,* and K. Shima**

The Institute of Physical and Chemical Research (RIKEN),
Wako, Saitama 351-01, Japan

*GSI, D-6100 Darmstadt, West Germany

**Tandem Accelerator Center, University of Tsukuba,
Ibaraki 305, Japan

Target-thickness dependent measurements of X rays emitted in collisions of fast heavy ions and solid targets have been recognized to be important technique to study the inner-shell processes of heavy ions in solids, where the relaxation times of excited states are not short enough compared to a mean collision interval. With respect to K-shell, such experimental data have been analyzed by using the two- or three-component model, which contains several fixed parameters (vacancy formation cross section, fluorescence yield, lifetime of vacancy, and cross section of electron capture to K-vacancy) to be determined to reproduce experimental data.¹⁾ Such a model is, however, inadequate even for K-shell, at least in the thickness region where the equilibrium of L-shell is not attained, because some parameters assumed to be constant are actually depend on the target thickness through the change of L-shell configuration. Here we report our high-resolution X ray measurements as a function of target thickness and projectile charge state, and show the importance of the effect of L-shell configuration on K-vacancy formation.

Target-thickness dependence of Ar $K\alpha$ satellite intensities from Ar⁴⁺ ions colliding with thin C foils of which thicknesses were 2 - 100 $\mu\text{g}/\text{cm}^2$ was measured. For Ar^{6+,12+,13+}, the thickness dependence was measured over the region 2 - 20 $\mu\text{g}/\text{cm}^2$ where L-shell non-equilibrium region is

contained, and for Ar^{11+} only one (thinnest) target was examined. Experimental set-up is shown in Fig. 1. 50 Mev Ar ions from the RIKEN linear accelerator were used and Ar K x-ray spectra were measured by using a broad-range crystal spectrometer.²⁾ The product of target thickness and a number of incident particles was monitored by counting recoil C atoms with a surface-barrier detector (SBD). The ions passed through the target were stripped again by a $20 \mu\text{g}/\text{cm}^2$ C foil for the ions to be brought into charge equilibrium, and finally collected with a Faraday cup to determine the number of the incident ions.

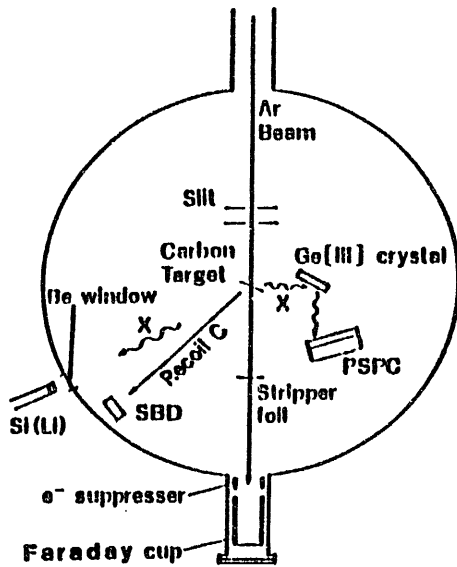
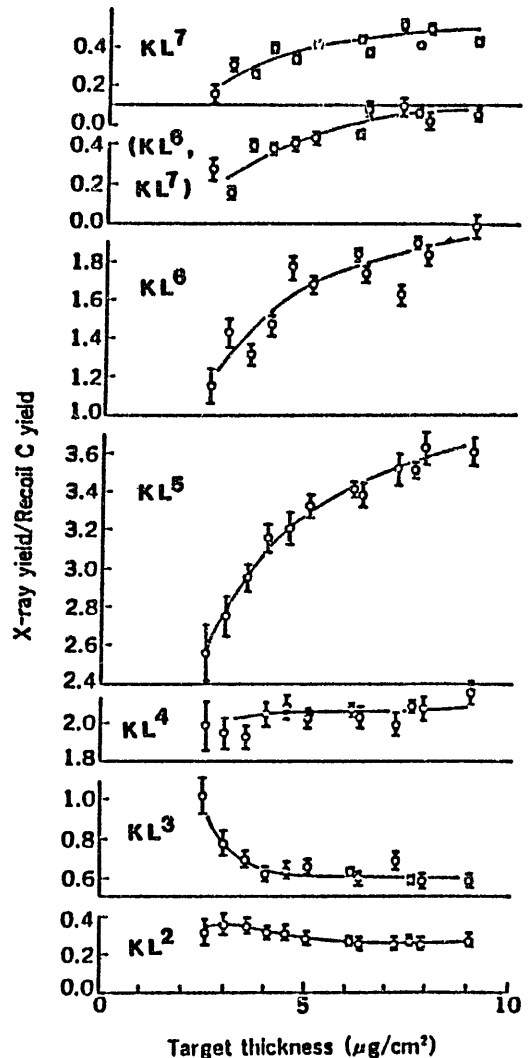


Fig. 1. Experimental set-up.

Fig. 2. Target-thickness dependence of K_{α} satellite intensities. Error bars indicate statistical errors only. Solid lines are drawn only for eye-guide.



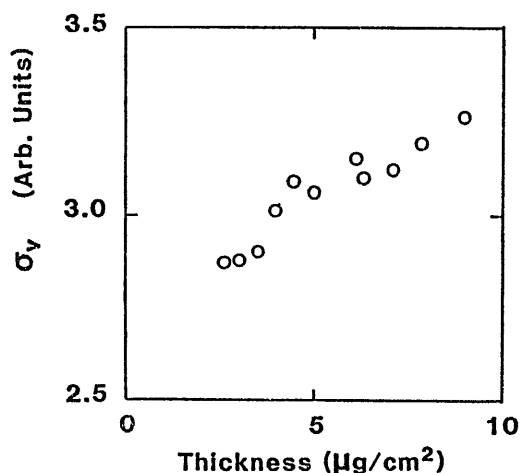
A part of the results for Ar^{4+} is shown in Fig. 2. The vertical scale is the intensity of each satellite divided by recoil C yield, i. e. the value proportional to X-ray

production cross section for each satellite. It can be seen that the high-energy group of the satellites grows with an increase in target thickness, and the low-energy group tends to decrease. Such behavior cannot be understood by the two- or three-component model. It will be explained by 1) the increase of L-holes with the thickness and 2) the increase of K-vacancy formation cross section itself with the thickness. The latter can be caused by the enhancement of K-L excitation due to the increase of L-holes. Using our data and the calculated values of fluorescence yield and transition rate for each defect configuration,³⁾ we can estimate the average K-vacancy formation cross section σ_v as a function of the target thickness. For thin target ($\lesssim 10 \mu\text{g}/\text{cm}^2$) we tentatively assume that the collisional quenching of K-hole is negligible. Thus

$$\sigma_v = \sum_n \sigma_x(n)/\omega(n) .$$

where $\sigma_x(n)$ and $\omega(n)$ are average X ray production cross section and fluorescence yield, respectively, for n-th satellite. In Fig. 3 σ_v for Ar^{4+} are plotted against C thickness. The increase of σ_v with the thickness is considered to be due to K-L excitation. If the collisional quenching is taken into account, the increase of σ_v may be further enhanced. The results for Ar^{6+} show essentially same feature as Ar^{4+} .

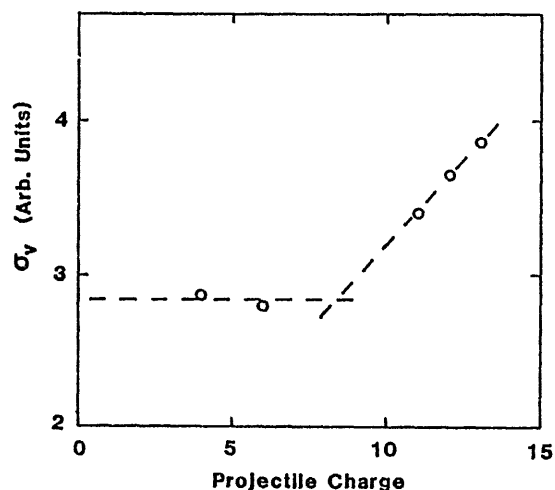
Fig. 3. σ_v for Ar^{4+} as a function of target thickness.



In Fig. 4 σ_V for the thinnest target ($\sim 2.6 \mu\text{g}/\text{cm}^2$) is plotted as a function of projectile charge state. The values for Ar^{4+} and Ar^{6+} are approximately same, whereas σ_V for Ar^{11+} , Ar^{12+} , and Ar^{13+} seem to increase linearly with the charge. The bend is near $8+$, just before the start of L-hole existence. This increase of σ_V is further evidence of the effect of L-hole existence on K-vacancy formation. If extremely thin target can be examined, more drastic increase of σ_V will be observed. Therefore the increased part of σ_V is considered to be lower-side estimate of K-L excitation cross section.

Full analysis of our data is still in progress.

Fig. 4. σ_V as a function of incident charge for the thinnest target ($2.6 \mu\text{g}/\text{cm}^2$).



References

- 1) See for example, H.-D. Betz, F. Bell, H. Panke, G. Kalkoffen, M. Welz, and D. Evers, Phys. Rev. Lett. 33, 807 (1974).
- 2) A. Hitachi, H. Kumagai, and Y. Awaya, Nucl. Instr. Meth., 195, 631 (1982).
- 3) C. P. Bhalla, Phys. Rev. A8, 2877 (1973).

K-ELECTRON CAPTURE FROM TARGET ATOMS BY ^3He IONS

I. Katayama, M. Fujiwara, T. Noro, H. Ikegami, F. Fukuzawa*, K. Yoshida*,
Y. Haruyama**, A. Aoki**, H. Ogawa*** and K. Sugai****

RCNP, Osaka Univ., Mihogaoka, Ibaraki, Osaka 567

*Dept. of Nuclear Engineering, Kyoto Univ., Sakyo-ku, Kyoto 606

**Lab. of Applied Physics, Kyoto Prefectural Univ., Kyoto 606

***Dept. of Physics, Nara Women's Univ., Nara 630

****INS, Univ. Tokyo, Midoricho, Tanashi, Tokyo 188

Abstract: By using 72 and 52 MeV $^3\text{He}^{2+}$ beams, electron capture from Ag and Sn target K shells has been successfully measured with a high resolution magnetic spectrograph. The results are reasonably well explained by eikonal approximations.

Inner shell electron capture at intermediate energies remains to be studied both theoretically and experimentally. Electron capture at asymptotically high energies, on the contrary, has been well explained by a second order plane wave Born approximation and at low energies by a perturbed stationary state model¹⁾. At intermediate energies where the cross section increases to the maximum, electron capture becomes highly complicated process to be understood, which is a reason for the emergence of several theoretical treatments. Among them are the full peaking of the strong potential Born (SPB) by Macek et al.^{2,3)}, the transverse peaking in the SPB by Alston⁴⁾, another approximation in the SPB by McGuire et al.⁵⁾ and an eikonal approximation by Eichler⁶⁾. Our present experiment is intended to provide data to test these theories. It is also our intention that the present data may help in theoretical investigation of the inner shell shielding problem, which is normally discussed with an effective charge, in electron capture process⁵⁾.

The $^3\text{He}^{2+}$ beams were employed in the present experiment. This is because they allow us to use the largest projectile velocity among available particles of which electron capture products have charge to permit the energy analysis using a magnetic spectrograph. Details of our method and Sn data were already reported elsewhere⁷⁾. Some details of the Ag data are reported here. The $^3\text{He}^{2+}$ beams were accelerated and extracted from the

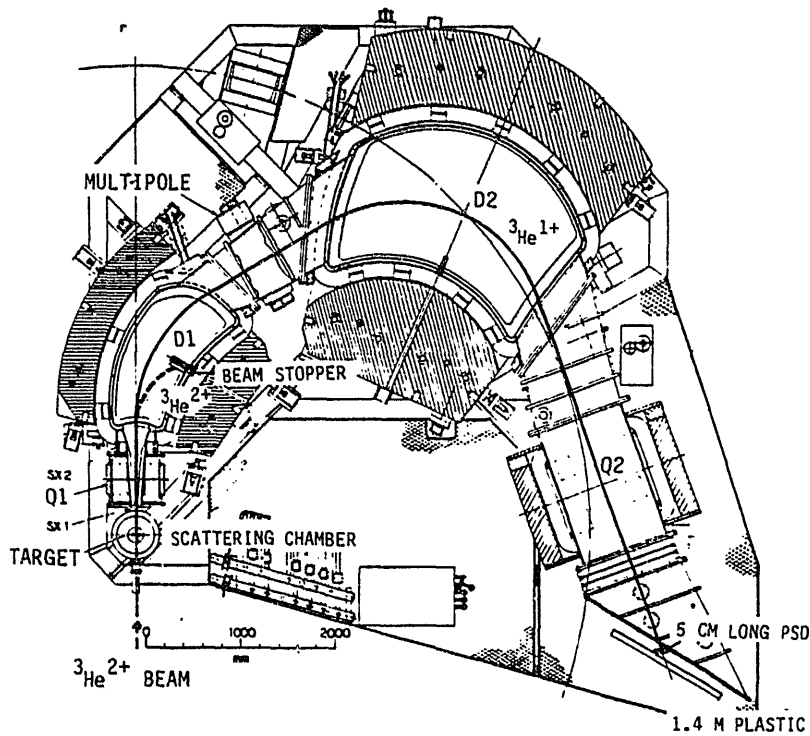


Fig. 1. Present experimental arrangement using the high resolution magnetic spectrograph RAIDEN at RCNP, Osaka University.

AVF cyclotron at RCNP, Osaka University. Momentum analyzing system of the beam which consists of two 90 degree magnets is designed to give the energy resolution of $\Delta E/E = 1 \times 10^{-4}$ on the target. Fig. 1 shows the present experimental arrangement using the magnetic spectrograph RAIDEN⁸⁾. The spectrograph was used at zero degree. The magnetic field was adjusted to measure electron capture product ${}^3\text{He}^{1+}$ and the ${}^3\text{He}^{2+}$ beams were stopped at an insulated aluminium plate inside the first dipole magnet. The focal plane counter was a 5 cm long position sensitive semiconductor detector (PSD), later replaced by a 2 cm long drift counter. The target thickness dependences of ${}^3\text{He}^{1+}$ total yields obtained are shown in fig. 2a for the Ag target case, from which electron loss cross sections (fig. 2b) and electron capture cross sections (fig. 2c) were deduced. Theoretical work by N. Bohr for electron loss (second equation in ref. 9 employed) and Nikolev's work for total capture cross sections¹⁰⁾ as well as high energy data from Jülich¹¹⁾ are also shown for comparison. Fig. 3 shows the energy spectrum of ${}^3\text{He}^{1+}$ from ${}^3\text{He}^{2+} + \text{Ag} \rightarrow {}^3\text{He}^{1+} + \text{Ag}^*$ process at 72 and 52 MeV measured by using the PSD. A deconvolution to deduce the K shell component was performed using the ${}^3\text{He}^{1+}$ line of the pure carbon target as a response curve. Note that the low energy tail of the carbon response curve had to be

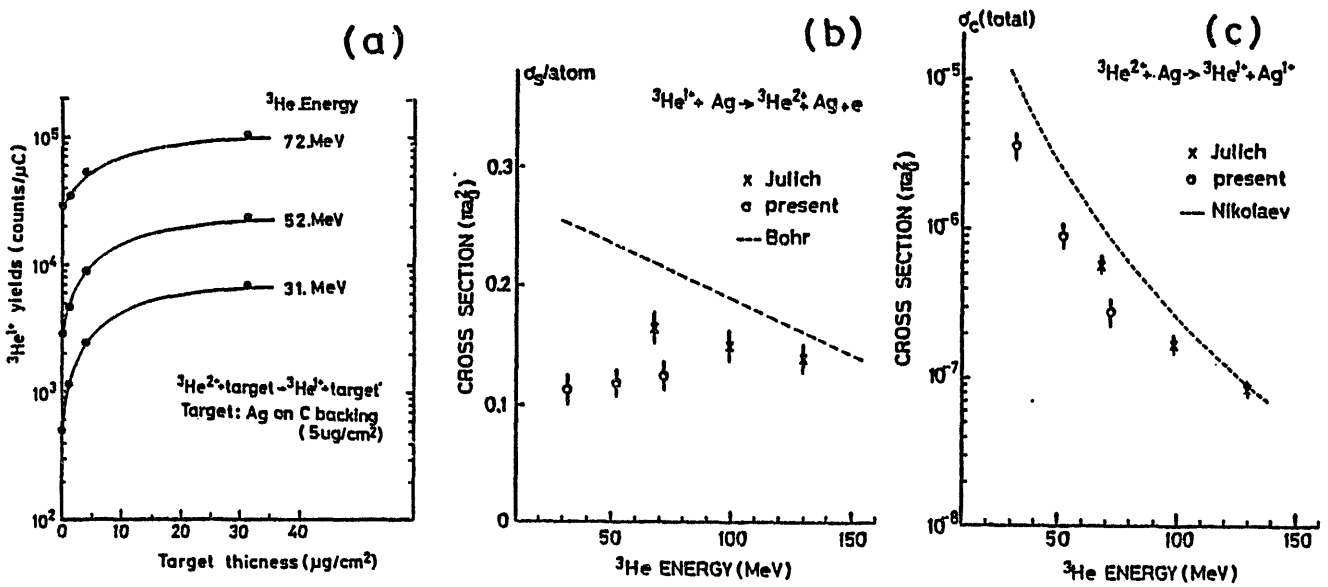


Fig. 2. (a) Target thickness dependence of ${}^3\text{He}^{1+}$ yields for Ag target. (b) Electron loss cross sections obtained from the curves in (a). The dashed line shows the result calculated by using Bohr's second formula⁹. (c) Total electron capture cross sections obtained from the curves in (a). The dashed line shows the results of Nikolaev's OBK calculations for L+M shells¹⁰. High energy data in (b) and (c) are taken from ref. 10.

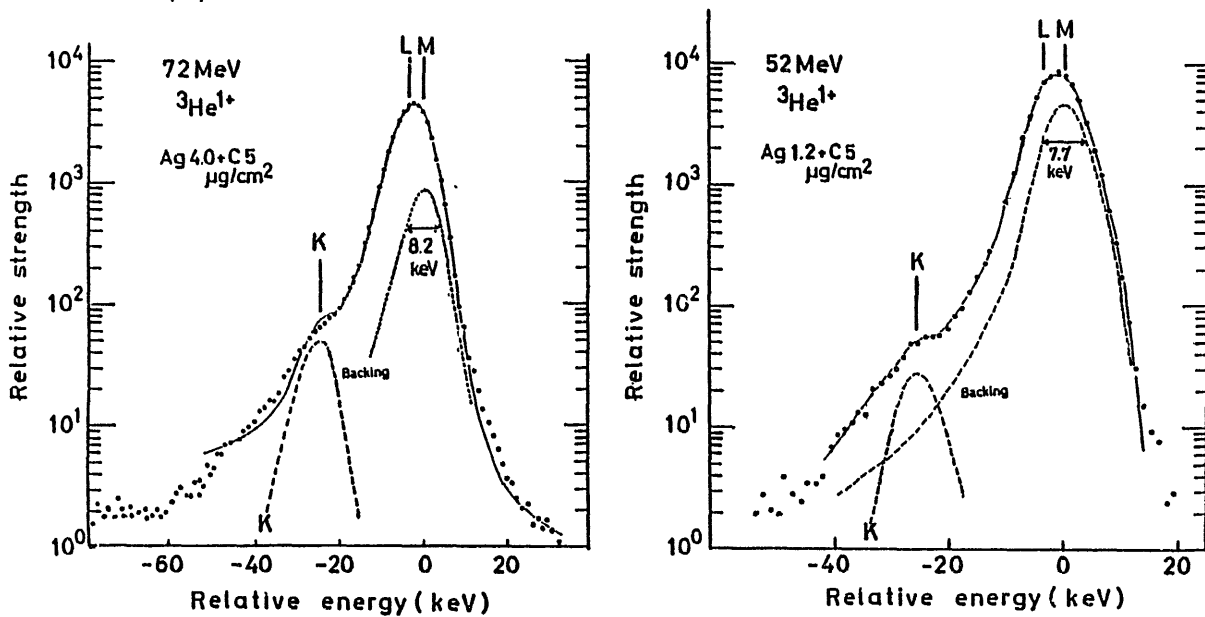


Fig. 3. Energy spectra of electron capture products ${}^3\text{He}^{1+}$ for Ag target measured by using the spectrograph RAIDEN. The contribution of the K shell and C backing is shown together with the final fitting result.

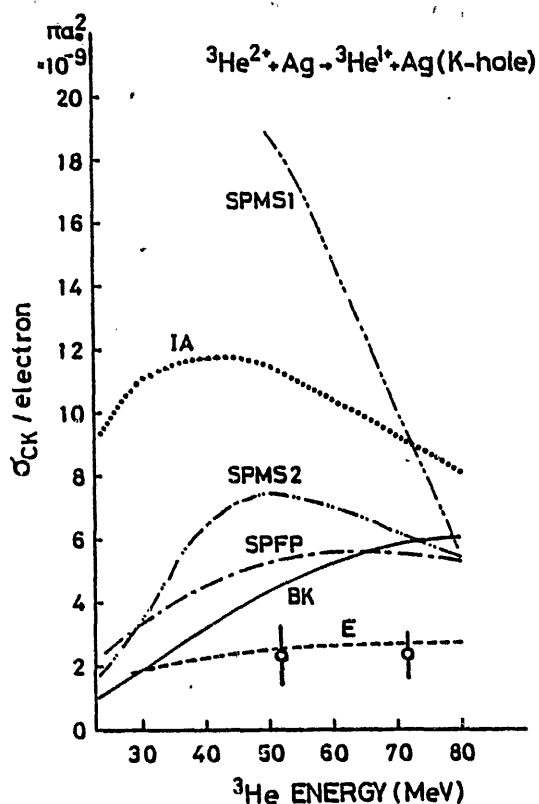


Fig. 4. Comparison of the present data with theoretical results for K shell electron capture of ${}^3\text{He}^{2+}$ from Ag target. SPFP is the full peaking SPB calculations by Macek et al.^{2,3)}. SPMS1,2 are the SPB calculations by McGuire et al.⁵⁾. E is the eikonal approximation by Eichler⁶⁾. I is the impulse approximation by Briggs¹²⁾. BK is the first order calculation by Brinkman-Kramers¹³⁾.

slightly increased at 52 MeV so as to explain the spectrum. The deconvolution result is also shown in the figure. The contribution of carbon backing was determined from the thickness dependence of the ${}^3\text{He}^{1+}$ total yield (fig. 2a). The ${}^3\text{He}$ energy dependence of the K shell electron capture cross sections is shown in fig. 4 in comparison with several theoretical calculations.

It should be mentioned that further accumulations of data and considerations on the deconvolution procedure have brought us to the conclusion that the 52 MeV result in ref. 7 should be changed to the present one. The Sn result in ref. 7 at 52 MeV is also reduced by a factor of two. With revised results for Ag and Sn at 52 MeV, the velocity dependence of the present data seems to be explained reasonably well by the eikonal approximation.

We acknowledge Dr. S. Morinobu for his cooperation at early stage of the experiment and Profs. J.H. McGuire and J. Eichler for sending us the SPB calculations and eikonal calculations.

References

- 1) J. Briggs, J. Macek and K. Taulbjerg, *Comments At. Mol. Phys.* 12 (1982) 1.
- 2) J. Macek and K. Taulbjerg, *Phys. Rev. Lett.* 46 (1981) 170.
- 3) J. Macek and S. Alston, *Phys. Rev.* A26 (1982) 250.
- 4) S. Alston, *Phys. Rev.* A27 (1983) 2342.
- 5) J.H. McGuire, R.E. Kletke and N.C. Sil, *Phys. Rev.* A32 (1985) 815.
- 6) J. Eichler, *Phys. Rev.* A23 (1981) 498.
- 7) I. Katayama, M. Fujiwara, S. Morinobu, T. Noro, H. Ikegami, F. Fukuzawa and K. Sugai, the Proceedings of the Second Asia-Pacific Physics Conf. held at Bangalore, India in 1986 (to be published).
- 8) H. Ikegami, S. Morinobu, I. Katayama, M. Fujiwara and S. Yamabe, *Nucl. Instr. Methods* 173 (1980) 335.
- 9) N.K. Bohr, *Danske Vidensk. Selsk., Mat.-Fys. Meddr* 18 (1948) No.8.
- 10) V.S. Nikolaev, *Sov. Phys. JETP* 24 (1967) 847.
- 11) I. Katayama et al., preprint (to be published).
- 12) J.S. Briggs, *J. Phys.* B10 (1977) 3075.
- 13) M.R.C. McDowell and J.P. Coleman, Introduction to the Theory of Ion Atom Collision (Amsterdam, North Holland, 1970) ch.8.

WHAT IS NEW IN CONVOY ELECTRON PHYSICS?*

I. A. Sellin

University of Tennessee, Knoxville, TN 37996,
and Oak Ridge National Laboratory, Oak Ridge, TN 37830, USA

In preference to attempting to review the already voluminous literature¹ concerning electron capture (ECC) and loss (ELC) to continuum states in ion-atom and ion-solid collisions -- referred to here under the collective term convoy electron production -- space and time constraints suggest a wiser course. I choose to focus on the rapid advances in understanding that have occurred in the past year owing to the development of new and powerful techniques^{2,3} for making doubly differential measurements of convoy electron distributions having comparably high resolution in longitudinal and transverse components of electron ejection velocity in the projectile rest frame.

By now familiar to most of us is the sharp cusp in the velocity spectrum of electrons observed when the ejected electron velocity \vec{v}_e matches that of the emergent ion \vec{v}_p in both speed and direction. Although the occurrence of a cusp is simply a signature of the Coulomb interaction, the shape depends on the contributions of individual partial waves to a multipole (P_κ) expansion of the cross section and thus is sensitive to fine details of the collision dynamics. For high \vec{v}_p , ECC cusps typically differ from ELC cusps by virtue of greater longitudinal spread and large dipole moments¹⁻³ parallel to \vec{v}_p . Corresponding ELC cusps have larger transverse spreads characterized by even κ : P_2, P_4, \dots . By continuity these multipole distributions are also predicted for similar collisions in which high Rydberg states are populated.

Until very recently most ECC and ELC measurements have been effectively singly differential, even though collection cones of $\sim 1^\circ$ near 0° were used. To get a more accurate picture of the shape of the doubly differential cross section, it is desirable to subdivide this cone so that the effective angular resolution corresponds to a differential slice in

transverse electron velocity \vec{v}_{et} of a size comparable to that of the longitudinal slice, centered on a particular \vec{v}_{el} fixed by the analyzer pass energy and resolution chosen. A straightforward angular-scanning method employing spectra obtained as a function of stepwise changes in collection angle has been used by Meckbach et al.³ for this purpose. The alternative method used in our laboratory employs a position-sensitive detector to simultaneously collect data at all polar and azimuthal emission angles from $\theta = 0$ to 5° and $\phi = 0$ to 360° in an array of 256×256 pixels. The key advantage of our method is its speed.

Figure 1 displays sample data concerning the κ distribution observed

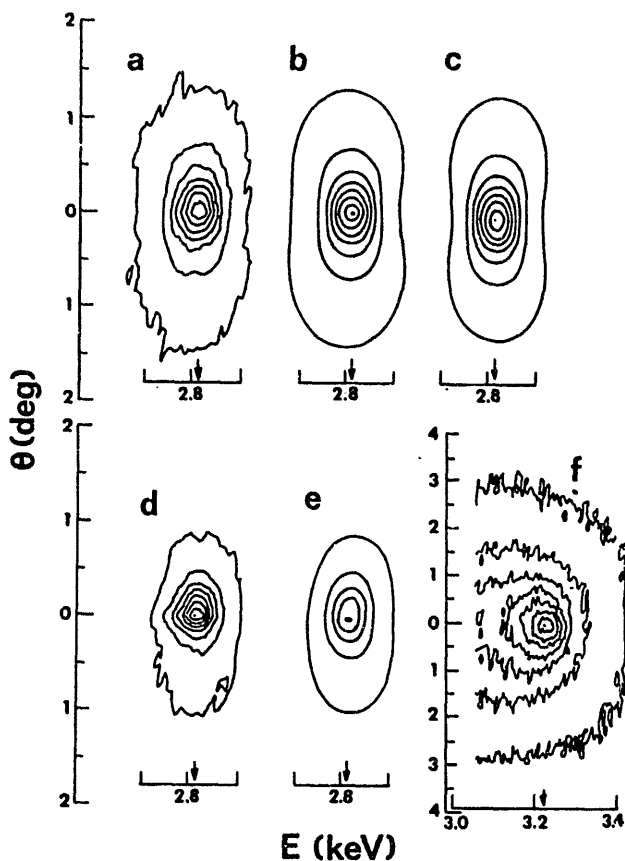


Fig. 1. Contour plots for ELC by O^{5+} in Ar and He at $\vec{v}_p = 14.4$ a.u., and ECC by O^{8+} in Ne at 15.4 a.u. Contours shown represent multiples of 12.5% of peak height. The horizontal scale indicates laboratory-frame electron energy; the vertical scale indicates electron ejection angle. Isotropic angular distributions would have nearly circular contours. (a) Measured distribution for Ar target. (b) Corresponding fit to (a), normalized to the peak height of the data. (c) Theoretical distribution (Ref. 4) after convolution with analyzer acceptance. (d) Measured distribution for He. (e) Fit for (d), normalized to the peak height of (d). (f) ECC distribution for O^{8+} in Ne.

for electrons ejected by $\vec{v}_p = 10.1, 14.4, \text{ and } 16.2 \text{ a.u.}$ O^{5+} ions undergoing single collisions in He and Ar². As expected from Burgdörfer's theory⁴ the distribution is dominated by ELC from the loosely bound $n = 2$ levels by an order of magnitude compared to the combined contributions from ECC and K-shell ELC. For $n=2$, the doubly differential cross section is given by

$$d\sigma/dv = (\sigma/v) [1 + \beta_2 P_2(\cos\theta) + \beta_4 P_4(\cos\theta)].$$

There can be no doubt concerning the strongly transverse character of the ELC angular distributions: the presence of appreciable P_2 and P_4 multipole strengths is confirmed; and a striking contrast with the strong dipole character of the ECC distribution illustrated for 15.4-a.u. O^{5+} in Ne is seen. Also plotted is the theoretical angular distribution for ELC in Ar, after convolution with a reasonable approximation to the spectrometer acceptance function.

Figure 2 displays sample data⁵ concerning the κ distribution observed

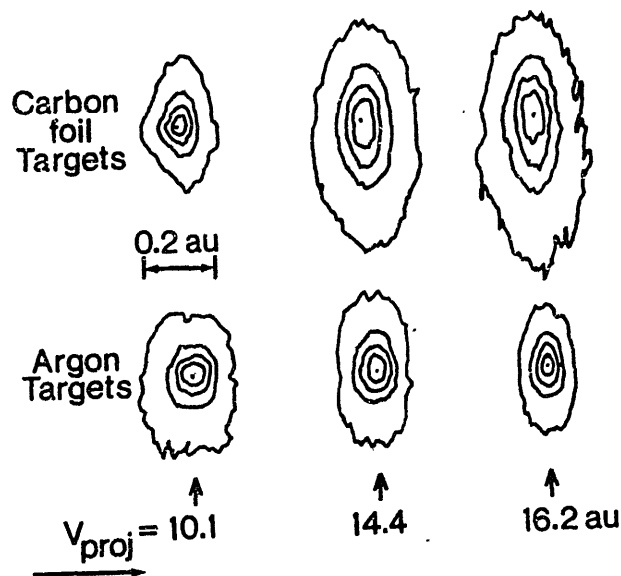


Figure 2. Contour plots of velocity distributions for convays produced in thin C targets vs. those for ELC in Ar. Contour levels shown represent intervals of 20% of each peak height. Longitudinal and transverse velocity components are represented horizontally and vertically, respectively, with equal velocity scales for all figures; 0.2 au is shown. Numbers at bottom of figure indicate v_p . Isotropic angular distributions would have circular contours.

for convoy electrons from thin C targets together with corresponding data for O^{5+} ions undergoing ELC in Ar at equal \vec{v}_p values. The striking resemblance contrasts markedly with typical ECC distributions, whose strong dipole content is absent. Table 1 compares measured multipole coefficients β_κ with corresponding experimental and theoretical values for ELC from isotachic O^{5+} projectiles on Ar. The quantity $B_\kappa \equiv \beta_\kappa(\text{convoy})/\beta_\kappa(\text{ELC})$ highlights the extent to which high κ values for convoy distributions from solid targets rise beyond those for ELC values. Though there is strong resemblance between ELC and convoy distributions, there are also important differences: the enhanced κ characteristic of convoy distributions in solid targets is seen to be a steeply rising function of \vec{v}_p .

If one applies ELC theory formulated for ion-atom collisions to convoy electron production in solids, this skew toward higher κ may be viewed as evidence for high n state populations in the penetrating ions. In this picture excited ions signal their presence by giving birth to convoy electron distributions of corresponding high κ . Either excitation or capture to excited n, l states would then precede ELC. The relative importance of high κ would be enhanced for high n and l , because ELC cross sections rise rapidly with increasing orbital size and decreasing binding energy E_b . If this interpretation is correct, the multipole content we observe is a quantitative measure of projectile ion n and l state populations during the short time (≤ 1 fs) of projectile penetration. An interesting question arises: is the κ content of the multipole distribution likely to change materially upon entry into vacuum? A negative answer, at least for the relatively high v_p beams of concern up to now can be given. In the sudden approximation, ionic bound states screened within the solid project onto atomic excited states in the vacuum. That the net phase change of each of the wave function components in the coherent superposition of electronic eigenstates describing a convoy state is likely to be small can be seen by considering a typical phase integral $\phi = \int \Delta E dt \approx (1/\vec{v}_p) \int \Delta E dx \approx 0.04$, a small value. Here ΔE is the size of the potential step (about 0.2 a.u.); the integration over path length dx extends over about 2 a.u. and $\vec{v}_p \geq 10$ a.u.

TABLE I. Comparison of β_k values for convoy distributions with those for ELC. Also shown are the even order coefficient ratios B_k defined in the text. The estimated uncertainties in B_k are ± 0.04 .

v_p (au)	Target	β_2	β_4	β_6	β_8	β_{10}
16.2	Carbon	-0.78	0.25	-0.32	0.19	-0.16
	Ar ^a	-0.68	0.13			
	Ar ^b	-0.70	0.18			
	B_k	1.1	1.9			
14.3	Carbon	-0.82	0.29	-0.26	0.07	-0.03
	Ar ^a	-0.62	0.12			
	Ar ^b	-0.67	0.16			
	B_k	1.3	2.4			
10.1	Carbon	-0.48	0.11	-0.18	0.09	-0.05
	Ar ^a	-0.26	0.05			
	Ar ^b	-0.56	0.10			
	B_k	1.8	2.2			

^aExperimental values from Reference 2.

^bTheoretical values from Reference 2,4.

How different results for light ions (H, He) at lower velocities (≥ 1 au) can be (and often are) is a point that has been mentioned in the past¹⁻⁵, has not generally been adequately appreciated by workers in the field, and which can scarcely be overemphasized. For light ions of low velocity it is physically very plausible to expect that secondary electron generation and scattering phenomena will be less dominated by the electronic charge of the accompanying ionic particle than in the fast heavy ion case, will be relatively more sensitive to solid state effects at, for example, the exit surface, and may well be qualitatively different owing to the longer time scale over which secondary electron distribution characteristics can adjust. For example, the adjustment to the potential step at the exit surface just discussed cannot then be expected to be either small or sudden.

Notable examples have been uncovered recently by Meckbach et al.⁶⁻⁸ in doubly differential studies of secondary electron spectra by hydrogenic particles in He and in thin foils of C, Al, and Au at ionic kinetic energies in the range 100-200 keV. For example, high resolution electron spectra for electrons ejected in the forward direction by protons and neutral hydrogen in collisions with He gas showed the expected convoy peak, but also showed a zero degree ridge extending to the lowest electron energies measured. The authors propose that this new secondary electron component represents electrons which propagate on the saddle of the potential surface produced by the two positive ions H^+ and He^+ in the intermediate collision complex. Figure 3 illustrates this result.

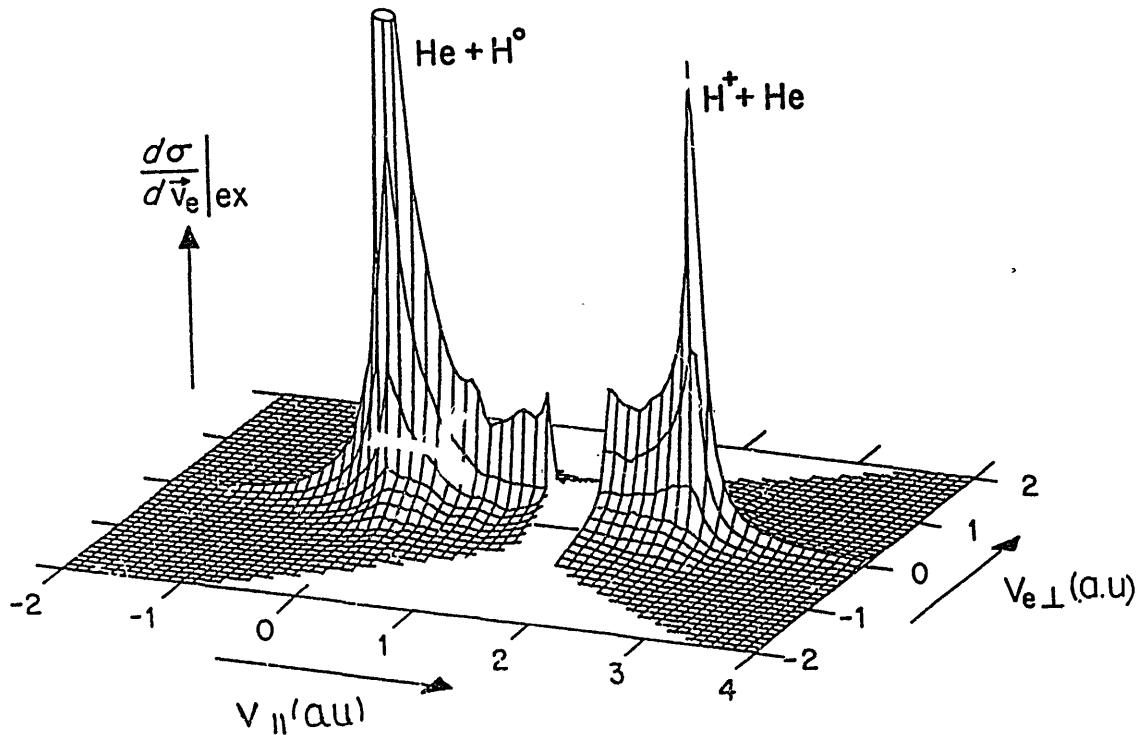


Figure 3. Combined velocity distribution of electrons produced in $H^+ + He$ and $He + H^0$ collisions. The data for $\vec{v}_e > 1.8$ au are for $H^+ + He$ collisions and include the ECC peak. The data for $\vec{v}_e < 1.5$ au are for $He+H^0$ collisions and include the peak due to direct ionization of H^0 at $\vec{v} = 0$. The two peaks are joined by a ridge of secondary electrons concentrated at zero transverse electron velocity. From Ref. 6.

In an even more remarkable example, Gofni et al. ^{7,8} presented doubly differential distributions of convoy electrons when 100 and 170 keV protons traversed thin carbon, gold and aluminum foils and compared them to those obtained with He targets. The ridge they attributed to electrons moving in the two Coulomb center potential saddle determined by the target and projectile ions, also appeared in the ion-solid convoy electron distributions. In addition two strong lateral humps also appeared, which were explained as due to diffraction of the ridge electrons in the polycrystalline foil material. Figure 4 illustrates these results.

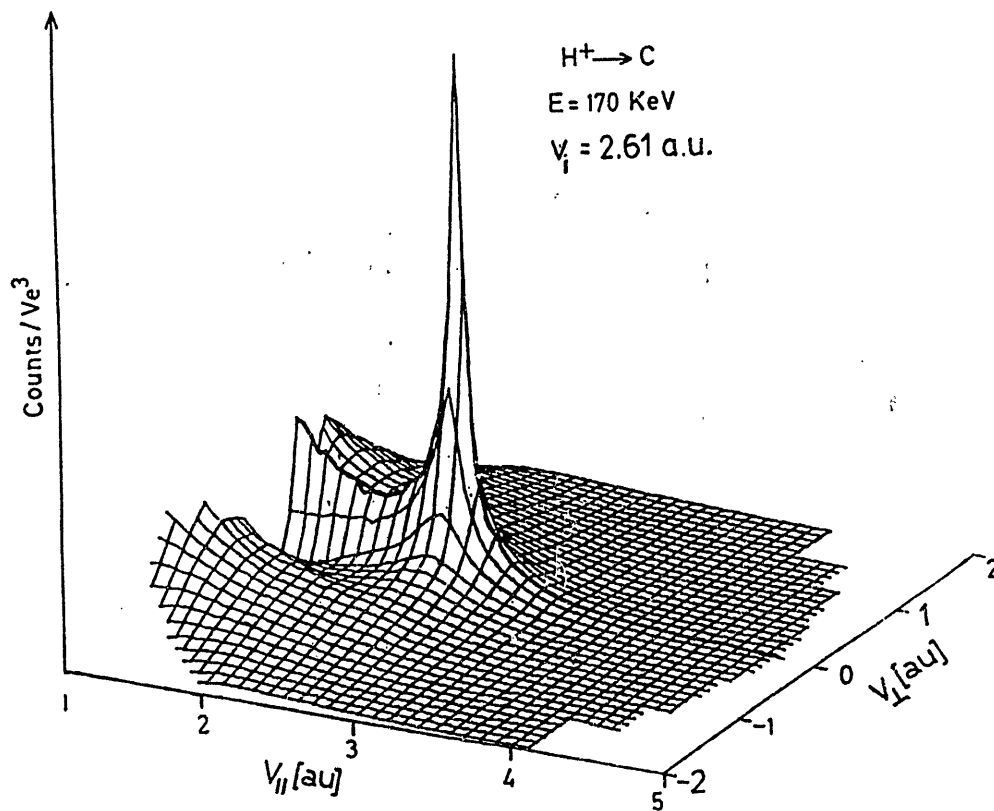


Figure 4. Doubly differential distribution of secondary electrons emitted when 170keV protons traverse a $5\mu\text{g}/\text{cm}^2$ carbon foil. Diffracted ridge electrons are claimed to be found in the lateral humps. Fro Refs. 7 & 8.

They also found that the diffraction of convoy electrons is impeded by their strong correlation to the moving ions. In the case of Al targets the observed "diffraction" was found to be typical for Al_2O_3 . This was interpreted as an indication that the observed electrons originate from a thin polycrystalline oxide layer close to the downstream surface of emission.

This work was supported by the National Science Foundation and the U.S. Dept. of Energy under contract No. DE-AC05-84OR21400 with Martin Marietta Energy Systems, Inc.

References

- 1) M. Breinig et al., Phys. Rev. A 25, 3015 (1982), and many reference therein; S. D. Berry et al., Phys. Rev. A31, 1392 (1985); and numerous authors in Forward Electron Ejection in Ion Collisions, edited by K. O. Groeneveld, W. Meckbach, and I. A. Sellin (Springer-Verlag, Heidelberg, 1984).
- 2) S. B. Elston et al., Phys. Rev. Lett. 55, 2281 (1985).
- 3) W. Meckbach et al., in Forward Electron Ejection in Ion Collisions, edited by K. O. Groeneveld, W. Meckbach, and I. A. Sellin (Springer-Verlag, Heidelberg, 1984).
- 4) See Ref. 2; also J. Burgdörfer, Z. Phys. A 309, 285 (1983); and J. Burgdörfer et al., Phys. Rev. A 28, 3277 (1983).
- 5) S. D. Berry et al., J. Phys. B 19, L149 (1986).
- 6) W. Meckbach et al., submitted to Phys. Rev. Letters.
- 7) A. R. Gofni et al., submitted to Phys. Rev. Letters
- 8) A.R. Gofni et al., submitted to Z. Phys. D.

Strong Forward-Backward Asymmetries in Electron Emission from
Overlapping Resonance States in Fast C^{3+} on He Collisions

Yasunori Yamazaki*

University of Tennessee and Oak Ridge National Laboratory

and

P.D.Miller, H.F.Krause, P.L.Pepmiller, S.Datz, I.A.Sellin,
and N.Stolterfoht**

Oak Ridge National Laboratory

Autoionizing electrons from the configuration $1s^2 2pnl$ produced by transfer and excitation were measured for 2.5-5.0 MeV C^{3+} + He-gas collision employing the method of zero-degree Auger spectroscopy¹⁾. The electron analyser was operated with an energy resolution of 300 meV (FWHM), which corresponds to the projectile rest frame energy resolution ~ 40 meV.

In figure 1, are shown the electron spectra referring the energy scale to the projectile rest frame for both the electrons emitted in forward (0°) and backward (180°) directions. Autoionization peaks corresponding to the Coster-Kronig transitions $1s^2 2pnl \rightarrow 1s^2 2s_\epsilon l'$ are clearly resolved up to $n=10$. For $n=5$ and 6 each group splits into several lines due to the quantum defect and the term splitting produced by the coupling of the nl electron with the $2p$ electron. At higher energies a step-like decrease at the series limit ($n \rightarrow \infty$) appear for ~ 8 eV. Surprisingly, for $n=5$ to 7 the fourth line in each group is strongly enhanced in the backward direction. At these peaks which show strong 90° asymmetry in projectile rest frame, it is found that two autoionizing states with opposite parities ($1s^2 2pnp^1S$ and

$1s^2 2pnd^1F$) overlap within their natural widths (i.e., overlapping resonances) . Coherent superposition of two electronic states, which have opposite parities, can be represented by a spatially polarized electron cloud. This cloud oscillates with the period corresponding to the energy difference between the two states and the states decay in a time corresponding to the natural widths. If the lifetimes of the states are shorter than the oscillation period, the decay occurs before there is a significant oscillation of the electron cloud, and the distribution of the decay products (e.g., ejected electrons) may show strong forward-backward asymmetry .

It is noted that this experiment indicates that electrons captured into bound states, may be strongly polarized at the time of capture and that the method of zero degree electron spectroscopy may, in some cases, be used to measure this polarization.

*Permanent address: Research Laboratory for Nuclear Reactors, Tokyo Institute of Technology.

**Permanent address: Hahn-Meitner-Institut fuer Kernforschung Berlin GmbH.

References

1. The experiment was performed at Oak Ridge National Laboratory EN Tandem facility using the apparatus temporarily transported from Hahn-Meitner-Institut fuer Kernforschung Berlin (see e.g., A.Itoh, D.Schneider, T.Schneider, T.J.M.Zouros, G.Nolte, G.Schiwietz, W.Zeitz, and N.Stolterfoht, Phys.Rev.A31, 684(1985)).
2. D.C.Griffin, M.S.Pindzola, and C.Bottcher, Phys.Rev.A31, 568 (1985) and D.C.Griffin, private communication.
3. Y.Yamazaki, P.D.Miller, H.F.Krause, P.L.Pepmiller, S.Datz, I.A.Sellin, and N.Stolterfoht, to be published.

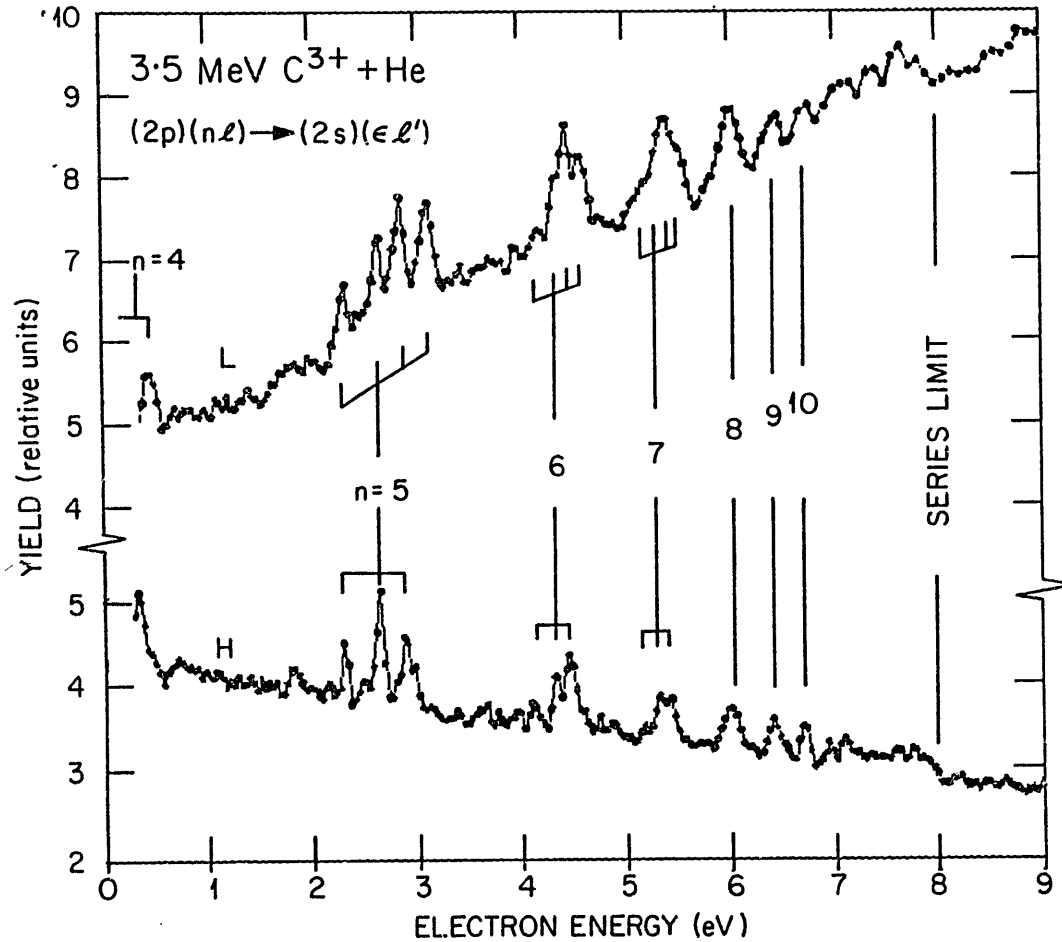


Figure 1. Electron spectra produced in 3.5 MeV $C^{3+} + He$ collisions. A number of peaks due to the Coster-Kronig transitions $1s^2 2pn\ell \rightarrow 1s^2 2s\epsilon\ell'$ are observed. The electron energy refers to the projectile rest frame. H and L correspond to the spectra of electrons emitted in forward (0°) and backward (180°) directions, respectively.

STATE-SELECTIVE MEASUREMENTS IN LOW-ENERGY ION-ATOM
AND ELECTRON-ATOM COLLISIONS

B.A. Huber

Institut für Experimentalphysik AG II, Ruhr-Universität
D 4630 Bochum, FRG

Among different experimental methods the so called translational energy spectroscopy (TES) is a rather powerful tool, which allows a detailed study of state distributions of multiply charged ions either created by electron or by ion impact. In recent years this method has been applied extensively in order to investigate electron capture reactions by multiply charged ions.

In principle the kinetic energies of the colliding particles are measured for a given scattering geometry with high precision. The measured energy gain or energy loss of the detected projectile can be transferred into the energy defect of the preceding reaction and therefore contains information on the excitation energies of the product particles as well as on the internal state of the incoming ion. For experimental reasons only the ground state or long-lived metastable states of the projectile have to be considered. However, this method works only effectively, if high energy- and angular resolution are obtained.

The following applications of the translational energy spectroscopy will be briefly discussed below:

- 1) Analysis of the final state population after electron capture by multiply charged ions.
- 2) Preparation of specific ion states and reactions with state-prepared ions.
- 3) Detection of metastable states of multiply charged ions.
- 4) State-selective measurements of multi-ionization of atoms by single electron impact.

As an example for studying electron capture by the aid of normal TES figure 1 shows the energy distribution of secondary Ar^{2+} ions formed in Ar^{3+}/Ar collisions. The parameter characterizing different curves is the electron energy, which is used in the electron impact ion source. At high electron energies a large number of different peaks occurs, which are caused by capture into different excited states of Ar^{2+} (indicated by vertical lines), whereby the Ar^{3+} projectile may be in the $^4\text{S}^{\circ}_{3/2}$ ground state or the weakly excited metastable states $^2\text{D}^{\circ}$ and $^2\text{P}^{\circ}$. A detailed analysis of this spectrum is given in ref. 1 and ref. 2. The identification of various reaction channels is simplified if only one ion state is present in the primary beam. This can be achieved by reducing the electron energy in the ion source below the threshold values for the production of excited Ar^{3+} states. The lowest curve in figure 1 represents the energy gain spectrum caused by pure ground state Ar^{3+} projectiles. By taking into account these contributions and by deconvoluting the more complex spectra at higher electron energies, we are able on the one hand to determine the relative beam fractions as function of the electron energy; on the other hand energy gain spectra can be generated for individual metastable projectile states.

The energy gain spectrum of Ar^+ ions produced in Ar^{2+}/Ar collisions (shown in figure 2) is even more complex and the corresponding procedure of lowering the electron energy is not very successful in identifying at least the exoergic reaction channels (for a detailed analysis see ref. 3). We therefore applied the technique of preparing the ionic state of the projectile before the collision occurs. In a first step excited states of Ar^{2+} are produced by electron capture reactions in Ar^{3+}/Ar collisions and selected by the setting of the energy analyser. In a second step the selected ions interact in a second collision chamber with Ar and the energy gain or loss of tertiary Ar^+ ions is analysed by TES.

Due to the finite drift time of 40 μs , which the ions need

to cover the distance between both collision chambers, only ions in metastable states remain excited, whereas the others decay into the ground state or low-lying metastable states. Analysing the decay schemes of Ar^{2+*} we have been able to prepare Ar^{2+} in various states. The result is summarized in figures 3 a,b,c, showing the energy gain spectra of Ar^+ ions where the projectile states of Ar^{2+} have been (^3P), ($^1\text{D}_2$), ($^3\text{F}_4^0$) and ($^5\text{D}_4^0$) as well. By applying this technique it was found, that cross sections for electron capture by highly excited metastable states exceed those for ground state and weakly excited species by a factor of about 100. This explains their dominant contribution to the energy gain spectrum, although their relative abundance is rather small in an unprepared beam ($\leq 1\%$).

As already shown in figs. 1 and 2 translational energy spectra vary strongly with the electron energy used in the ion source. As individual peaks are correlated with different projectile states, we can study the production of multiply charged ions in specific (metastable) states by single electron impact as function of the electron energy. The exact method of determining cross sections for multi-ionization into specific states is described in detail in ref. 4.

Results for double ionization of Ar atoms by electron impact are shown in figure 4, where the total double ionization cross section is subdivided into 5 'state-selective' cross sections. In some cases (metastable states) there is a weak structure at electron energies between 200 eV and 300 eV, which refers to contributions from L-vacancy production processes. The importance of these reactions increases strongly, if ions in higher charge states are produced.

Another subject of these studies has been the threshold behaviour of individual ionization functions, in particular a test of threshold laws as function of the final charge state and the populated internal state. Figure 5 shows the threshold

region for double ionization of Ar. The experimental cross sections for the production of individual Ar^{2+} states are fitted accordingly to the equation $\sigma \sim (E_{\text{el}} - E_{\text{thr}})^\kappa$, where E_{el} is the electron energy and E_{thr} determines the threshold value. The κ values are found to be close to 2, whereas in the case of the total cross section (shown as a dotted line) a steeper increase is measured, corresponding to $\kappa = 2,65$. This results from the superposition of state-resolved cross sections with different threshold values. Similar experiments have been performed for higher charge states showing no linear increase of κ with q ; for $q=4$ we measured a κ -value between 2 and 3.

References

- /1/ B.A. Huber, H.J. Kahlert, K. Wieseemann; J. Phys. B 17, 2883 (1984)
- /2/ J. Binder, B.A. Huber, H.R. Koslowski, K. Wieseemann; submitted to J. Phys. B (1986)
- /3/ J. Puerta, B.A. Huber; J. Phys. B 18, 4445 (1985)
- /4/ K. Wieseemann, J. Puerta, B.A. Huber; J. Phys. B 19, in press (1986)

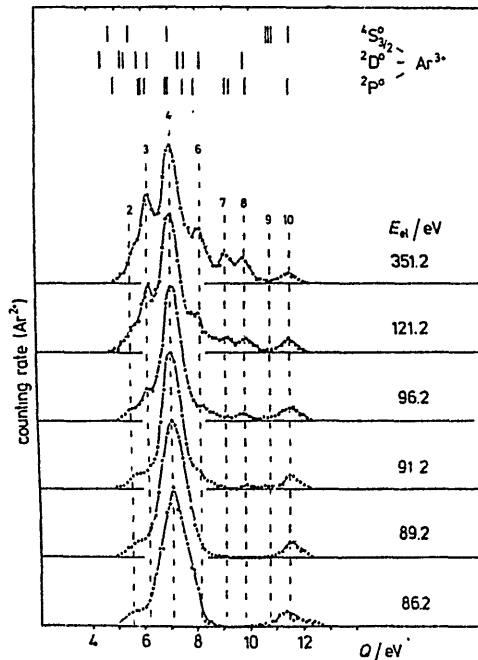


Fig. 1: Energy gain spectra of Ar^{2+} ions formed in Ar^{3+}/Ar collisions

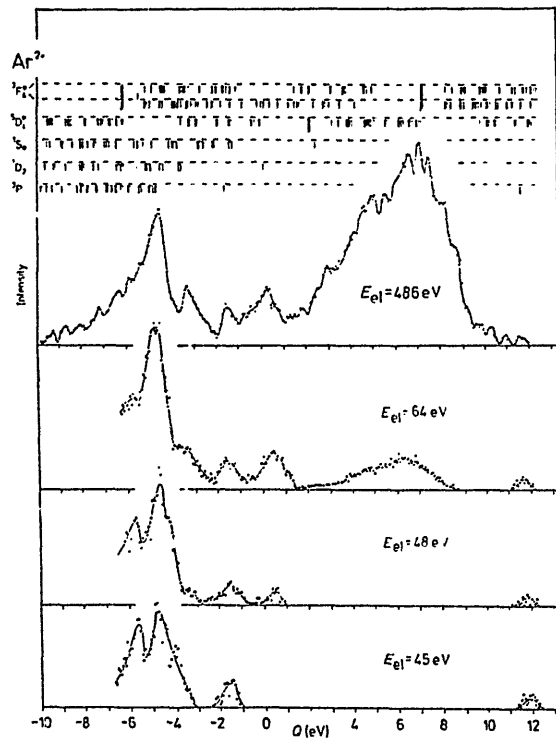


Fig. 2: Translational energy spectra of Ar^+ ions produced in Ar^{2+}/Ar collision as function of the electron energy E_{el} .

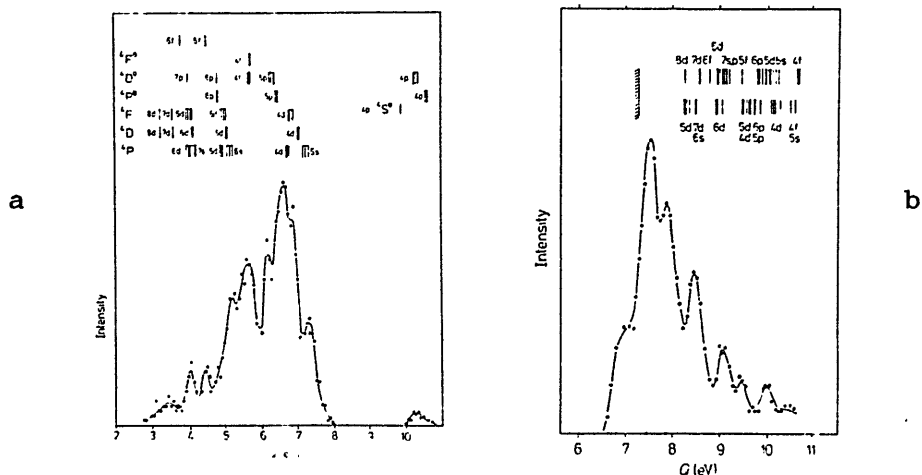
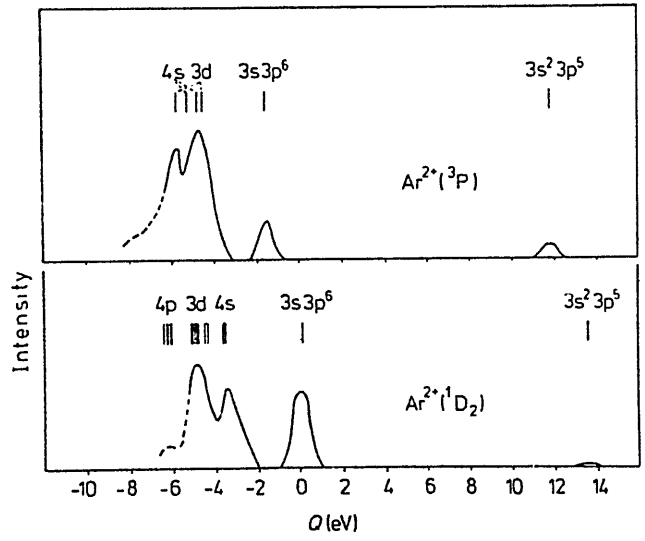


Fig. 3: Energy gain spectra of Ar^+ ions formed in Ar^{2+}/Ar collisions
 a) $\text{Ar}^{2+}: ({}^5\text{D}_{4}^{\circ})$; b) $({}^3\text{F}_{4}^{\circ})$;
 c) $({}^3\text{P})$ and $({}^1\text{D}_{2})$



c

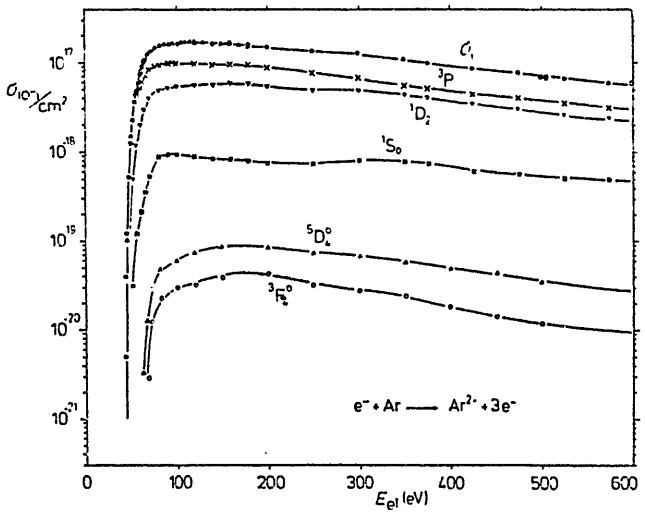


Fig. 4: State-selective cross sections for double ionization of Ar atoms by electron impact

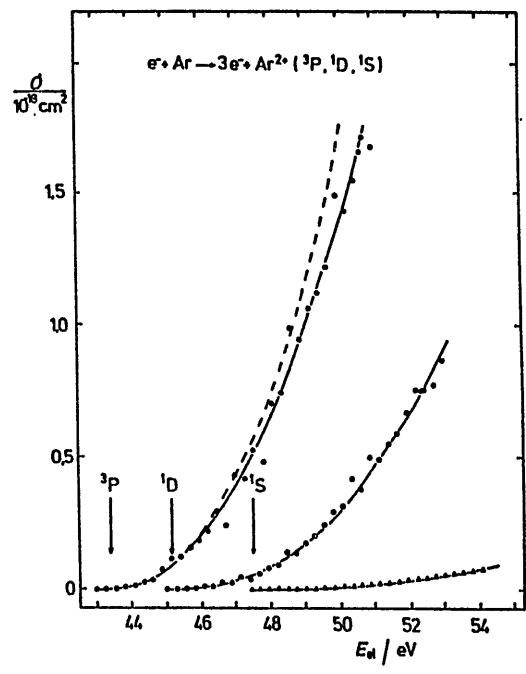


Fig. 5: Threshold behaviour of double ionization cross sections in Ar

STATE SELECTIVE ELECTRON CAPTURE BY HIGHLY STRIPPED IONS FROM ATOMS

Masahiro KIMURA

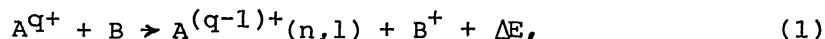
Department of Physics, Osaka University, Toyonaka, Osaka 560, Japan

Experimental study on final-state distribution in one-electron capture from slow fully-stripped and hydrogen-like projectile ions from H and He atoms is discussed. After a short review of the available results state-selectiveness of the process is interpreted using the Landau-Zener model.

1. INTRODUCTION

At an earlier stage total cross sections as a function of projectile charge and the collision energy have been the main subject of the study on electron capture from neutral targets by slow multiply charged ions. It has also been recognized that the information on the final state distribution of the captured electron is indispensable for the full understanding of such processes. Last year at XIV ICPEAC in Palo Alto a symposium "State Resolved Electron Capture by Multicharged Ions" [1] was devoted to review the current status of this actively developing field (see also ref.2 for a recent review). Since then new experimental information has been added quite recently by the NICE group in Nagoya on final state distributions in one-electron capture by fully stripped and hydrogenlike C, N and O ions from atomic and molecular hydrogen. No experimental final state analysis has been reported so far on these rather simple one- or two-electron systems. Though most theoretical calculations have been performed for electron capture by fully stripped projectiles colliding with atomic hydrogen, experimental study has been scarce because of the difficulties associated with the production of an atomic hydrogen target with good quality as well as the production of highly stripped projectiles.

In the present talk I will limit myself to the following one-electron capture process at low velocity ($v \ll 1$ a.u.),



where the target B is H or He atom and projectiles A^{q+} represents fully stripped, hydrogenlike and heliumlike C, N and O ions. The observed results will be interpreted by using the Landau-Zener model.

2. EXPERIMENTAL STUDY

The following two experimental methods have been widely used to analyze the final state distribution.

1) Photon spectroscopy, in which radiation from the excited levels produced by one-electron capture processes are analyzed. Since the resolution of photon spectroscopy is superior to the other method, it offers the possibility to investigate the l-distribution as well as the n-distribution even for hydrogenlike projectiles. Drawbacks of this method are very low sensitivity and difficulties in evaluation of transition probabilities and absolute calibration. This technique has been most successfully utilized by the FOM-Groningen group. They have measured the partial cross sections in slow collisions of C^{4+} , N^{5+} and O^{6+} ions with H, H_2 and He [3], and C^{6+} , N^{6+} and O^{6+} ions with H_2 and He [4].

2) Translational energy spectroscopy, in which the energy gain (or loss) of the projectiles is determined. This method has the advantage of getting direct information on the final state distribution with a very high detection efficiency. We have used this technique to analyze the final state distribution in slow collisions of fully stripped, hydrogenlike, heliumlike and lithiumlike ions of C, N and O with He atoms [5]. Furthermore, highly stripped ions of F, Ne, Kr and I, including I^{38+} , were employed in the subsequent study. This technique has also been used by the Belfast, Kansas and Stockholm groups, and Huber for projectiles with more than two electrons.

The apparatus and the experimental procedure we have used for translational energy spectroscopy are practically the same as those described previously [6] except for the target gas cell. The ion beam extracted from an electron beam ion source, NICE-1, is mass-analyzed and passed through a hot tungsten tube furnace containing dissociated hydrogen gas for the H-target study. Charge-changed ions scattered in forward direction are then energy-analyzed by an electrostatic analyzer before detection. The degree of dissociation in the furnace was found to be almost complete.

In Fig.1 are shown energy spectra for the collisions of fully stripped ions of C, N and O with H at the energy of 1.5q keV. As seen evidently the electron is captured predominantly into a particular single n shell; $n=4$ for the C^{6+} -H collision, and $n=5$ for the N^{7+} -H and O^{8+} -H collisions. These dominantly populated n-shells are found to be higher by one unit than the corresponding ones for the He-target owing to the smaller ionization poten-

tial of H. In O^{8+} -H, the observed peak is mainly due to the electron-capture into $n=5$ shell but we cannot exclude a possibility that the peak is somewhat contributed by the $n=6$ population. Shipsey et al.[7] have predicted the contribution of $n=6$ population to total one-electron capture cross section is about 30% at this energy by using traveling molecular orbital calculation, while Fritsch and Lin [8] have estimated it at about 10% by using extended atomic orbital method. From our observed spectrum we can say that the contribution should be at least smaller than 30%. As for the H-target we have also observed spectra for projectiles $C^{4,5+}$, $N^{5,6+}$ and $O^{6,7+}$. These results will be published elsewhere together with data for molecular hydrogen target.

The FOM-Groningen group has also measured the (n,l) -distribution in the collisions of He-like C, N and O ions with H and He. Their observations are consistent with ours as far as n -distribution is concerned.

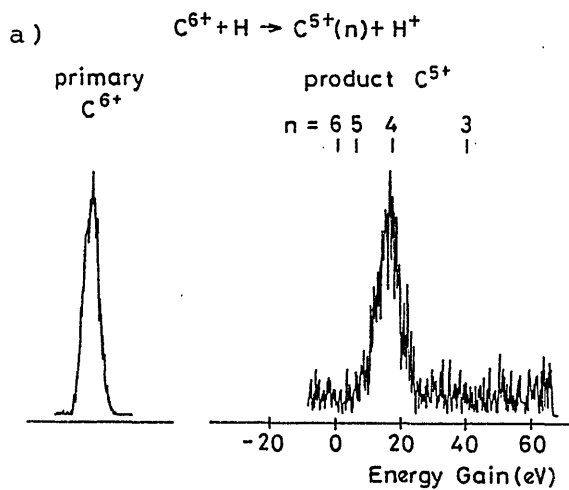
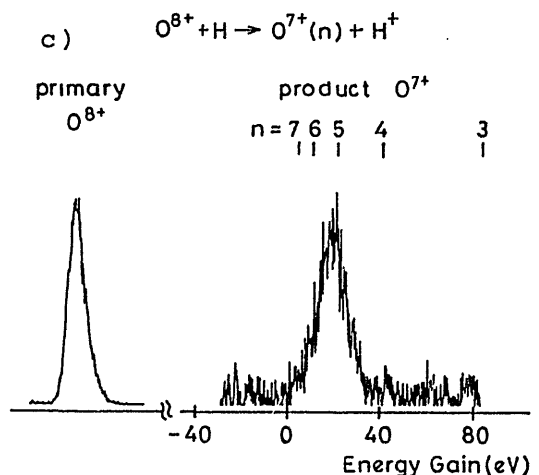
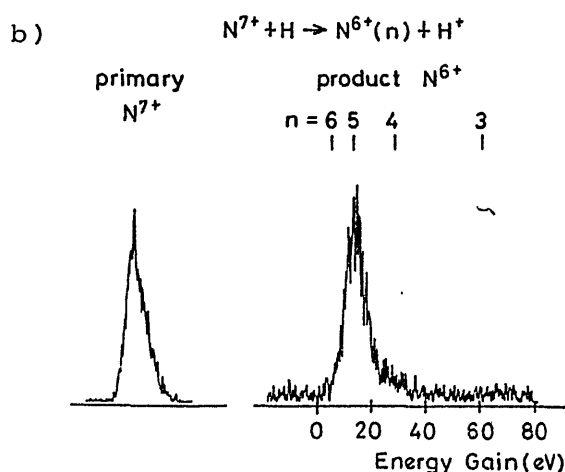


Fig.1. Energy gain spectra of forward scattered C^{5+} , N^{6+} and O^{7+} ions in a) C^{6+} -H, b) N^{7+} -H and c) O^{8+} -H collisions at 1.5q keV.



As reported for He-target [6] good similarity is again observed in the spectra for different ions with the same charge q for the H-target; a particular single n -shell is dominantly populated, and the capturing level becomes higher as the charge q becomes larger and as the ionization potential of target smaller.

3. LANDAU-ZENER MODEL AND REACTION WINDOW

Many-state close-coupling calculation is indispensable for accurate prediction of the electron capturing processes. Nevertheless Landau-Zener model calculation has not lost its advantage owing to its simplicity and straightforwardness. By using this model the observed state-selectivity can be interpreted and the concept of the reaction window is elucidated.

Strong Coulomb repulsion between the product two ions causes the crossings of potential energy curves of the product system with the curve of rather weakly interacting initial ion-atom system if the reaction is exothermic. In slow collisions the transitions are strongly favored at such crossings. Since the important crossings occur at large internuclear separations, the crossing distance R_c is expressed simply by (in a.u. except where indicated)

$$R_c = (q-1)/\Delta E. \quad (2)$$

Here ΔE is the energy gain of the reaction and equals to the difference between the ionization potential of the excited product $A^{(q-1)+}(n)$ ion, which takes a final hydrogenic state with the principal quantum number n , and that of the target atom I ;

$$\Delta E = q^2/2n^2 - I. \quad (3)$$

The transition probability at the crossing is taken to be $2p(1-p)$, where p is the standard Landau-Zener probability. This probability is integrated over impact parameter to obtain the cross section σ . Probability p is a function of interaction matrix element H_{12} , the radial component of the collision velocity and the difference in slopes of the diabatic potential curves at the crossing. Analytical expression for H_{12} has been obtained by Olson and Salop for the fully-stripped-projectile and atomic-hydrogen system and extended to the systems of targets other than atomic hydrogen [9]. Since the electron capture is dominated through the crossings within the limited region of internuclear distance, only final states with a particular single n -shell are generally favored. Therefore a single crossing approximation is enough for rough estimation. The application of multi-

channel Landau-Zener model is discussed in ref.10.

Fig.2 shows cross sections divided by πR_C^2 for various projectile charges as a function of crossing distance R_C at the collision velocity of 600 eV/amu. As seen the reaction window, i.e., the range of nuclear separation in which the cross section is significant, shifts to larger distances and becomes broader as the projectile charge increases.

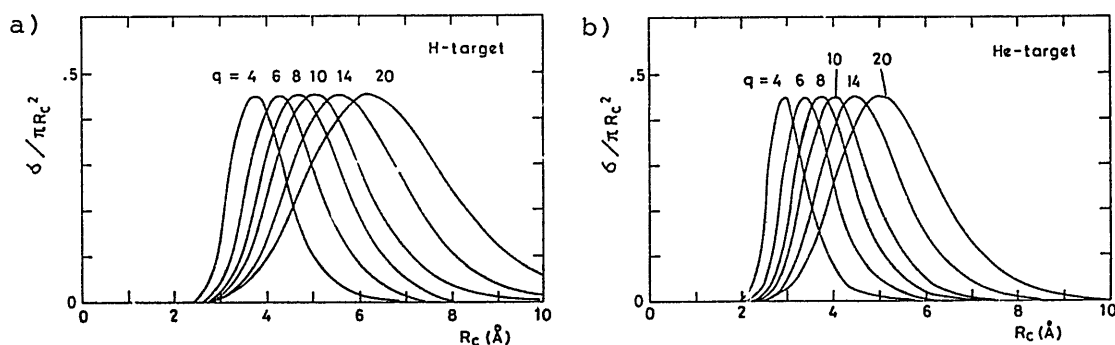


Fig.2. Calculated one-electron capture cross sections divided by πR_C^2 as a function of internuclear separation R_C for (a) H and (b) He targets. Collision energy is 600 eV/amu.

In Figs.3 a) and b) solid lines show combined relations (2) and (3) for H- and He-targets respectively with the boundaries of the reaction windows (broken lines). Here we define tentatively the reaction window as the region where $\sigma/\pi R_C^2$ is larger than 0.05. The positions of potential curve crossings are indicated by several symbols on the lines. Black circles are inside the window, and they are the states expected to be dominantly populated by one-electron capture but not yet confirmed experimentally. The dominantly populated n-shells actually observed by the NICE and/or FOM-Groningen groups are shown by black diamonds. The data for $q=10$ in b) is from Mann et al. for Ne^{10+} -He [11]. All the observed states are inside the window, or at least situated very closely to the window boundaries when no crossings are available inside the window. It is clear that only single n-shell is populated for $q \leq 10$ except for A^{9+} -He, in which both $n=4$ and 5 shells have been found to be appreciably populated in Ne^{9+} -He collision. At larger q more and more n-shells are populated as inferred from these figures and as demonstrated previously in Kr^{q+} ($q=7-25$)-He and I^{q+} ($q=10-38$)-He collisions [12,13].

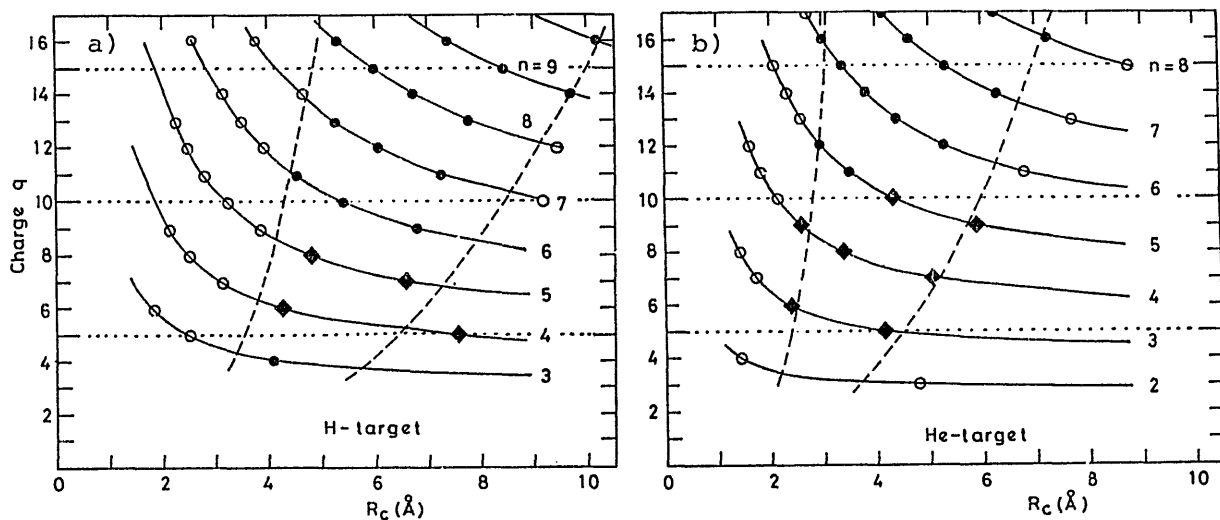


Fig.3. Positions of potential curve crossings as a function of n and q for a) H and b) He targets. The region between two broken lines is the reaction window.

ACKNOWLEDGMENT

The author is much indebted to all the members of the NICE group, especially to Dr. N. Kobayashi, Dr. S. Ohtani and Dr. H. Tawara for the collaboration work on one-electron capture from hydrogen.

References

- 1) In "Electronic and Atomic Collisions (Invited Papers)" eds. D.C.Lorents et al. (North-Holland, 1986) pp.431-478.
- 2) R.K.Janev and H.Winter, Phys. Reports 117 (1985) 265.
- 3) D.Dijkkamp et al., J. Phys. B 18 (1985) 4763.
- 4) D.Dijkkamp et al., J. Phys. B 18 (1985) 737.
- 5) S.Ohtani, in "Electronic and Atomic Collisions (Invited Papers)" eds. J.Eichler et al. (North Holland, 1984) p.353; M.Kimura, in Ref.(1) p.471; and references therein.
- 6) K.Okuno et al., Phys. Rev. A 28 (1983) 127.
- 7) E.J.Shipsey, T.A.Green and J.C.Browne, Phys. Rev. A 27 (1983) 821.
- 8) W.Fritsch and C.D.Lin, Phys. Rev. A 29 (1984) 3039.
- 9) R.E.Olson and A.Salop, Phys. Rev. A 14 (1976) 579.
- 10) M.Kimura et al., J. Phys. Soc. Japan 53 (1984) 2224.
- 11) R.Mann et al., Phys. Rev. Lett. 49 (1982) 1329.
- 12) T.Iwai et al., J. Phys. B 17 (1984) L95
- 13) H.Tawara et al., J. Phys. B 18 (1985) 337.

POLARIZATION PROPERTIES OF TOTAL EMISSION CROSS SECTION
IN He^+ -He COLLISIONS

R. Okasaka and H. Sakakibara

Department of Engineering Science, Kyoto University
Yoshida-honmachi, Sakyo-ku, Kyoto 606, Japan

1. Introduction

On ion-atom collisions of intermediate energy range ($10\text{-}10^4$ eV) colliding particles are in a quasi-molecular state during interacting period. Moments of transitions are rotational and radial coupling between two quasi-molecular states and transition occurs preferentially near the level crossing region. When the coupling scheme of dominant excitation process is specified, parallel component of angular momentum in respect to the molecular axis becomes definite on a excited state; rotational coupling excites Π -state and radial coupling excites Σ -state in He^+ -He collisions, for the incident channel of $\text{He}^+(1s)+\text{He}(1s^2)$ is in Σ -state. In the case where the angular momentum of the molecular state is conserved on the separated atoms, the former process produces alignment of magnetic sublevel of $m'=\pm 1$ and the latter produces that of $m'=0$. Observation of energy dependence of polarization of total emission cross section brings important informations about such excitation mechanisms, while polarization analysis of differential excitation cross section in coincidence with scattered particle at fixed colliding energy are useful to study alignment and orientation of excited atoms.

In the present studies, first, we decide the principal coupling scheme of a excitation by comparing the observed emission cross section with the calculated excitation function and, next, obtain the dependence of polarization on collision energy by solving coupled equations of two-level model. Then, we estimate, by making comparison between the calculated and the observed polarizations, a size of locking radius which is measure of transition region from body-fixed molecular state where the symmetry axis coincides with the molecular axis to spaced-fixed atomic state at large internuclear distance.

2. Experiments and coupling schemes

The apparatus is described in detail elsewhere.¹⁾ An ion-beam was

introduced into a collision cell and spectroscopic measurements of visible to extreme UV region were performed. Radiations polarized parallel ($I_{//}$) and perpendicular (I_{\perp}) to the beam axis were measured with a linear polarizer at 90° with respect to the beam direction. Typical examples of two-type emission cross sections are shown in Fig. 1 and 2. The behaviors exhibited in Fig. 1 and Fig. 2 correspond to that of a cross section populated by rotational coupling through potential crossing at small inter-nuclear distance (R) and that populated by radial coupling through crossing at finite R , respectively.²⁾ The broken lines in Fig. 1 and 2 show the cross sections of rotational excitation and of radial excitation calculated using the theoretically and experimentally determined potential curves.²⁾

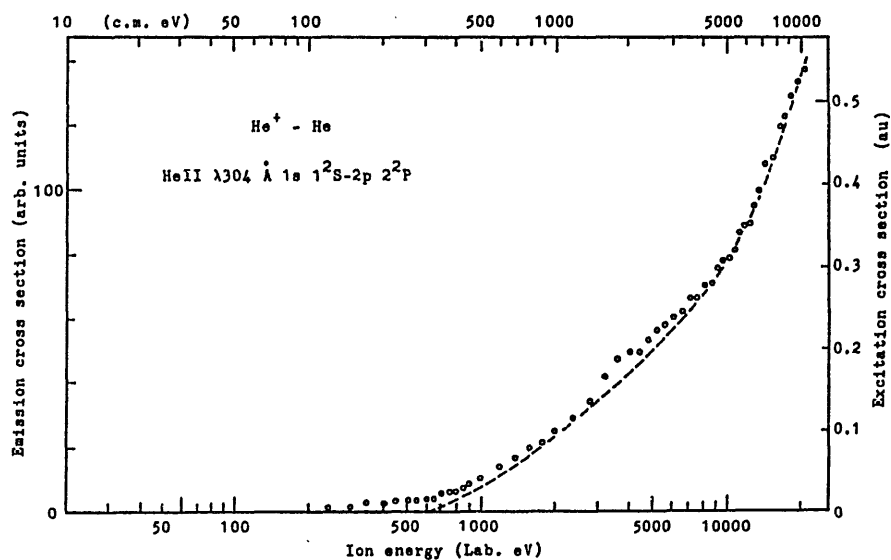


Fig.1 The observed emission cross section and the calculated excitation function for HeII 2p 2^2P level.

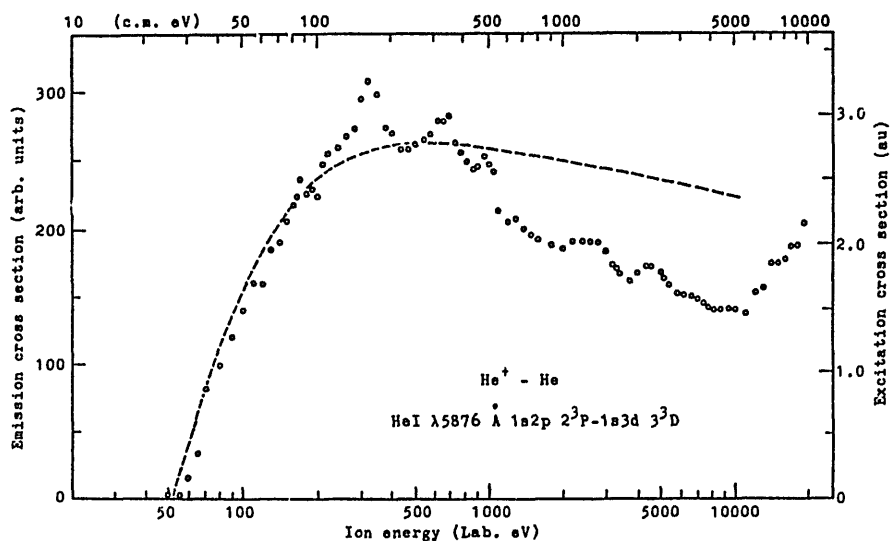


Fig.2 The observed emission cross section and the calculated excitation function for HeI 1s3d 3^3D level.

3. Polarization and locking radius

In the calculations of the excitation functions, we used the classical impact parameter method assuming that particle goes orbit of elastic scattering.¹⁾ When the direction of quantum axis of the separated atom coincides with the scattering angle, the population σ_m of magnetic sublevel m in laboratory system, where we take the quantum axis parallel to the beam direction, is given by equation (1),

$$\sigma_m^J = 2\pi \int \sum_{m'} [D_{mm'}(\theta(b))]^2 P(b) b db. \quad (1)$$

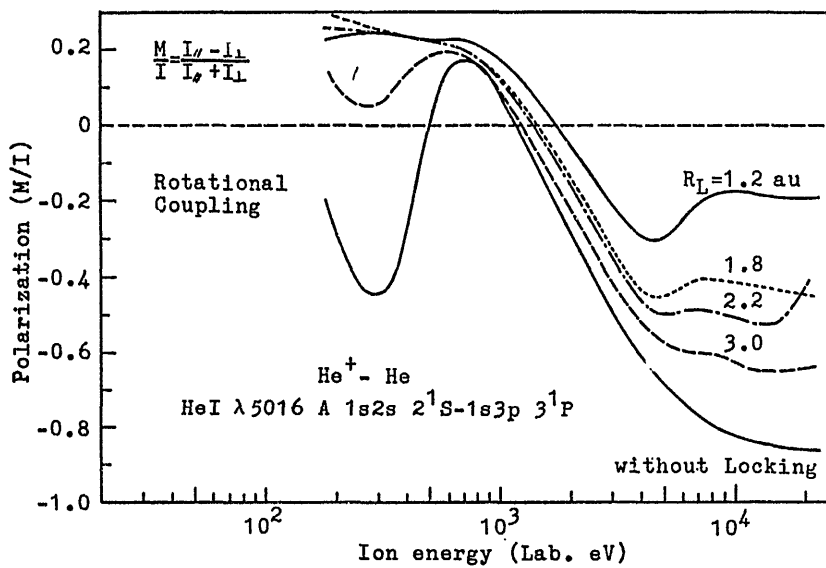


Fig.3 Polarization of HeI 5016 Å line at various locking radius in rotational excitation.

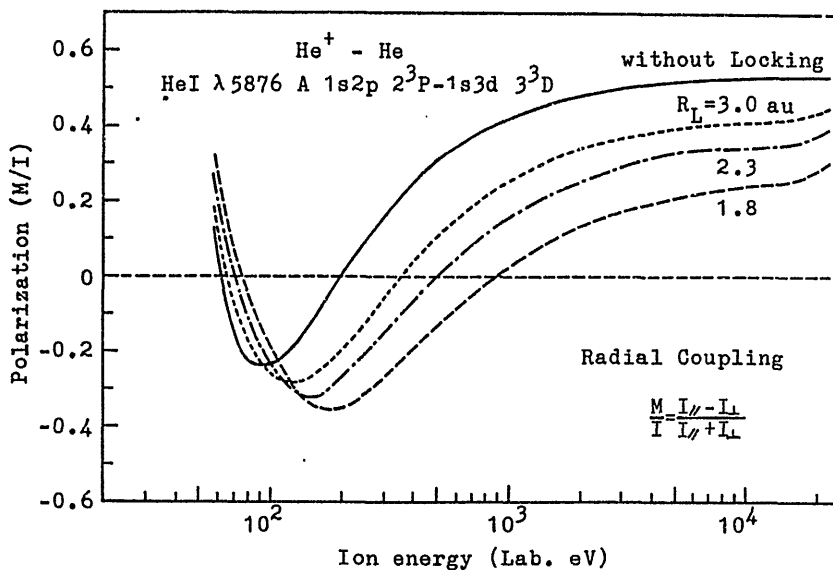


Fig.4 Polarization of HeI 5876 Å line at various locking radius in radial excitation.

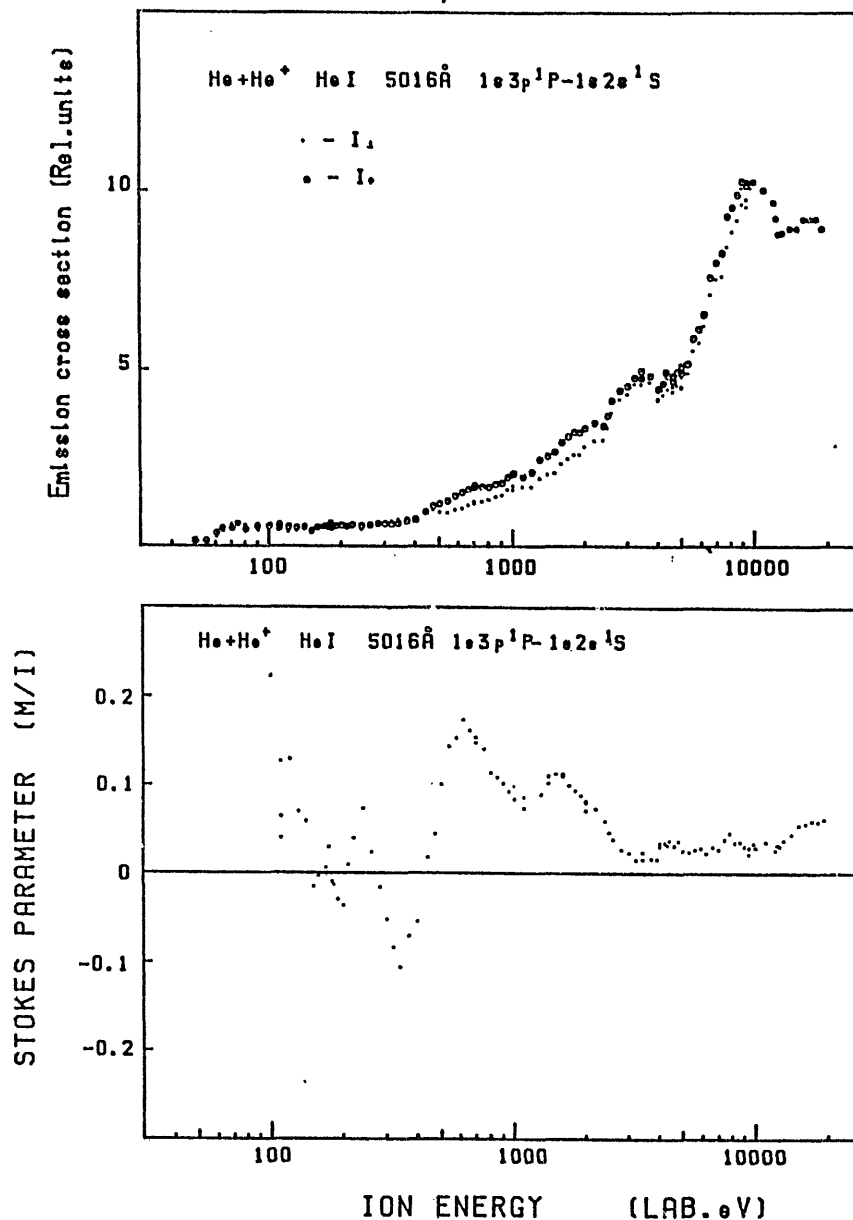


Fig.5 The emission cross section and polarization of HeI 5016 A line

Here, $P(b)$ is transition probability at impact parameter b , m' is magnetic quantum number in center-of-mass system and $D_{mm'}$ is transform matrix from C- to L-system. The solidlines noted "without locking" in Fig. 3 and 4 are profiles of the calculated Stokes parameter M/I of HeI 5016 Å line populated by rotational excitation and of HeI 5876 Å line populated by radial excitation, respectively.

The measured emission cross sections and polarizations corresponding to the results in Fig. 3 and 4 are shown in Fig. 5 and 6. It is quite probable that disagreements between the calculated and the measured polarizations in the figures result from the fact that rearrangement of electron clouds can not follow rotation of the molecular axis.

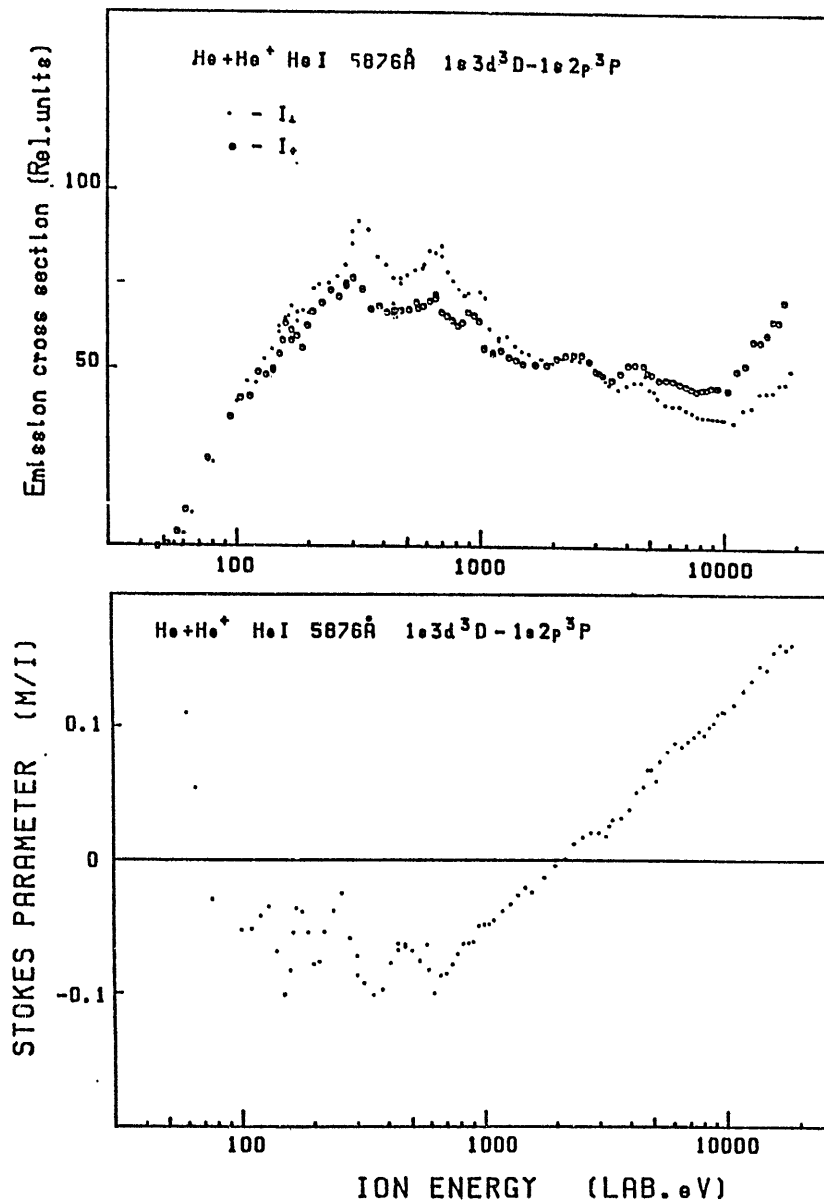


Fig.6 The emission cross section and polarization of HeI 5876 Å line

If there exists finite locking radius R_L at which the direction of symmetry axis of the system begins to deviate from the direction of molecular axis, the polarization depends on size of it. The calculated polarizations for various locking radius are shown in Fig. 3 and 4. The profiles of polarization for $R_L=1 \sim 2$ au in Fig. 3 and 4 agree qualitatively with corresponding profiles of the measured polarizations in Fig. 5 and 6.

References

- 1) R. Okasaka, Y. Konishi, Y. Sato and K. Fukuda, J. Phys. B: At. Mol. Phys. in press.
- 2) R. Okasaka, Y. Sato and K. Fukuda, J. Spectrosc. Soc. Japan, in press.

ANISOTROPY OF ELECTRON EMISSION FROM ALIGNED STATES OF NEON

F. Koike,[†] H. Sakaue, Y. Ikezaki, K. Wakiya, T. Takayanagi,
H. Suzuki, and A. Yagishita[§]

[†]School of Medicine, Kitasato University,
Sagamihara, Kanagawa 228 Japan

Department of Physics, Sophia University,
Chiyoda-ku Tokyo 102 Japan

[§]Photon Factory, National Laboratory for High Energy Physics,
Ohomachi, Ibaraki 305 Japan

An ejected electron spectroscopic study has been carried out on Li^+ + Ne collisions. The Li^+ -impact energy has been ranged from 0.45 keV up to 9 keV. The emission angle dependence of autoionizing electrons has been measured in absolute scale. For a peak due to the $\text{Ne}^{2+} 2p^4 (^1D) 3s^2 ^1D - \text{Ne}^+ 2p^5 ^2P$ autoionization, we have found a change of the angular distribution of the ejected electrons depending on the ion-impact energy.

Concerning the differential cross section $d\sigma(\theta)/d\Omega$ of the electron emission, we find that we can write it as

$$\frac{d\sigma}{d\Omega} = \frac{\sigma_t}{4\pi} \{ 1 + \beta P_2(\cos\theta) \}, \quad (1)$$

where σ_t is the total emission cross section, P_2 is the second order Legendre polinomial, and β is the anisotropy parameter. We have derived this relation under the assumptions firstly that the autoionizing state is excited by a transition between the quasimolecular states owing to the radial coupling in the vicinity of the avoided crossing between the initial and final potential energy curves, and secondly that it obtains a complete alignment with respect to the quasimolecular axis. We have obtained the ion-impact energy dependence of β as shown in Fig. 1. We want here to point out the presence of a minimum in β - vs - Li^+ -impact energy curve at around 0.6 keV of the ion-impact energy. This is quite consistent with the speculation that the center-of-mass scattering angle of Li^+ with dominant contribution to the excitation of the autoionizing state should exceed 90° along with the unbounded decrease of the Li^+ -impact energy.

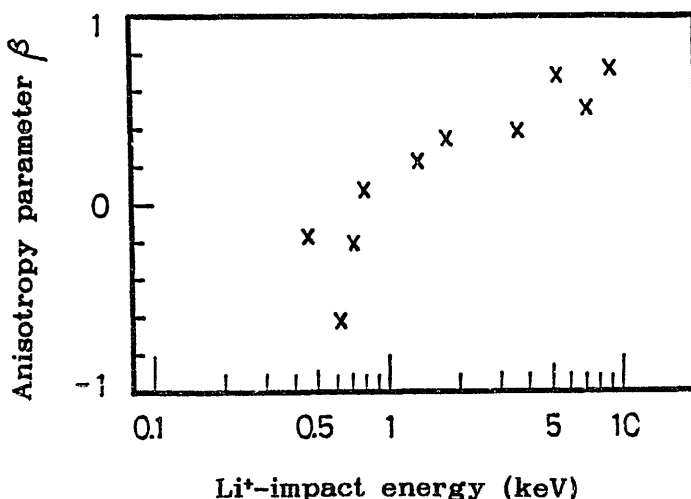


Fig.3. Li^+ -impact energy dependence of anisotropy parameter

Double- and Single-Charge Transfer in Collision of C^{6+} ion with He atom at Low Impact Energies

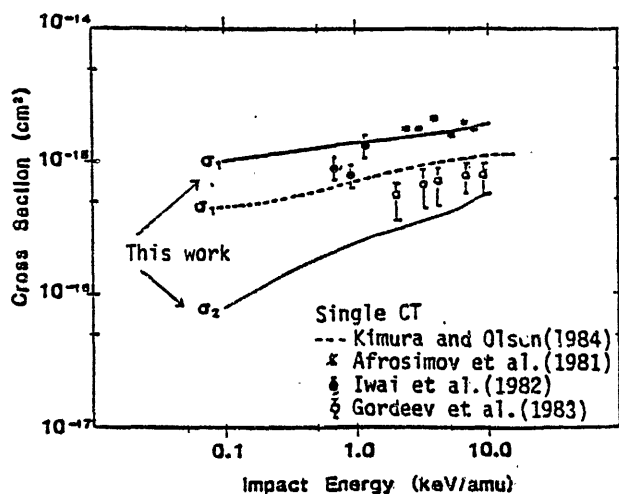
Tomoko Ohyama-Yamaguchi

Institute of Space and Astronautical Science, Komaba,
Meguro-ku, Tokyo 153, Japan

In the study of low energy charge transfer processes of multiply charged ions with atoms, most of theoretical and experimental studies have been concentrated on the single-charge transfer processes. On the other hand a few theoretical^{1,2)} and experimental³⁻⁵⁾ investigations have been carried out for the double-charge transfer processes in the low energy collision.

In this work we calculate the total single- and double-charge transfer cross sections in the collision of the C^{6+} ion with the He atom in the impact energy region $0.1 \leq E \leq 10$ keV/amu as another example to understand the double-charge transfer process. The electron transfer process in the low energy region is reasonably understood in terms of a quasi-molecular representation. In this procedure there are many curve crossings among the adiabatic potential curves. A diabatic treatment is, however, found to be useful for the most of curve crossings.

Fig. 1 shows results of the single- and double-charge transfer cross sections. The single-charge transfer mainly occurs through the avoided crossing near 5au, while the double-charge transfer takes place via a two-step one-electron transfer or a direct transition. Hence the double-charge transfer cross section obtained is about a tenth of the single-charge transfer cross section in these impact energies.



References

- 1) E. J. Shipsey et al.
Phys. Rev. A15(1977) 2166.
- 2) M. Kimura and R. E. Olson
J. Phys. B17(1984) L713.
- 3) D. H. Crandall et al.
Phys. Rev. Lett. 36(1976) 858.
- 4) R. A. Phaneuf and D. H. Crandall
(1981).
- 5) N. Stolterfoht et al.
Phys. Rev. Lett. 57(1986) 74.

Fig. 1

Low Velocity Collision of O^{6+} with He by MO Base Treatment

N. Shimakura, H. Sato*, M. Kimura[†] and T. Watanabe[&]

General Education Department, Niigata University, Niigata 950-21, Japan

*Physics Department, Ochanomizu University, Bunkyo-ku, Tokyo 113, Japan

[†]Joint Institute for Laboratory Astrophysics, University of Colorado

Boulder, Colorado 80309, USA

[&]Institute of Physical and Chemical Research, Wako-shi, Saitama 351, Japan

Partial and total cross sections of single electron capture processes by O^{6+} ion from He are calculated for the velocity range of 0.075 to 0.5 au. (0.14-7.0 keV/amu). A molecular orbital expansion method including two-electron-type electron translation factors has been employed along with classical trajectories.¹⁾ The adiabatic potential energies and wavefunctions for the $(O+He)^{6+}$ system are generated using a pseudopotential technique. This technique reduces four-electron system to a relatively simple two-electron system. Our pseudopotential for the $O^{6+}(1s^2)$ ion core is represented by an l -dependent gaussian type.²⁾ The cross sections were calculated using seven and eight channel close coupling treatment. Convergence of the cross section as a function of basis size is checked. Calculated total cross sections are relatively independent on velocity with a value of about 10^{-15} cm². On the other hand, partial cross sections are more sensitive to velocity at lower velocity region. These findings agree well with experimental observations³⁾ and results calculated with a atomic orbital expansion method⁴⁾.

References

- 1) M. Kimura, H. Sato, and R. E. Olson, Phys. Rev. A28, 2085 (1983).
- 2) J. N. Bardsley, B. R. Junker and D. W. Norcross, Chem. Phys. Lett. 37, 502 (1976).
- 3) D. Dijkamp, Yu S. Gordeev, A. Brazuk, A. G. Drentje and F. J. de Heer, J. Phys. B18, 737 (1985).
- 4) W. Fritsch and C. D. Lin, J. Phys. B. in press.

EVIDENCE FOR CORRELATED DOUBLE-ELECTRON CAPTURE IN
SLOW O^{6+} + He COLLISIONS

R. A. Phaneuf, F. W. Meyer, C. C. Havener, N. Stolterfoht,*
J. K. Swenson,[†] and S. M. Shafroth[†]
Oak Ridge National Laboratory,[‡] Oak Ridge, Tennessee 37831

Double electron capture by few-electron multicharged ions during slow collisions with He may result in Auger-decaying product states of the projectile, provided the initial projectile charge exceeds +4. These autoionizing states can be characterized by either (nearly) equivalent electron configurations, in which the two captured electrons occupy essentially the same or adjacent shells, or by non-equivalent configurations, in which one of the electrons is in a Rydberg state. Using the method of zero-degree Auger spectroscopy, we have verified population of both types of autoionizing states by double electron capture during slow collisions of O^{6+} with He: for these systems, both LMM Auger electrons, attributed to the (nearly) equivalent electron configurations $(1s^2)3l3l'$ or $(1s^2)3l4l'$, and L_1L_23M -Coster Kronig electrons, attributed to the non-equivalent electron configurations $(1s^2)2pnl$, were observed. The LMM Auger electrons can arise either from two sequential single electron transitions or from a simultaneous or correlated two-electron transition. On the other hand, production of the Coster-Kronig electrons is expected to result only from correlated double electron capture. Comparison of the LMM Auger electron and Coster Kronig electron production cross sections suggests that the correlated double capture process is of comparable importance to the sequential single capture mechanism.

*Permanent address: Hahn-Meitner-Institut für Kernforschung GmbH, Berlin, Germany.

[†]Permanent address: University of North Carolina, Chapel Hill, NC USA.

[‡]Operated by Martin Marietta Energy Systems, Inc. for the U.S. Department of Energy under Contract No. DE-AC05-84OR21400.

Evolution of Fast Heavy Ion Excitation in Solid Target

— 0.83–2.4 MeV/u Br^{q+}, Cu^{q+} + C —

K.Shima, K.Umetani, S.Fujioka, M.Yamanouchi, Y.Awaya*, T.Kambara*,
T.Mizogawa* and Y.Kanai*

Tandem Accelerator Center, University of Tsukuba, Ibaraki 305, Japan

*The Institute of Physical and Chemical Research (RIKEN), Saitama
351-01, Japan

To investigate the evolution of projectile inner shell excitation in solids, mean emission cross sections of projectile K and L x-rays $\overline{\sigma}_x$ (= x-ray yield/T) have been measured vs target thickness T. The collisions investigated are 52, 120, 150 MeV Cu^{q+} and 140 MeV Br^{q+} + C, where the projectile K-vacancy production takes place under the single collision condition, whereas projectile L-shell vacancies are dominated by the residual excitation collision. Our interest is focused on the $\overline{\sigma}_x$ vs T relation in thin T region where projectile L-shell configurations still vary before equilibration is attained, which has not been clarified.

Obtained relations for $\overline{\sigma}_{KX}$ (Fig.1) or $\overline{\sigma}_{LX}$ vs T have been analyzed with the aid of observed x-ray energy shifts as well as the calculated cross sections of projectile inner shell ionization and excitation. In the present collisions, the dominant factors to provide the variation of $\overline{\sigma}_x$ at T region of nonequilibrium L-shell configurations are considered to be in (a) the variation of projectile inner shell excitation (K to L, or L to M) and (b) the variation of fluorescence yield.

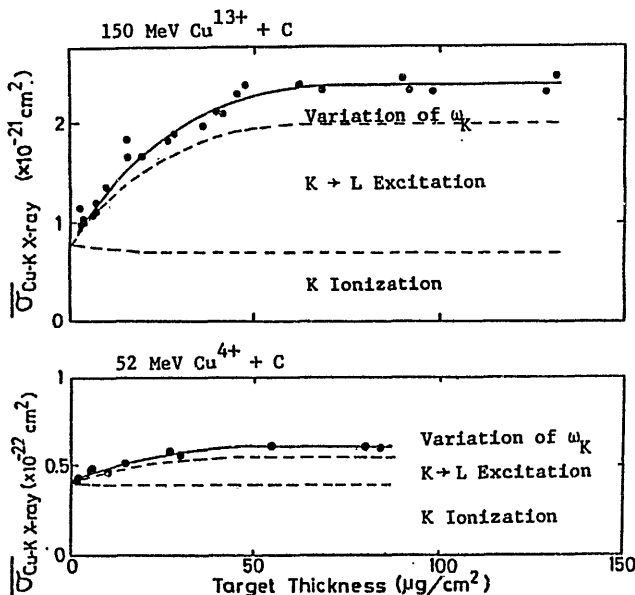


Fig.1. Mean emission cross sections of Cu-K x-rays vs carbon thickness T in the collisions of 150 MeV Cu¹³⁺ + C and 52 MeV Cu⁴⁺ + C.

ANGULAR DEPENDENCE OF LOSS ELECTRONS IN
0.5 MeV/amu H_2^+ -, H_3^+ - AND He^+ - Ar COLLISIONS

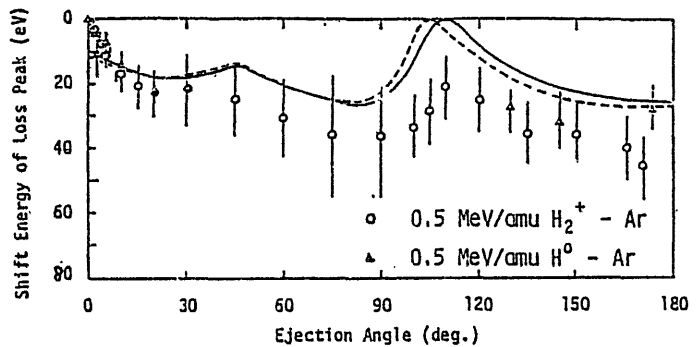
F. Nishimura and N. Oda*

Research Laboratory for Nuclear Reactors, Tokyo Institute
of Technology, O-okayama, Meguro-ku, Tokyo 152, Japan

*Dept. of Phys., Science University of Tokyo, Kagurazaka
Shinjuku-ku, Tokyo 162, Japan

The doubly differential cross sections differential in energy and electron ejection angle have been measured in this experiment over the energy range from 10 to 2000 eV at angles 0° to 165° for collisions of 0.5 MeV/amu H_2^+ , H_3^+ and He^+ with Ar. On the electron loss peak, the angular dependence of the peak energy and the peak width, and the single differential cross sections for the peak have been determined. These results are compared with other available experimental results as well as theoretical results.

Fig. 1. Energy shift of electron loss peak as a function of electron ejection angle.
o, Present results for H_2^+ - Ar;
 Δ , 0.5 MeV.amu H^0 - Ar³⁾;
—, electron impact approximation with inelastic effects for 0.5 MeV/amu H^0 - Ar¹⁾;
---, same as the solid line but without inelastic effects.



In the angular dependence of the peak energy for H_2^+ - Ar collision, as shown in Fig. 1, there exist two bumps at about 45° and 110° , which are compared with the result of the electron impact approximation for H^0 - Ar collision by Jakubassa¹⁾. Such bumps are not observed neither in the experimental nor theoretical results by Kövér et al.²⁾

References

- 1) D.H. Jakubassa, J. Phys. B: At. Mol. Phys. 13 (1980) 2099.
- 2) A. Kövér, D. Varga, Gy. Szabó, D. Berényi, I. Kádár, S. Ricz, J. Végh and G. Hock, J. Phys. B: At. Mol. Phys. 16 (1983) 1017.
- 3) M.M. Duncan and M.G. Menendez, Phys. Rev. A 23 (1981) 1085.

CONTINUUM X RAYS DURING ION-ATOM COLLISIONS

Kiyoshi KAWATSURA, Akio OOTUKA*, Masao SATAKA, Ken-ichiro KOMAKI*, Hiroshi NARAMOTO, Yasuaki SUGIZAKI, Kunio OZAWA, Yohta NAKAI and Fuminori FUJIMOTO*

Department of Physics, Japan Atomic Energy Research Institute

Tokai, Ibaraki 319-11, Japan

* College of General Education, University of Tokyo, Komaba, Tokyo 153, Japan

Radiative electron capture (REC) in fast ion-atom collisions was first observed by Schnopper et al. Since then, many investigations of REC processes have been reported. The experiments should be carried out under single collision conditions to compare with theoretical calculations. This work is done in order to extend our data to higher energies and different projectiles and also to study primary bremsstrahlung.

The JAERI tandem accelerator provided bare and one electron ions of F, S and Cl at 4.0 MeV/amu on He gas targets. Some data was also taken at different velocities. The x-ray spectra were taken with a HORIBA Si(Li) detector at 90° to the beam direction. Figure 1 shows the x-ray spectra for Cl¹⁷⁺ ion incident on a He gas target. They included projectile x rays, REC x rays and bremsstrahlung. The REC and bremsstrahlung x-ray spectra are analyzed. A more detailed discussion will be presented in this seminar.

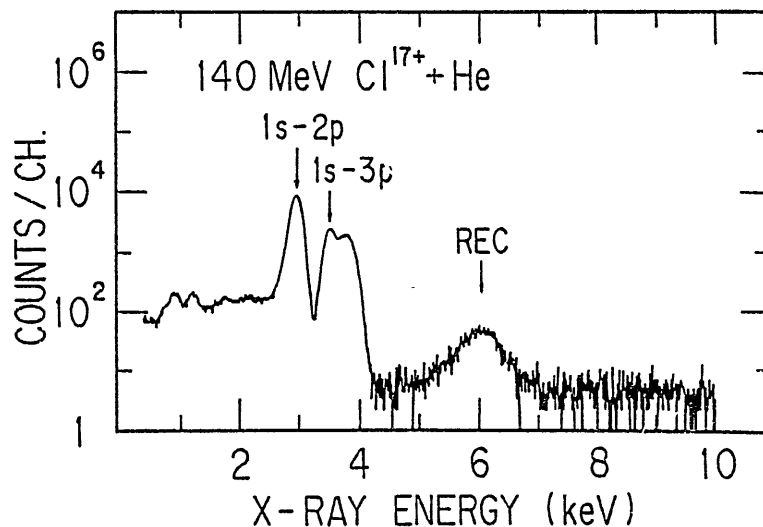


Fig. 1. The x-ray spectra for 140-MeV Cl¹⁷⁺ ion incident on a He gas target.

Photon Angular Distribution of Radiative Electron Capture
by Relativistic Strong Potential Born Calculation

Ken-ichi Hino

Department of Applied Physics, the University of Tokyo
7-3-1, Hongo, Bunkyo-ku, Tokyo 113, Japan

and

Tsutomu Watanabe

The Institute of Physical and Chemical Research
2 Hirosawa, Wako-shi, Saitama 351-01, Japan

We discuss the angular distribution of the relativistic radiative electron capture (REC) in the laboratory frame. By the plane-wave Born calculation, it is predicted that the angular distribution of photon depends on $\sin^2\theta$ (θ :the angle of the emitted photon in the laboratory frame) in spite of including the retardation effects.¹⁾ Such $\sin^2\theta$ -dependence is mostly due to the lowest-order Born term. On the contrary, using relativistic strong potential Born (SPB) wave functions, this term does not have dominant contributions to the REC cross section any longer because of the nearly orthogonal properties between the initial continuum state and the final bound state of the electron and the projectile ion. Therefore, the $\sin^2\theta$ angular dependence is expected to be modified to some extent.

We compare the present SPB calculation of REC with the recent experimental results.^{2),3)}

1)E. Spindler, H. Betz, and F. Bell, Phys. Rev. Lett. **42**, 832 (1979)

2)R. Anholt, W. E. Meyerhof, et. al., Phys. Rev. Lett., **53**, 234 (1984)

3)R. Anholt, Ch. Stoller, et. al., Phys. Rev. **A33**, 2270 (1986)

MANIFESTATION OF MINIMA IN THE GENERALIZED OSCILLATOR STRENGTHS AS
MINIMA IN THE INTEGRATED CROSS SECTIONS FOR ION-ATOM COLLISIONS

Masahiro Iwai, Isao Shimamura, and Tsutomu Watanabe

The Institute of Physical and Chemical Research (RIKEN)
Hirosawa, Wako, Saitama 351-01, Japan

The plane-wave Born approximation (PWBA) is valid for collisions of charged particles with atoms at sufficiently high energies T . The differential cross section in this approximation is expressible as the product of a simple factor and the generalized oscillator strength (GOS), which is a generalization of the optical oscillator strength. The GOS is defined as a function of the momentum K transferred from the incident particle to the target atom in the collision. The existence and the general significance of minima in GOS for many atomic and molecular transitions are discussed in the literature.¹⁻⁴ Effects of these minima on the integral cross sections have also been investigated especially for inner-shell ionization by heavy particles.^{3,4} These analyses have shown frequent appearance of shoulders in the impact energy dependence of the integral ionization cross sections.

We will show appearance of conspicuous minima, rather than shoulders, in the integral cross sections for some discrete excitation processes due to minima in the corresponding GOS. General conditions for appearance of minima in the integral cross section are also discussed.

The GOS is conveniently represented by a three-dimensional plot as a function of K and of the excitation energy E . Such a plot is called the Bethe surface. We have proposed to extend the Bethe surface to visualize the behavior of GOS along an isoelectronic sequence; an additional axis for the inverse of the (effective) nuclear charge is useful for this purpose.⁵⁾ This extended surface serves to clarify the physics behind minima in the GOS.

We have calculated, as an example, the GOS for the $2s^2 1S \rightarrow 2s3p 1P$ transitions of Be-like systems, using configuration-interaction wave functions for both the initial and final states. The result will be reported in the conference.

References

- 1) M. Inokuti: Rev. Mod. Phys. **43**, 297 (1971); M. Inokuti, Y. Itikawa, and J. E. Turner: *ibid.* **50**, 23 (1978).
- 2) I. Shimamura: J. Phys. Soc. Jpn. **30**, 824 (1971).
- 3) M. Matsuzawa, K. Omidvar, and M. Inokuti: J. Phys. B: Atom. Molec. Phys. **9**, 2173 (1976).
- 4) S. T. Manson and A. Msezane: J. Phys. B: Atom. Molec. Phys. **8**, L5 (1975).
- 5) M. Iwai, I. Shimamura, and T. Watanabe: Book of Abstracts, Tenth International Conference on Atomic Physics (Tokyo, August 1986) eds. H. Narumi and I. Shimamura, p.436.

ELECTRON IMPACT EXCITATION OF OXYGEN-LIKE KRYPTON*

A. Z. Msezane, J. Lee, K. J. Reed⁺ and R. J. W. Henry⁺⁺
 Atlanta University, Atlanta, Georgia 30314

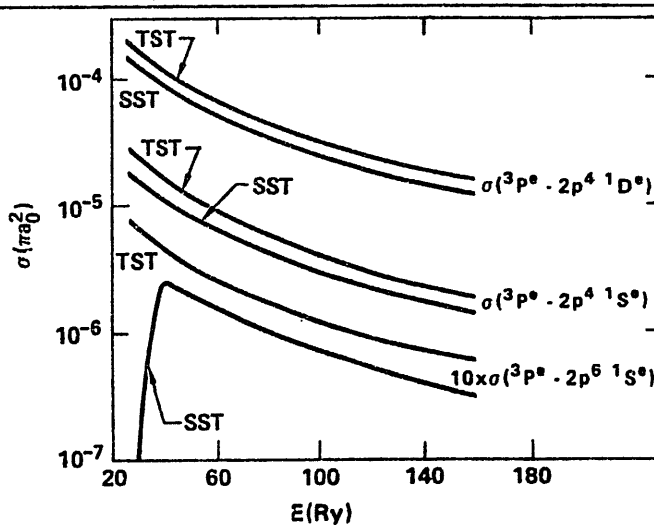
⁺University of California, Lawrence Livermore National Laboratory
 Livermore, California 94550

⁺⁺Louisiana State University, Baton Rouge, Louisiana 70803

Electron impact excitation cross sections are calculated for transitions from the ground state $2s^2 2p^4 \ ^3P$ to the $n=2$ and $n=3$ excited states of oxygen-like krypton for impact energies ranging from near threshold to 10keV. Configuration-interaction type wave functions are employed and the cross sections are calculated in a close-coupling (CC) approximation. Coupling effects among the channels for collisional excitation of the $2s^2 2p^4$, $2s2p^5$ and $2p^6$ configurations are also investigated by comparing six-, five-, four-, three-, and two-state CC results (6CC, 5CC, 4CC, 3CC and 2CC).

We discovered the surprising result that the calculated cross sections for the transitions from the $2s^2 2p^4 \ ^3P$ to the $2p^6 \ ^1S$, $2s^2 2p^4 \ ^1S$ and 1D excited states are reduced considerably (~45%) and moderately (32% and 22%) respectively compared to their corresponding 2CC results when the $2s2p^5 \ ^3P^0$ state is coupled. This addition also diminishes the 2CC cross section $\sigma(2s^2 2p^4 \ ^3P-2p^6 \ ^1S)$ at 26.2Ry by a factor of about 100. Comparison between the 6CC(SST) and the 2CC (or 3CC)(TST) results for the various transitions is summarized in the figure for the energy range $26.2 \leq E \leq 160$ Ry.

Effects of couplings in Kr⁺²⁸



We conclude that the $2s2p^5 \ ^3P^0$ state provides an extremely important coupling mechanism; its effects are expected to be important for intermediate coupling results which are obtainable from the LS coupling data and are currently being investigated. Any level of approximation which fails to incorporate the coupling from the $2s2p^5 \ ^3P^0$ is expected to overestimate the excitation cross sections to the $n=2$ levels.

*Work performed under the auspices of the U.S. Department of Energy by Lawrence Livermore National Laboratory under contract #W-7405-Eng-48. AZM and RJWH are supported in part by U.S. DOE, Office of Basic Energy Sciences

¹A. Z. Msezane, K. J. Reed and R.J.W. Henry, Phys. Rev. A. (in press)(1986)

LIST OF PARTICIPANTS

AWAYA Yohko

The Institute of Physical and
Chemical Research (RIKEN)
Wako-shi, Saitama 351-01
JAPAN

BADRINATHAN C.

Tata Institute of Fundamental
Research
Colaba, Bombay-400 005
INDIA

BEYER Heinrich F.

GSI
Postfach 110541
D-6100 Darmstadt
WEST GERMANY

DANJO Atsunori

Department of Physics
Niigata University
Ikarashi, Niigata 950-21
JAPAN

DUNN Gordon H.

JILA / NBS
Campus Box 440
University of Colorado
Boulder, Colorado 80309-0440
USA

EGAN Patrick O.

Lawrence Livermore National
Laboratory
Mail Stop L-296
P. O. Box 808
Livermore, CA 94550
USA

EICHLER Jorg

Hahn-Meitner-Institut
Glienicke Str. 100
D-1000, Berlin 39
WEST GERMANY

FROELICH Piotr

Department of Quantum
Chemistry
Uppsala University
Box 518, 75120 Uppsala
SWEDEN

FUJIMOTO Fuminori

College of General Education
University of Tokyo
Komaba, Meguro-ku
Tokyo 153
JAPAN

GALSTER Wilfried

Faculty of Science and
Technology
University of Tsukuba
Sakura-mura, Ibaraki 305
JAPAN

HAHN Yukap

Physics Department
University of Connecticut
Storrs, CT 06268
USA

HARUYAMA Yoichi

Laboratory of Applied Physics
Kyoto Prefectural University
Shimogamo, Sakyo-ku, Kyoto 666
JAPAN

HENRY Ronald J.

Department of Physics and
Astronomy
Louisiana State University
Baton Rouge, LA 70803
USA

HIRAYAMA Takato

Department of Physics
Sophia University
Kioicho, Chiyodaku, Tokyo 102
JAPAN

HUBER Bernd A.

Institut für Experimentalphysik
AG II
Ruhr-Universität Bochum
Universitätsstr. 150
Postfach 102148
D-4630 Bochum 1
WEST GERMANY

ICHIMURA Atsushi

Institute of Space and
Astronautical Science
Komaba 4-6-1, Meguro-ku
Tokyo 153
JAPAN

ISHIHARA Takeshi

Institute of Applied Physics
University of Tsukuba
Sakura-mura, Niihari-gun
Ibaraki 305
JAPAN

ISHII Keizo
Cyclotron and Radioisotope
Center
Tohoku University
Sendai 980
JAPAN

ITO H Akio
Rigaku Industrial Corporation
Takatsuki, Osaka 569
JAPAN

KAMBARA Tadashi
The Institute of Physical and
Chemical Research (RIKEN)
Wako-shi, Saitama 351-01
JAPAN

KANAI Yasuyuki
The Institute of Physical and
Chemical Research (RIKEN)
Wako-shi, Saitama 351-01
JAPAN

KANEKO Yozaburo
Department of Physics
Tokyo Metropolitan University
Fukasawa, Setagaya-ku
Tokyo 158
JAPAN

KATAYAMA Ichiro
RCNP
Osaka University
Mihogaoka 10, Ibaraki
Osaka 567
JAPAN

KAWATSURA Kiyoshi
Department of Physics
JAERI
Tokai, Ibaraki 319-11
JAPAN

KIMURA Masahiro
Department of Physics
Osaka University
Toyonaka, Osaka 560
JAPAN

KOBAYASHI Nobuo
Department of Physics
Tokyo Metropolitan University
Fukasawa, Setagaya-ku
Tokyo 158
JAPAN

KOHNO Isao
The Institute of Physical and
Chemical Research (RIKEN)
Wako-shi, Saitama 351-01
JAPAN

KOIKE Fumihiro
School of Medicine
Kitasato University
Kitasato 1-15-1, Sagamihara
Kanagawa 228
JAPAN

LIN Chii-Dong
Department of Physics
Kansas State University
Manhattan, KS 66506
USA

MANSON Steven T.
Department of Physics and
Astronomy
Georgia State University
Atlanta, Georgia 30303
USA

MARTINEZ Jose' Vergara
U S Department of Energy
ER-141; GTN
Washington, D C 20545
USA

MATSUMOTO Atsushi
Hiroshima Institute of
Technology
Itsukaichi, Saiki-ku
Hiroshima 731-51
JAPAN

MIKUMO Takashi
Institute of Physics and
Tandem Accelerator Center
University of Tsukuba
Sakura-mura, Ibaraki 305
JAPAN

MIZOGAWA Tatsumi
The Institute of Physical and
Chemical Research (RIKEN)
Wako-shi, Saitama 351-01
JAPAN

MOORE Fred L.
31 Physics Hall, FM-15
University of Washington
Seattle, WA 98195
USA

MORITA Susumu

Research Center of Ion Beam
Technology
Hosei University
3-7-2 Kajinocho, Koganei
Tokyo 184
JAPAN

MSEZANE Alfred Z.

Department of Physics
Atlanta University
223 James P. Brawley Drive S.W.
Atlanta, Georgia 30314
USA

MUKOYAMA Takeshi

Institute for Chemical Research
Kyoto University
Kyoto 606
JAPAN

NISHIMURA Fumio

Research Laboratory for
Nuclear Reactors
Tokyo Institute of Technology
Ookayama, Meguro-ku, Tokyo 152
JAPAN

OGAWA Hidemi

Department of Physics
Nara Women's University
Kitauoya Nishimachi, Nara 630
JAPAN

OHTANI Shunsuke

Institute of Plasma Physics
Nagoya University
Nagoya 464
JAPAN

OKASAKA Rei

Faculty of Engineering
Kyoto University
Yoshida-honmachi, Sakyo-ku
Kyoto 606
JAPAN

OKUNO Kazuhiko

Department of Physics
Tokyo Metropolitan University
Fukasawa, Setagaya-ku
Tokyo 158
JAPAN

PHANEUF Ronald A.

Oak Ridge National Laboratory
P. O. Box X, Bldg. 6003
Oak Ridge, TN 37831
USA

SAKAMOTO Naoki

Department of Physics
Nara Women's University
Kitauoya Nishimachi, Nara 630
JAPAN

SATAKA Masao

Department of Physics
JAERI
Tokai, Ibaraki 319-11
JAPAN

SELLIN Ivan A.

Oak Ridge National Laboratory
1008 W. Outer Drive
Oak Ridge, TN 37830
USA

SHIBATA Hiromi

Research Center for Nuclear
Science and Technology
University of Tokyo
22-2 Shirane Shirakata
Tokai-mura, Naka-gun
Ibaraki 319-11
JAPAN

SHIMA Kunihiro

Tandem Accelerator Center
University of Tsukuba
Sakura-mura, Ibaraki 305
JAPAN

SHIMAKURA Noriyuki

Division of Chemistry
General Education Department
Niigata University
8050 Ikarashi Nino-cho
Niigata 950-21
JAPAN

SHIMAMURA Isao

The Institute of Physical and
Chemical Research (RIKEN)
Wako-shi, Saitama 351-01
JAPAN

SMITH Anthony Charles Hugh

Department of Physics and
Astronomy
University College London
London WC1E 6BT
UK

TONUMA Tadao

The Institute of Physical and
Chemical Research (RIKEN)
Wako-shi, Saitama 351-01
JAPAN

WATANABE Tsutomu

The Institute of Physical and
Chemical Research (RIKEN)
Wako-shi, Saitama 351-01
JAPAN

WU Victor Wei-Keh

Institut für Experimentalphysik
AG II
Ruhr-Universität Bochum
Universitätsstr. 150
Postfach 102148
D-4630 Bochum 1
WEST GERMANY

YAMAGUCHI Tomoko

Institute of Space and
Astronautical Science
Komaba 4-6-1, Meguro-ku
Tokyo 153
JAPAN

YAMAZAKI Yasunori

Research Laboratory for
Nuclear Reactors
Tokyo Institute of Technology
Ookayama, Meguro-ku
Tokyo 152
JAPAN

YOUNGER Stephen M.

Lawrence Livermore National
Laboratory
P. O. Box 808
Livermore, CA 94550
USA

LIST OF IPPJ-AM REPORTS

- IPPJ-AM-1* “Cross Sections for Charge Transfer of Hydrogen Beams in Gases and Vapors in the Energy Range 10 eV–10 keV”
H. Tawara (1977) [Published in Atomic Data and Nuclear Data Tables 22, 491 (1978)]
- IPPJ-AM-2* “Ionization and Excitation of Ions by Electron Impact –Review of Empirical Formulae–”
T. Kato (1977)
- IPPJ-AM-3 “Grotrian Diagrams of Highly Ionized Iron FeVIII-FeXXVI”
K. Mori, M. Otsuka and T. Kato (1977) [Published in Atomic Data and Nuclear Data Tables 23, 196 (1979)]
- IPPJ-AM-4 “Atomic Processes in Hot Plasmas and X-Ray Emission”
T. Kato (1978)
- IPPJ-AM-5* “Charge Transfer between a Proton and a Heavy Metal Atom”
S. Hiraide, Y. Kigoshi and M. Matsuzawa (1978)
- IPPJ-AM-6* “Free-Free Transition in a Plasma –Review of Cross Sections and Spectra–”
T. Kato and H. Narumi (1978)
- IPPJ-AM-7* “Bibliography on Electron Collisions with Atomic Positive Ions: 1940 Through 1977”
K. Takayanagi and T. Iwai (1978)
- IPPJ-AM-8 “Semi-Empirical Cross Sections and Rate Coefficients for Excitation and Ionization by Electron Collision and Photoionization of Helium”
T. Fujimoto (1978)
- IPPJ-AM-9 “Charge Changing Cross Sections for Heavy-Particle Collisions in the Energy Range from 0.1 eV to 10 MeV I. Incidence of He, Li, Be, B and Their Ions”
Kazuhiko Okuno (1978)
- IPPJ-AM-10 “Charge Changing Cross Sections for Heavy-Particle Collisions in the Energy Range from 0.1 eV to 10 MeV II. Incidence of C, N, O and Their Ions”
Kazuhiko Okuno (1978)
- IPPJ-AM-11 “Charge Changing Cross Sections for Heavy-Particle Collisions in the Energy Range from 0.1 eV to 10 MeV III. Incidence of F, Ne, Na and Their Ions”
Kazuhiko Okuno (1978)
- IPPJ-AM-12* “Electron Impact Excitation of Positive Ions Calculated in the Coulomb-Born Approximation –A Data List and Comparative Survey–”
S. Nakazaki and T. Hashino (1979)
- IPPJ-AM-13 “Atomic Processes in Fusion Plasmas – Proceedings of the Nagoya Seminar on Atomic Processes in Fusion Plasmas Sept. 5-7, 1979”
Ed. by Y. Itikawa and T. Kato (1979)
- IPPJ-AM-14 “Energy Dependence of Sputtering Yields of Monatomic Solids”
N. Matsunami, Y. Yamamura, Y. Itikawa, N. Itoh, Y. Kazumata, S. Miyagawa, K. Morita and R. Shimizu (1980)

- IPPJ-AM-15 "Cross Sections for Charge Transfer Collisions Involving Hydrogen Atoms"
Y. Kaneko, T. Arikawa, Y. Itikawa, T. Iwai, T. Kato, M. Matsuzawa, Y. Nakai,
K. Okubo, H. Ryufuku, H. Tawara and T. Watanabe (1980)
- IPPJ-AM-16 "Two-Centre Coulomb Phaseshifts and Radial Functions"
H. Nakamura and H. Takagi (1980)
- IPPJ-AM-17 "Empirical Formulas for Ionization Cross Section of Atomic Ions for Elec-
tron Collisions –Critical Review with Compilation of Experimental Data–"
Y. Itikawa and T. Kato (1981)
- IPPJ-AM-18 "Data on the Backscattering Coefficients of Light Ions from Solids"
T. Tabata, R. Ito, Y. Itikawa, N. Itoh and K. Morita (1981) [Published in
Atomic Data and Nuclear Data Tables 28, 493 (1983)]
- IPPJ-AM-19 "Recommended Values of Transport Cross Sections for Elastic Collision and
Total Collision Cross Section for Electrons in Atomic and Molecular Gases"
M. Hayashi (1981)
- IPPJ-AM-20 "Electron Capture and Loss Cross Sections for Collisions between Heavy
Ions and Hydrogen Molecules"
Y. Kaneko, Y. Itikawa, T. Iwai, T. Kato, Y. Nakai, K. Okuno and H. Tawara
(1981)
- IPPJ-AM-21 "Surface Data for Fusion Devices – Proceedings of the U.S.–Japan Work-
shop on Surface Data Review Dec. 14-18, 1981"
Ed. by N. Itoh and E.W. Thomas (1982)
- IPPJ-AM-22 "Desorption and Related Phenomena Relevant to Fusion Devices"
Ed. by A. Koma (1982)
- IPPJ-AM-23 "Dielectronic Recombination of Hydrogenic Ions"
T. Fujimoto, T. Kato and Y. Nakamura (1982)
- IPPJ-AM-24 "Bibliography on Electron Collisions with Atomic Positive Ions: 1978
Through 1982 (Supplement to IPPJ-AM-7)"
Y. Itikawa (1982) [Published in Atomic Data and Nuclear Data Tables 31,
215 (1984)]
- IPPJ-AM-25 "Bibliography on Ionization and Charge Transfer Processes in Ion-Ion
Collision"
H. Tawara (1983)
- IPPJ-AM-26 "Angular Dependence of Sputtering Yields of Monatomic Solids"
Y. Yamamura, Y. Itikawa and N. Itoh (1983)
- IPPJ-AM-27 "Recommended Data on Excitation of Carbon and Oxygen Ions by Electron
Collisions"
Y. Itikawa, S. Hara, T. Kato, S. Nakazaki, M.S. Pindzola and D.H. Crandall
(1983) [Published in Atomic Data and Nuclear Data Tables 33, 149 (1985)]
- IPPJ-AM-28 "Electron Capture and Loss Cross Sections for Collisions Between Heavy
Ions and Hydrogen Molecules (Up-dated version of IPPJ-AM-20)
H. Tawara, T. Kato and Y. Nakai (1983) [Published in Atomic Data and
Nuclear Data Tables 32, 235 (1985)]

- IPPJ-AM-29 "Bibliography on Atomic Processes in Hot Dense Plasmas"
T. Kato, J. Hama, T. Kagawa, S. Karashima, N. Miyanaga, H. Tawara,
N. Yamaguchi, K. Yamamoto and K. Yonei (1983)
- IPPJ-AM-30 "Cross Sections for Charge Transfers of Highly Ionized Ions in Hydrogen
Atoms (Up-dated version of IPPJ-AM-15)"
H. Tawara, T. Kato and Y. Nakai (1983) [Published in Atomic Data and
Nuclear Data Tables 32, 235 (1985)]
- IPPJ-AM-31 "Atomic Processes in Hot Dense Plasmas"
T. Kagawa, T. Kato, T. Watanabe and S. Karashima (1983)
- IPPJ-AM-32 "Energy Dependence of the Yields of Ion-Induced Sputtering of Monatomic
Solids"
N. Matsunami, Y. Yamamura, Y. Itikawa, N. Itoh, Y. Kazumata, S. Miyagawa,
K. Morita, R. Shimizu and H. Tawara (1983) [Published in Atomic Data and
Nuclear Data Tables 31, 1 (1984)]
- IPPJ-AM-33 "Proceedings on Symposium on Atomic Collision Data for Diagnostics and
Modelling of Fusion Plasmas, Aug. 29 – 30, 1983"
Ed. by H. Tawara (1983)
- IPPJ-AM-34 "Dependence of the Backscattering Coefficients of Light Ions upon Angle of
Incidence"
T. Tabata, R. Ito, Y. Itikawa, N. Itoh, K. Morita and H. Tawara (1984)
- IPPJ-AM-35 "Proceedings of Workshop on Synergistic Effects in Surface Phenomena
Related to Plasma-Wall Interactions, May 21 – 23, 1984"
Ed. by N. Itoh, K. Kamada and H. Tawara (1984) [Published in Radiation
Effects 89, 1 (1985)]
- IPPJ-AM-36 "Equilibrium Charge State Distributions of Ions ($Z_1 \geq 4$) after Passage
through Foils – Compilation of Data after 1972"
K. Shima, T. Mikumo and H. Tawara (1985) [Published in Atomic Data and
Nuclear Data Tables 34, 357 (1986)]
- IPPJ-AM-37 "Ionization Cross Sections of Atoms and Ions by Electron Impact"
H. Tawara, T. Kato and M. Ohnishi (1985)
- IPPJ-AM-38 "Rate Coefficients for the Electron-Impact Excitations of C-like Ions"
Y. Itikawa (1985)
- IPPJ-AM-39 "Proceedings of the Japan-U.S. Workshop on Impurity and Particle Control,
Theory and Modeling, Mar. 12 – 16, 1984"
Ed. by T. Kawamura (1985)
- IPPJ-AM-40 "Low-Energy Sputterings with the Monte Carlo Program ACAT"
Y. Yamamura and Y. Mizuno (1985)
- IPPJ-AM-41 "Data on the Backscattering Coefficients of Light Ions from Solids (a
Revision)"
R. Ito, T. Tabata, N. Itoh, K. Morita, T. Kato and H. Tawara (1985)

- IPPJ-AM-42 "Stopping Power Theories for Charged Particles in Inertial Confinement Fusion Plasmas (Emphasis on Hot and Dense Matters)"
S. Karashima, T. Watanabe, T. Kato and H. Tawara (1985)
- IPPJ-AM-43 "The Collected Papers of Nice Project/IPP, Nagoya"
Ed. by H. Tawara (1985)
- IPPJ-AM-44 "Tokamak Plasma Modelling and Atomic Processes"
Ed. by T. Kawamura (1986)
- IPPJ-AM-45 Bibliography of Electron Transfer in Ion-Atom Collisions
H. Tawara, N. Shimakura, N. Toshima and T. Watanabe (1986)
- IPPJ-AM-46 "Atomic Data Involving Hydrogens Relevant to Edge Plasmas"
H. Tawara, Y. Itikawa, Y. Itoh, T. Kato, H. Nishimura, S. Ohtani, H. Takagi, K. Takayanagi and M. Yoshino (1986)
- IPPJ-AM-47 "Resonance Effects in Electron-Ion Collisions"
Ed. by H. Tawara and G. H. Dunn (1986)
- IPPJ-AM-48 "Dynamic Processes of Highly Charged Ions (Proceedings)"
Ed. by Y. Kanai and S. Ohtani (1986)

Available upon request to Research Information Center, Institute of Plasma Physics, Nagoya University, Nagoya 464, Japan, except for the reports noted with*.

